Tomasz Kalwarczyk

FROM SELF-DIFFUSION TO SCALE DEPENDENT VISCOSITY

- FLUORESCENCE CORRELATION SPECTROSCOPY STUDIES

Advisor: Prof. dr hab. Robert Hołyst

Department of Soft Condensed Matter and Fluids

The presented dissertation was prepared within

the International Ph.D. in Chemistry Studies at the

Institute of Physical Chemistry of the Polish Academy of Sciences

Kasprzaka 44/52, 01-224 Warsaw, Poland.

Warsaw, August 19, 2011

Acknowledgments

I would like to thank my advisor Professor Robert Hołyst for his support, advices and for creating excellent research environment. Thanks to Professor Marcin Fiałkowski for fruitful discussions and all kind of suggestions about the scientific work. Thank to all members of the Soft Condensed Matter and Fluids department of the Institute of Physical Chemistry of the Polish Academy of Sciences for creating inspiring scientific atmosphere.

I would like to acknowledge Professor Adam Patkowski for creating the opportunity to get training in fluorescence correlation spectroscopy technique at the Laboratory of Molecular Biophysics at the Adam Mickiewicz Univeristy in Poznań. Thanks to Dr Jacek Gapiński for giving me advices and teaching the fluorescence correlation spectroscopy technique.

I would like to acknowledge Professor Hans-Jürgen Butt and Dr Kaloian Koynov for providing me experimental results of diffusion in the polystyrene matrices. I would like to thank Dr Jędrzej Szymański for providing me experimental results of diffusion in the surfactant solutions.

I would like to thank Msc. Urszula Rak, Msc. Ewa Zaboklicka for their contribution to the results of my research.

The work was supported by the Project operated within the Foundation for Polish Science Team Programme co-financed by the EU "European Regional Development Fund" TEAM/2008-2/2 and the "Mistrz" Programme.

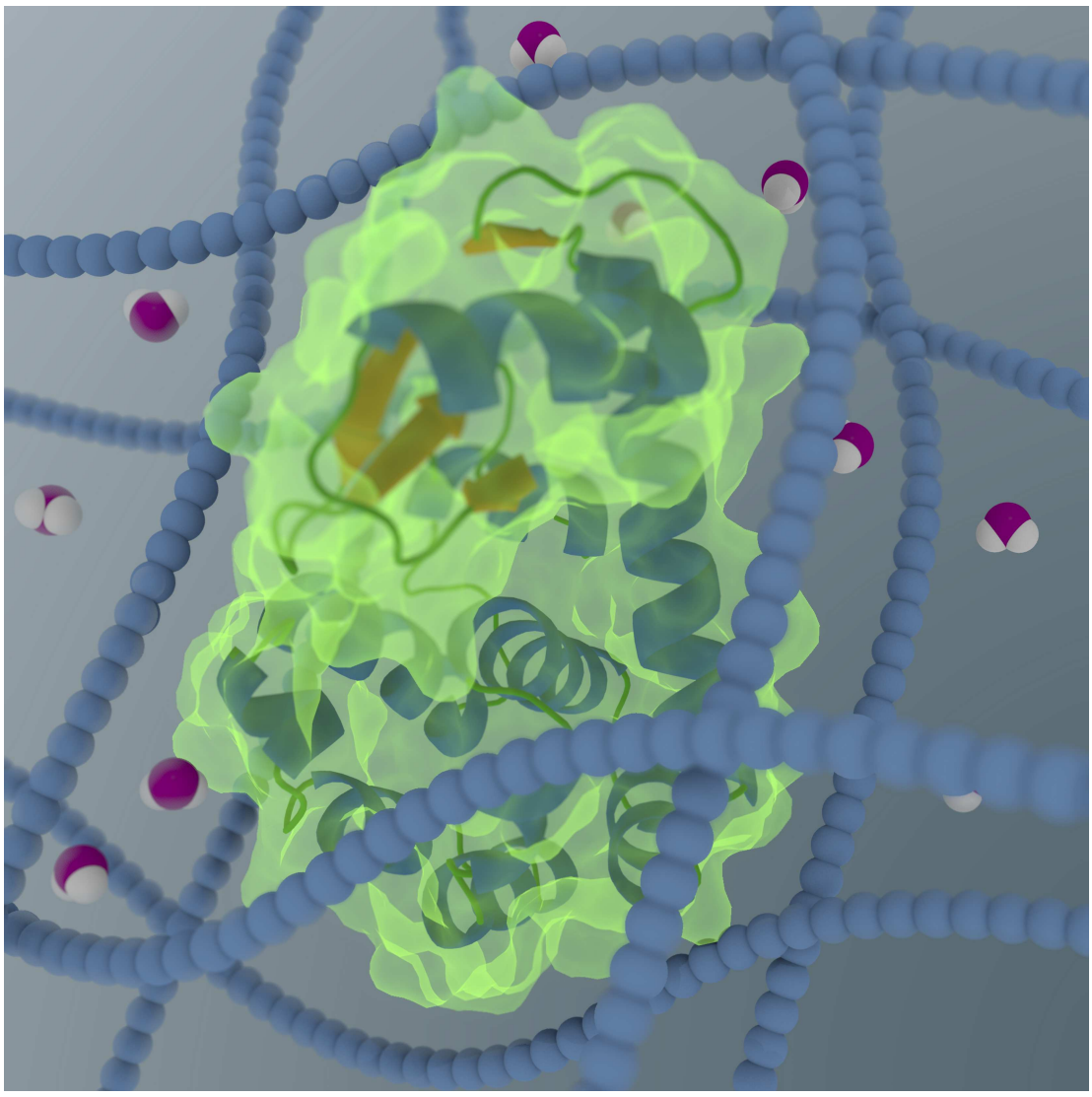

Cartoon represents the motion of nanoscopic probe through a network composed of polymer chains.

Publications

1. Kalwarczyk, T., Ziębacz, N., Wieczorek, S. A., and Hołyst, R. “Kinetics and dynamics of dissolution/mixing of a high-viscosity liquid phase in a low-viscosity solvent phase” *J. Phys. Chem. B* **111**(41), 11907–11914 (2007) (IF=3.603)

2. Kalwarczyk, T., Ziębacz, N., Fiałkowski, M., and Hołyst, R. “Late stage of the phase-separation process: Coalescence-induced coalescence, gravitational sedimentation, and collective evaporation mechanisms” *Langmuir* **24**(13), 6433–6440 (2008) (IF=4.268)

3. Hołyst, R., Bielejewska, A., Szymański, J., Wilk, A., Patkowski, A., Gapiński, J., Żywociński, A., Kalwarczyk, T., Kalwarczyk, E., Tabaka, M., Ziębacz, N., and Wieczorek, S. A. “Scaling form of viscosity at all length-scales in poly(ethylene glycol) solutions studied by fluorescence correlation spectroscopy and capillary electrophoresis” *Phys. Chem. Chem. Phys.* **11**(40), 9025–9032 (2009) (IF=3.453)

4. Li, H., Wieczorek, S. A., Xin, X., Kalwarczyk, T., Ziębacz, N., Szymborski, T., Hołyst, R., Hao, J., Górecka, E., and Pociecha, D. “Phase Transition in Salt-Free Catanionic Surfactant Mixtures Induced by Temperature” *Langmuir* **26**(1), 34–40 (2010) (IF=4.268)

5. Li, H., Xin, X., Kalwarczyk, T., Kalwarczyk, E., Nitoń, P., Hołyst, R., and Hao, J. “Reverse Vesicles from a Salt-Free Catanionic Surfactant System: A Confocal Fluorescence Microscopy Study” *Langmuir* **26**(19), 15210–15218 (2010) (IF=4.268)

6. Hou, S., Ziębacz, N., Kalwarczyk, T., Kamiński, T. S., Wieczorek, S. A., and Hołyst, R. “Influence of nano-viscosity and depletion interactions on cleavage of DNA by enzymes in glycerol and poly(ethylene glycol) solutions: qualitative analysis” *Soft Matter* **7**(7), 3092–3099 (2011) (IF=4.457)

7. † Kalwarczyk, T., Ziębacz, N., Bielejewska, A., Zaboklicka, E., Koynov, K., Szymański, J., Wilk, A., Patkowski, A., Gapiński, J., Butt, H.-J., and Hołyst, R. "Comparative analysis of viscosity of complex liquids and cytoplasm of mammalian cells at the nanoscale" *Nano Letters* **11**(5), 2157–2163 (2011) (IF=12.186)

8. Hou, S., Ziębacz, N., Wieczorek, S. A., Kalwarczyk, E., Sashuk, V., Kalwarczyk, T., Kamiński, T.S., Hołyst, R. "Formation and Structure of PEI/DNA Complexes: Quantitative Analysis" *Soft Matter* **7**(7), 3092–3099 (2011) (IF=4.457)

9. Ziębacz, N., Wieczorek, S.A., Kalwarczyk T., Fiałkowski, M., Hołyst R. "Crossover regime for the diffusion of nanoparticles in polyethylene glycol solutions: influence of the depletion layer" *Soft Matter* **DOI:** 10.1039/C0SM01357A (IF=4.457)

10. † Kalwarczyk, T., Tabaka, M., Hołyst R. "Size-dependent viscosity and DNA/protein crowding of the cytoplasm of Escherichia coli" **Submited to** *PNAS* (IF=9.771)

Patent applications

1. Maciej Paszewski, Marcin Fiałkowski, Ewelina Kalwarczyk, Tomasz Kalwarczyk, Katarzyna Winkler, Robert Hołyst; **P-391217** „Metoda pokrywania powierzchni nanocząstkami"

2. Maciej Paszewski, Marcin Fiałkowski, Ewelina Kalwarczyk, Tomasz Kalwarczyk, Katarzyna Winkler, Robert Hołyst; **EN.700114.GB** „Method of coating material surfaces with nanoparticles"

3. Yuriy Stepanenko, Maciej Paszewski, Marcin Fiałkowski, Ewelina Kalwarczyk, Tomasz Kalwarczyk, Katarzyna Winkler, Robert Hołyst, Joanna Niedziółka-Jonsson, Izabela Kamińska, Marcin Opałło; **P-393843** "Nanoczastki pokryte ligandami hydrofilowymi, warstwa takich nanoczastek i powierzchnia pokryta taka warstwa."

† Works which directly relates to this Thesis.

Thesis

Complex liquids such as polymer or surfactant solutions appear in many branches of modern chemistry, from cosmetic industry, through pharmacy to the synthesis of nanoparticles. Viscosity of those liquids may be orders of magnitude higher than the solvent viscosity. Such high viscosity is due to the presence of overlapped polymer chains or micelles. Small proteins and nanoparticles diffuse surprisingly fast in living cells and in other high viscosity complex liquids. Their diffusion coefficients are often orders of magnitude larger than expected from the Stokes-Sutherland-Einstein (SSE) equation $D = kT/6\pi\eta_{\mathrm{m}}r_{\mathrm{p}}$ where η_{m} is the macroscopic viscosity of polymer solution (measured traditionally with falling ball viscometer or rheometer) and r_{p} is the hydrodynamic radius of the probe.

High mobility of small objects in complex fluids can be explained by the dependence of viscosity on the scale at which it is measured (the size of the probe used to measure the viscosity). I propose the following modification of the Stokes-Sutherland-Einstein (SSE) equation:

$$D = \frac{kT}{6\pi\eta_{\mathrm{eff}}r_{\mathrm{p}}}$$

where η_{eff} is the effective viscosity experienced by the probe, which is, a function of hydrodynamic radius of the probe:[†]

$$\eta_{\mathrm{eff}} = \eta_0 \, exp\left[\left(\frac{R_{\mathrm{eff}}}{b\xi}\right)^a\right]$$

[†] η_0 is the viscosity of the solvent; $R_{\mathrm{eff}}^{-2} = R_{\mathrm{h}}^{-2} + r_{\mathrm{p}}^{-2}$; ξ is the correlation length; a and b are constants of the order of 1.

In order to check whether the hypothesis of scale dependent viscosity is correct, measurements of viscosity of polymer solutions as a function of the size of the probe as well as a function of the polymer concentration, were performed. In my measurements a technique called fluorescence correlation spectroscopy (FCS) was used. In addition, the above hypothesis was tested for the systems that are different from polymer solutions. For this purpose data of diffusion in surfactant solutions, literature data concerning the viscosity of the cytoplasm of living cells, and data of viscosity of the solutions of colloidal particles were analyzed.

Koncepcja pracy doktorskiej

Płyny złożone takie jak roztwory polimerów bądź środków powierzchniowo czynnych znajdują zastosowanie w wielu dziedzinach współczesnej chemii począwszy od przemysłu kosmetycznego, przez farmację, na syntezie nanocząstek kończąc. Roztwory płynów złożonych charakteryzują się lepkościami rzędy wielkości większymi w stosunku do lepkości rozpuszczalnika. Wynika to z obecności wzajemnie zahaczających się łańcuchów polimerowych lub agregatów cząsteczkowych (micel). Pomimo dużych wartości lepkości, współczynniki dyfuzji małych białek mogą być znacząco wyższe niż można by wyliczyć z równania Stokesa-Sutherlanda-Einsteina $D = kT/6\pi\eta_{\mathrm{m}}r_{\mathrm{p}}$ gdzie η_{m} jest lepkością roztworu polimerowego a r_{p} jest promieniem hydrodynamicznym próbnika. Przy założeniu że powyższe równanie jest poprawne, jedynym wytłumaczeniem takich obserwacji może być fakt że współczynnik lepkości η jest funkcją rozmiaru próbnika.

Niniejsza rozprawa doktorska poświęcona jest zagadnieniu lepkości zależnej od skali pomiaru (rozmiaru użytego próbnika). Pomiary opisane w rozprawie wykonane były dla wodnych roztworów polimerowych. Lepkość roztworów wyznaczana była z pomiarów samo dyfuzji cząsteczek w badanych roztworach. W badaniach została zastosowana spektroskopia korelacji fluorescencji (FCS). Układem pomiarowym były roztwory glikolu polietylenowego oraz próbniki w postaci znakowanego fluorescencyjnie białka oraz barwnika fluorescencyjnego. Przeprowadzona została też analiza danych dostępnych w literaturze dla innych układów celem wyprowadzenia równania

opisującego lepkość w funkcji rozmiaru próbnika. Równanie to zostało następnie zastosowane do analizy lepkości cytoplazmy żywych, komórek oraz lepkości koloidalnego roztworu twardych kul.

Table of contents

Thesis **1**

Koncepcja pracy doktorskiej **3**

Table of contents **5**

Nomenclature and Abbreviations **7**

1 Intoduction **11**

1.1 Viscosity of fluids 11

1.2 Self-diffusion and the Stokes-Sutherland-Einstein equation 12

1.3 Experimental technique 17

1.3.1 Fluorescence and phosphorescence 17

1.3.2 Fluorescence correlation spectroscopy 19

Autocorrelation function 22

Three dimensional diffusion 29

Photophysics of the fluorophore 30

1.4 Complex liquids 33

1.4.1 Introduction to polymer solutions 33

1.4.2 Introduction to surfactant solutions 37

1.4.3 Introduction viscosity of complex liquids 42

Viscosity of dilute solutions 42

Viscosity of concentrated solutions 43

2 Experimental section **47**

2.1 Materials 47

Labeling of the Lysozyme 49

2.2 Methods 50

Sample preparation 50
FCS Experimental setup 51
Falling ball Viscometry 51
FCS calibration and experimental procedure 53
Fluctuation Dissipation Theorem 55

3 Results, data analysis, and discussion **57**
3.1 Viscosity of complex liquids 57
Measurements of diffusion in poly(ethylene glycol) solutions . . 57
3.1.1 Scaling form of the viscosity of complex liquids 59
Viscosity of poly(ethylene glycol) solutions 59
Viscosity of polystyrene solutions 61
Viscosity of $C_{12}E_6$ solutions 63
3.1.2 Validation of the scaling formula 64
3.2 Viscosity of the cytoplasm of mammalian cells 68
3.3 Viscosity of the cytoplasm of *Escherichia coli* 77
3.4 Viscosity of colloidal suspensions 83
3.4.1 Calculation of the effective viscosity of colloidal suspensions . 83
3.4.2 Application of the scaling law to the literature data 84

4 Summary and conclusions **91**

Nomenclature and Abbreviations

$\check{\beta}$	Sliding friction coefficient, see Eq.(1.2.4), page 14
η	Viscosity coefficient
η_{m}	Macroscopic viscosity
η_{eff}	Effective viscosity (scale dependent)
κ	Structure parameter, see Eq.(1.3.26), page 30
$\mathbb{T}$	Fraction of molecules in the triplet state
ν	Excluded volume exponent
ω	Radiuis of the focal volume
ϕ	Volume fraction of hard spheres
Π	Osmotic pressure
ψ	Concentration of hard spheres understand as volume of the spheres divided by the volume of the slovent. $\psi = \phi/\left(1-\phi\right)$
R_{eff}	Effective hydrodynamic radius, see Eq.(1.4.15), page 45
R_{g}	Polymer radius of gyration
R_{h}	Polymer hydrodynamic radius
r_{p}	Hydrodynamic radius of a probe

τ Correlation time (Lag time)

τ_T Time which molecules spend in the triplet state

τ_D Time of diffusion, time which molecule spends in the focal volume, see Eq.(1.3.24), page 30

d Dimensionality

S_0 Singlet ground electronic state

S_1,S_2 Singlet excited electronic states

T_1 First triplet state

ϑ Addition to the hydrodynamic radius of the rigid sphere, see Eq.(3.4.12), page 88

ξ Mesh (blob) size, correlation length, distance between entanglement points, see Eq.(1.4.5), page 36

ζ Half length of the focal volume

C Concentration

c Concentration in g·cm^{-3}

c^* Overlap concentration, see Eq.(1.4.4), page 35

D Diffusion coefficient

d_p Diameter of the probe

E Electric field

F Force

F_{r} Force exerted on a sphere with given radius immersed in a fluid of given viscosity, see Eq.(1.2.3), page 13

J Flux

k The Boltzmann constant

M_{n} Number averaged molecular weight

M_{w} Weight averaged molecular weight

N Number of molecules, particles, *etc.*

n Number of monomers in polymer chain

n_{v} Number of molecules per unite volume

N_{A} Avogadro's number

R The gas constant

T Temperature

t Time

U Velocity of the sphere, see Eq.(1.2.3), page 13

V Volume

SSE The Stokes-Sutherland-Einstein equation, see Eq.(1.2.12), page 16

ACF Autocorrelation function, see page 22

CMC Critical micelle concentration

DCR Diffusion coefficient ratio – diffusion coefficient of the probe related to its diffusion coefficient in a pure solvent

FCS Fluorescence correlation spectroscopy

FDT Fluctuation-dissipation theorem

FRAP Fluorescence recovery after photobleaching

FV Focal volume – small spot illuminated by the light of the laser

MDE(r) Molecular detection efficiency in a given point,$\boldsymbol{r}$, inside the focal volume

PEG Polymer – poly(ethylene glycol), see Figure 14**a**, page 47

RhB Rhodamine B, see Figure 14**b**, page 47

SPAD Single photon avalanche diode – FCS detector

TAMRA Fluorescent dye (5-(and-6)-carboxytetramethylrhodamine), see Figure 14**c**, page 47

1 Introduction

1.1 Viscosity of fluids

Viscosity is a transport property which is related to the migration of the momentum from one point of the space to another. The definition of the viscosity of hypothetical homogeneous fluid is given below. The fluid is bounded by a solid wall and a plate of the area equal to A at a distance z from the wall. Let the fluid be composed of hypothetical, infinitesimally thin layers (Figure 1). Let neglect the effect of plate's edges. If an external force F (parallel to the wall) is applied to the plate, force needed to move the plate along the X axis, according to the Newton law (Eq.(1.1.1)), is proportional to the surface area of the plate A, velocity of the plate along X axis – v_{x}, and inversely proportional to the distance of the plate from the wall (Z axis). The proportionality constant denoted as η is the viscosity of the fluid and is also called the internal friction.

$$F = \eta A \frac{\mathrm{d}v_{\mathrm{x}}}{\mathrm{d}z} \tag{1.1.1}$$

Eq.(1.1.1) can be applied not only to the plate which bounds the fluid but also to each of hypothetical layers.

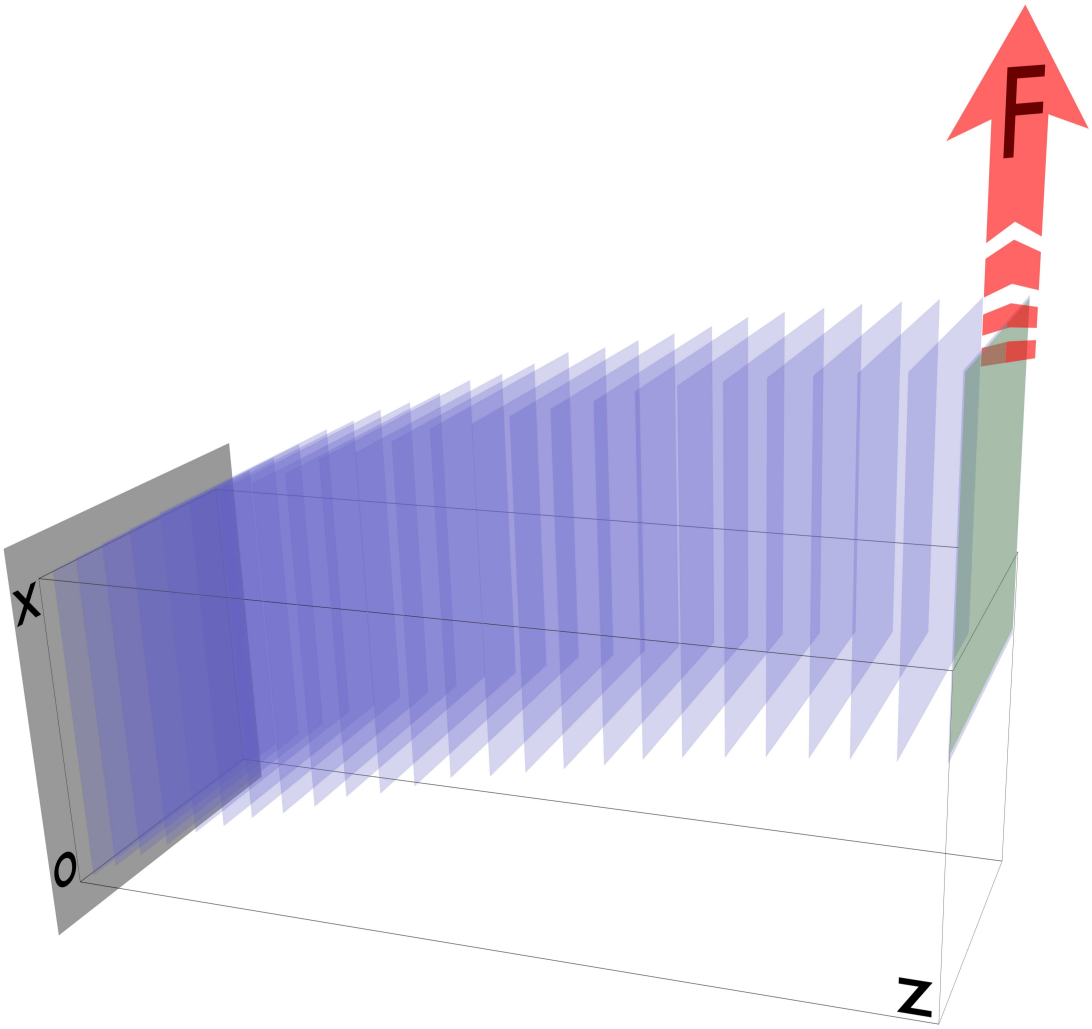

Figure 1: Schematic representation of the fluid bounded by the solid wall and the plate. The force F is applied to the plate in the direction of the X axis. Displacement of the plate along X axis with the velocity v_{x} causes displacements of each layer. The displacement of each layer is governed by Eq.(1.1.1).

1.2 Self-diffusion and the Stokes-Sutherland-Einstein equation

The concept of diffusion was introduced by Thomas Graham in 1833 [1]. Adolf Fick followed Graham's concept and introduced [2] his diffusion laws (Eqs.(1.2.1) and (1.2.2)).

$$J = -D\frac{\mathrm{d}N}{\mathrm{d}x} \tag{1.2.1}$$

where J denotes the flux of molecules through the unit of area in the unit of time, N is the number of molecules, and D is their diffusion coefficient. Eq.(1.2.1) is known as the first Fick's law. The second Fick's law is given by the relation:

$$\frac{\mathrm{d}C}{\mathrm{d}t} = D\frac{\mathrm{d}^2C}{\mathrm{d}x^2} \tag{1.2.2}$$

Here C is the concentration, and t is time. Graham and Fick focused their studies of diffusion on the collective motion of molecules and on their transport.

Sir George Gabriel Stokes was more interested in the fluid mechanics and the flow past immersed bodies. In 1850, he calculated from the Navier-Stokes equations, the force F_r exert on a sphere of radius r_p by a fluid of viscosity η moving with velocity U[3]:

$$F_\mathrm{r} = 6\pi\eta r_\mathrm{p} U \tag{1.2.3}$$

He assumed that velocity of the fluid vanishes at the surface of the sphere. He also assumed that the fluid overflowing the sphere is homogeneous and the flow itself is non-turbulent. Eq.(1.2.3) is equivalent to the situation when the liquid remain immobile and the sphere moves with the velocity U. The work of Stokes allowed to improve the description of molecular motion. In the year of 1902 William Sutherland used the Stokes formula (Eq.(1.2.3)) to investigate the motion of ions, dissolved in the liquid, after application of an external electric field $E = \mathrm{d}u/\mathrm{d}x$ (u – applied voltage). He assumed that the force exerted on the ions can be described by the Stokes law (Eq.(1.2.4))

[4].

$$F = qE = 6\pi\eta r_{\mathrm{p}} U \frac{1 + 2\eta/\check{\beta} r_{\mathrm{p}}}{1 + 3\eta/\check{\beta} r_{\mathrm{p}}} \tag{1.2.4}$$

Here q is the charge of the ion, $\check{\beta}$ is a coefficient of sliding friction. $\check{\beta} = 0$ when the velocity of the fluid on the surface of the ion does not vanished and $\check{\beta} = \infty$ when the fluid velocity on the ion surface goes to zero.

Three years later Sutherland [5] in March, and Einstein [6] in May of 1905 published their works about diffusion of small solutes. Both proposed the same equation describing random, thermal motion of spherical particles. Both researchers used the Stokes equation to describe the drag exerted on the sphere moving in a fluid in the random manner. Their derivation is summarized below.

Consider a system containing a liquid with a volume V at temperature T. In this fluid, there are N spherical particles, whose concentration satisfies the assumption of infinite dilution. Molecules are located in volume V, as shown in Figure 2. In such a system, the osmotic pressure difference is generated, such that at the point x, $\Pi = \Pi(x)$ and at $x + \mathrm{d}x$, $\Pi = \Pi(x + \mathrm{d}x)$. Suppose that the fluid surrounding the particles is immobile. In this case the change of the Gibbs free energy (the work) associated with the movement of particles (for simplification only in the direction x) is equal to:

$$\mathrm{d}G = V\mathrm{d}\Pi = V\mathrm{d}(CRT) = \mathrm{d}CRTV \tag{1.2.5}$$

where C is the concentration of particles, and R is the gas constant. According to the Stokes equation (Eq.(1.2.3)) the force F_{r} (Eq.(1.2.3)) is exerted on a particle moving in

a fluid, hence for N particles, in equilibrium, we obtain the relationship:

$$\mathrm{d}CRTV = -NF_{\mathrm{r}}\mathrm{d}x \tag{1.2.6}$$

Transforming this equation, we obtain:

$$\nabla CRT = -\frac{NF_{\mathrm{r}}}{V} \tag{1.2.7}$$

The equation can be expressed as:

$$N_{\mathrm{A}}\nabla\left(\frac{N}{V}\right)RT = -6\pi\eta r_{\mathrm{p}}\frac{UN}{V} \tag{1.2.8}$$

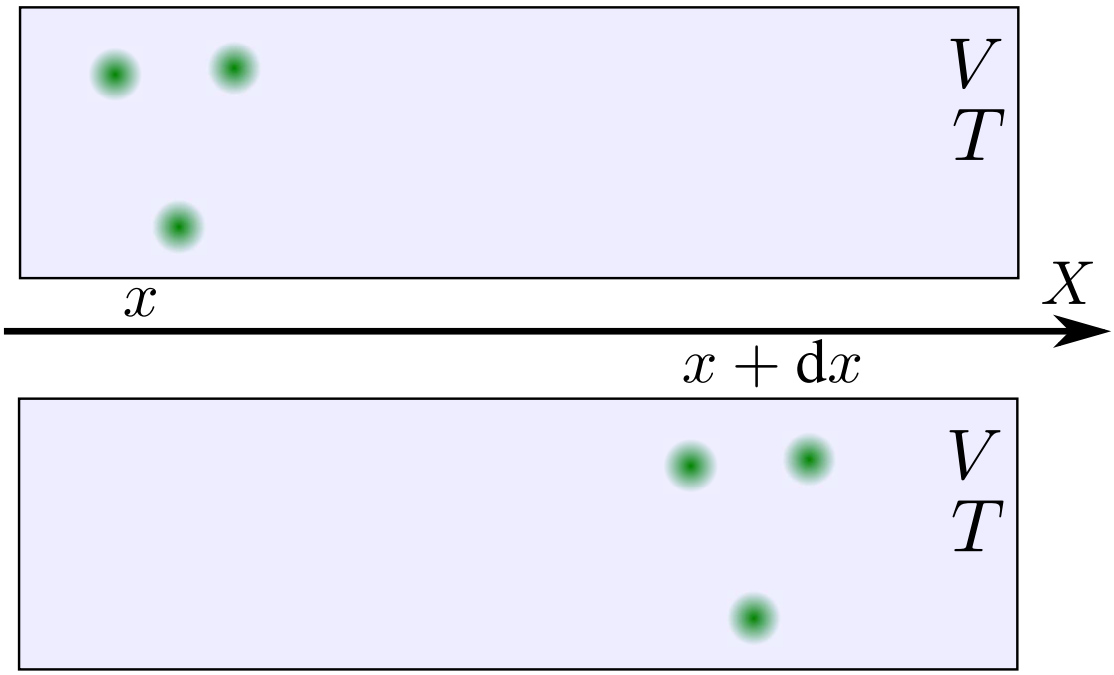

Figure 2: The system contains a fluid with a volume V and temperature T. In the liquid, are spherical particles at concentration, C, that satisfies the assumption of infinite dilution.

Because:

$$\frac{UN}{C} = J \tag{1.2.9}$$

then according to Fick's first law:

$$\nabla\left(\frac{N}{V}\right) = -\frac{J}{D} \tag{1.2.10}$$

where D is a diffusion coefficient. Finally we obtain:

$$-\frac{J}{D}kT = -6\pi\eta r_{\mathrm{p}}J \tag{1.2.11}$$

Thus, the diffusion coefficient of particles contained in the fluid under consideration is equal to:

$$D = \frac{kT}{6\pi\eta r_{\mathrm{p}}} \tag{1.2.12}$$

This dependence is called the Stokes-Sutherland-Einstein (SSE) equation. Although SSE equation was derived over 100 years ago it is still in use. Additionally as Edward shown in his review [7], the SSE equation is valid even for very small molecules. For example in water as the solvent SSE is valid for the molecules whose r_{p} is larger than 0.5 nm. When smaller molecules were considered, large deviations from SSE equation were observed. In addition, deviations from SSE equation are observed when the concentration of diffusing molecules is large.

1.3 Experimental technique

This section is devoted to the experimental technique used to study the diffusion of different probes. Currently, there are several techniques to measure diffusion coefficients of objects at different length scales, i.e., nuclear magnetic resonance (NMR) [8], allowing the determination of diffusion coefficient of small molecules (molecular length scale), fluorescence recovery after photobleaching and dynamic light scattering allowing to determine the diffusion coefficients for objects with sizes ranging from a few to several hundred nm [9, 10], and optical microscopy allowing to determine the diffusion coefficients of objects (based on measurements of mean-squared displacement) ranging in size from several hundred nm to several microns. For the measurements described in this dissertation, I use relatively novel technique called fluorescence correlation spectroscopy (FCS) [11]. It allows for measurements at a molecular scale (measurement of single molecules of a size less than a nanometer), and at the nanometric scale (size of probes from single to tens of nanometers). In the following sections I discuss photophysics of molecules used as probes in FCS and theoretical background of the FCS.

1.3.1 Fluorescence and phosphorescence

When light illuminates solutions of aromatic compounds one can observe a glowing effect which was described by John F. W. Herschel [12]. He investigated aqueous solution of quinine. Luminescence observed by Herschel is a general term describing two similar phenomena: fluorescence and phosphorescence. Both phenomena occur

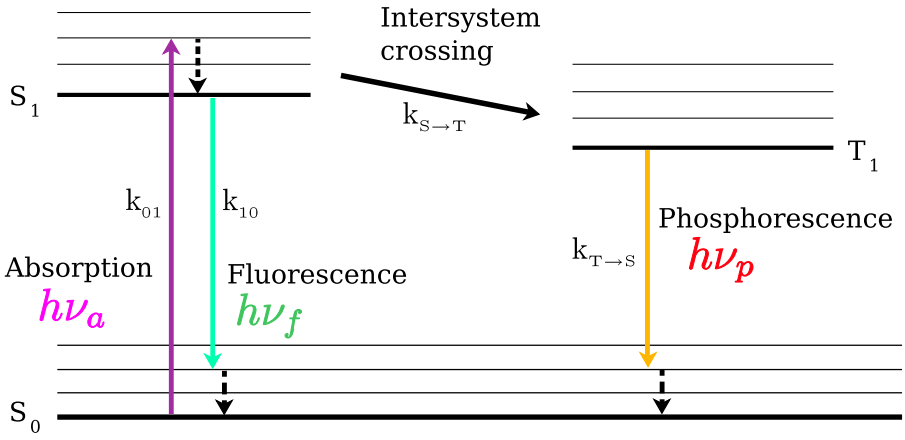

Figure 3: Picture shows simplified Jabłoński diagram. S_0, S_1, S_2 correspond to singlet ground, and excited electronic states of the molecule. T_1 represents excited, first triplet state. Rate constants of each process are as follows: k_{01} for transition from the ground state to S_1; k_{10} for transition from the excited state to S_0; $k_{S\to T}$ for intersystem crossing and $k_{T\to S}$ for the phosphorescence.

due to the relaxation of molecule from the excited state to the ground state. Both, fluorescence and phosphorescence can be explained using Jabłoński diagram shown in Figure 3. At the beginning of these processes, the particle is in the ground state (S_0). Next the molecule absorb a photon with energy equal $h\nu_a$. Due to absorption of energy, the molecule is excited to one of its vibrational levels in either electronic state S_1 or S_2. From S_2 the molecule non-radiatively relaxes to the lower excited state S_1 within picoseconds. When molecule reaches a thermally equilibrated state S_1 further decreases its energy by emission of photons with energy equal to $h\nu_f$. The transition between states $S_1 \rightarrow S_0$ takes usually few nanoseconds and is called fluorescence. When molecule is in the excited state S_1 apart of the fluorescence emission, transition between S_1 and T_1 may occur. Such transition is called intersystem crossing. When molecule decreases its energy to the level of T_1 it fall into a kind of energetic trap. T_1 has lower energy than the S_1 state so that a backward transition is impossible. On the

other hand transition $T_1 \rightarrow S_0$ is forbidden. During transition between first triplet state and ground singlet state phosphorescence photon is emitted with energy equal $h\nu_p$. Typical lifetime of the phosphorescence is of the order of microsecond or longer and is limited by probability of the $T_1 \rightarrow S_0$ transition.

In this work fluorescence phenomenon is used for detection of molecules presence in the observed part of the sample. Detailed information about photophysics of observed molecules, in particular information about vibrational levels of molecules are not important in our experiments and will be omitted in the introduction.

1.3.2 Fluorescence correlation spectroscopy

Fluorescence correlation spectroscopy was developed by Webb in early '70s of the XXth century [13], and improved by Rigler [11] in '90s. The technique was used to measure the rate constant of chemical reactions (binding of ethidium bromide to DNA) [13], translational diffusion coefficients of small molecules such as fluorescent dyes, proteins and polymers [14–16], and finally rotational diffusion coefficients [17].

Typical concentrations used in the FCS are of the order of nano moles. Usage of confocal microscope equipped with a laser as a source of coherent light, allows to obtain the detection volume, of the order of fraction of femto-liter. Additionally, by use of ultra-sensitive detectors that count photons at the level of tens to hundreds of thousands of photons per second, it is possible to detect fluctuations in the concentration of fluorescent molecules in the confocal volume with a precision of single molecules. Example of experimental system is shown in Figure 4. Laser beam (Figure 4 – (1)) with

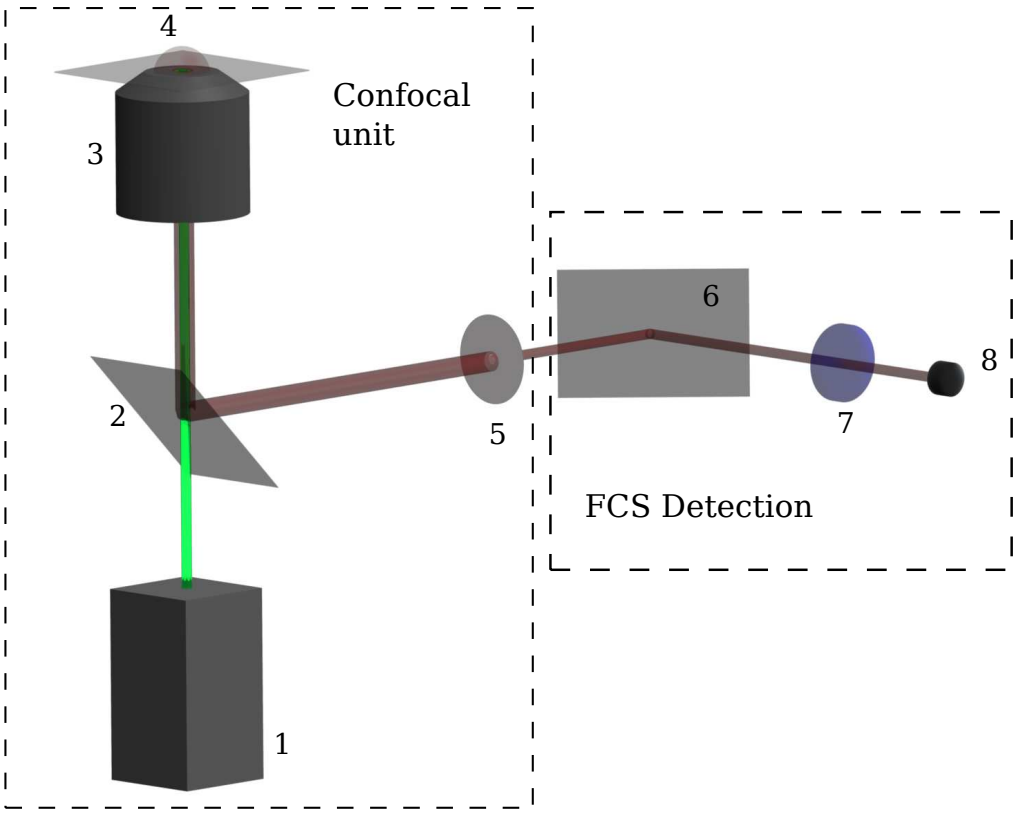

Figure 4: A scheme of the FCS equipment. 1 – source of laser light; 2 – dichroic mirror; 3 – microscope objective; 4 – sample; 5 – pinhole; 6 – mirror; 7 – filter; 8 – SPAD (Single Photon Avalanche Diode) detector.

proper wavelenght excites invetigated molecules. The beam is focused in the sample (Figure 4 – (4)) by the objective of the microscope (Figure 4 – (3)). Small spot which is illuminated by the laser is called the focal volume FV. Fluorescent molecules present in the FV and illuminated by the light of the laser emit photons which are further collected by the lens of the objective. Since molecules are not only exited in the focal volume but also in a whole laser beam passing through the sample, collected signal should be spatially confined in order to detect signal from the FV only. Therefore dichroic mirror (Figure 4 – (2)) reflect collected light onto a pinhole (Figure 4 – (5)). Pinhole from the origin signal remove only those photons which are emitted from outside the FV. Next

the signal is directed into the FCS detection unit, consisting of a set of filters (Figure 4 – (7)) and detector (Single Photon Avalanche Diode – SPAD (Figure 4 – (8))).

Fluorescence correlation spectroscopy can be presented in the following manner. Suppose that the concentration of a fluorophore in the studied solution is 5 nM. Now, from the considered sample extract a hypothetical cylinder (assume that this is the confocal volume FV), whose height is equal to 1 micrometer, and the radius is 0.2 micrometers. The volume of this cylinder is 0.126 μm^3, which is equivalent to 0.126 fL. Average number of a fluorophore molecules in the considered FV is equal to 0.38. This value reflects the equilibrium concentration of the fluorophore in the solution. On the other hand, instantaneous concentration (number of molecules) in the FV fluctuates, due to diffusion of the fluorophore. A concentration change in the FV, causes changes in the intensity of the detected signal, which constitutes basis of measurements of the fluorescence correlation spectroscopy. The presence of molecules in the FV is described by the Poisson statistics. This means that the probability of finding m fluorophores in a given confocal volume, while their average number equals N, is given by the Poisson distribution (Eq.(1.3.1).

$$P\left(m,N\right)=\frac{N^{m}}{m!}e^{-N} \tag{1.3.1}$$

According to Eq.(1.3.1) the probability that in the considered volume of investigated solution one can find no molecules $P\left(0,0.38\right)=68\%$, The probability that only one molecule will be found in the FV – $P\left(1,0.38\right)=26\%$, whereas $P\left(2,0.38\right)=5\%$.

For three molecules the probability $P\left(3, 0.38\right) < 1\%$. Signal detected from the FV is schematically shown in Figure 6. Two main variables which can be determined from the collected signal are the average number of molecules occupying the FV and time which molecules spend in the FV. Diffusion of molecules in the focal volume produce

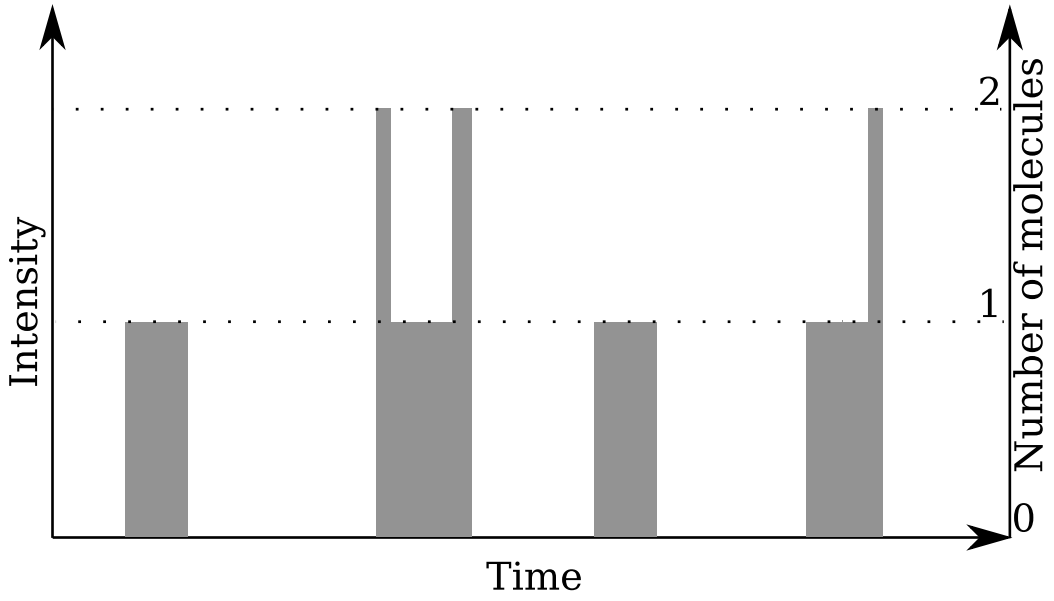

Figure 5: Fluorescence signal from the theoretical FV. For 68% of time there is no molecules in FV (no signal). For 26% of time one fluorescent molecule can be found in the FV. Two molecules occupy the FV in 5% of the whole time.

intensity fluctuations – a noise. To find out whether the noise exhibit some temporal correlation, an autocorrelation function (ACF) is used.

Autocorrelation function

The autocorrelation function used in the fluorescence correlation spectroscopy is a product of detected fluorescence intensity at time equal t, ($F\left(t\right)$) and of the intensity in the time, delayed of time τ ($F\left(t+\tau\right)$), averaged over t, i.e., over the whole time of the experiment. Rapid diffusion through the FV results in rapid intensity fluctuations.

On the contrary slow diffusion, results in slow fluctuations. When the amplitude of the

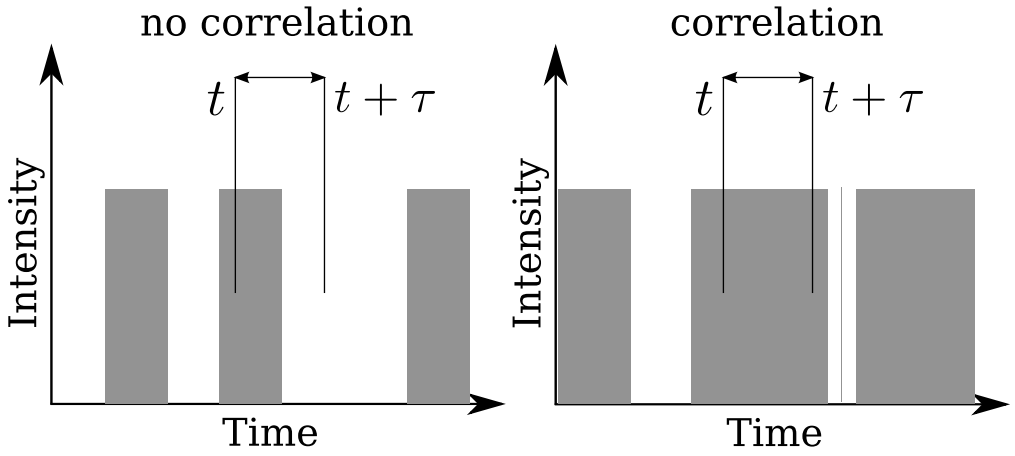

Figure 6: Figure present basis of the autocorrelation function. Rapid diffusion of the entities results in short times of the fluorescence fluctuations. On the other hand slow motion of the molecules through the focal volume produces fluctuations more elongated in time. When correlation time τ is longer than fluctuation time there is no temporal correlation in the analyzed noise. On the contrary for long fluctuations (longer than τ) correlation occurs.

---

intensity $F(t)$ is higher than the average value of the fluorescence signal $\langle F \rangle$, and is comparable with the amplitude $F(t+\tau)$ the temporal correlation occurs. The value of the autocorrelation is given by the following relation (following the reference [18, page 800]).

$$R(\tau) = \langle F(t) F(t+\tau) \rangle = \frac{1}{\mathfrak{T}} \int_0^{\mathfrak{T}} F(t) F(t+\tau) \, dt \tag{1.3.2}$$

Here $\mathfrak{T}$ denotes the time of data accumulation, and its inverse is a normalization factor. When fluorescent particles diffuse in and out of the the focal volume, the fluorescence signal fluctuates around the mean value and those fluctuations can be written as:

$$\delta F(t) = F(t) - \langle F \rangle \tag{1.3.3}$$

Finally the autocorrelation function of fluorescence fluctuations can be written in a form of Eq.(1.3.4) [18, page 800].

$$G(\tau) = \frac{\langle F(t)\, F(t+\tau)\rangle}{\langle F\rangle^2} - 1 = \frac{\langle \delta F(t)\, \delta F(t+\tau)\rangle}{\langle F\rangle^2} \tag{1.3.4}$$

Here we introduce theoretical model describing fluctuations of the fluorescence. Intensity of the detected signal is proportional to the number of photons emitted from a single molecule in a given period of time. Let B is a number of photons emitted by one molecule per unit of time. Let $\boldsymbol{r}$ is a position of the fluorophore at time $t = 0$. I assume that intensity profile of the laser beam focused by the objective is described by the three dimensional Gaussian distribution. This is the simplest model of the illumination spot and can be depicted as in the Figure 7.

For such defined focal volume, one can define a function that describes the detection efficiency. This function is given by the following equation:

$$\mathrm{MDE}(\boldsymbol{r}) = I_0 \exp\left[\frac{-2(x^2+y^2)}{\omega^2}\right] \exp\left[\frac{-2z^2}{\zeta^2}\right] \tag{1.3.5}$$

where I_0 is value of the maximal intensity, ω and ζ are semi-axes of the ellipsoidal profile shown in Figure 7. FV is described by the Gaussian function. The function does not exhibit sharp boundaries and ω and ζ represent values in which intensity decreases to the value of e^{-2} of the maximum intensity I_0 [18, page 801]. According to the shape

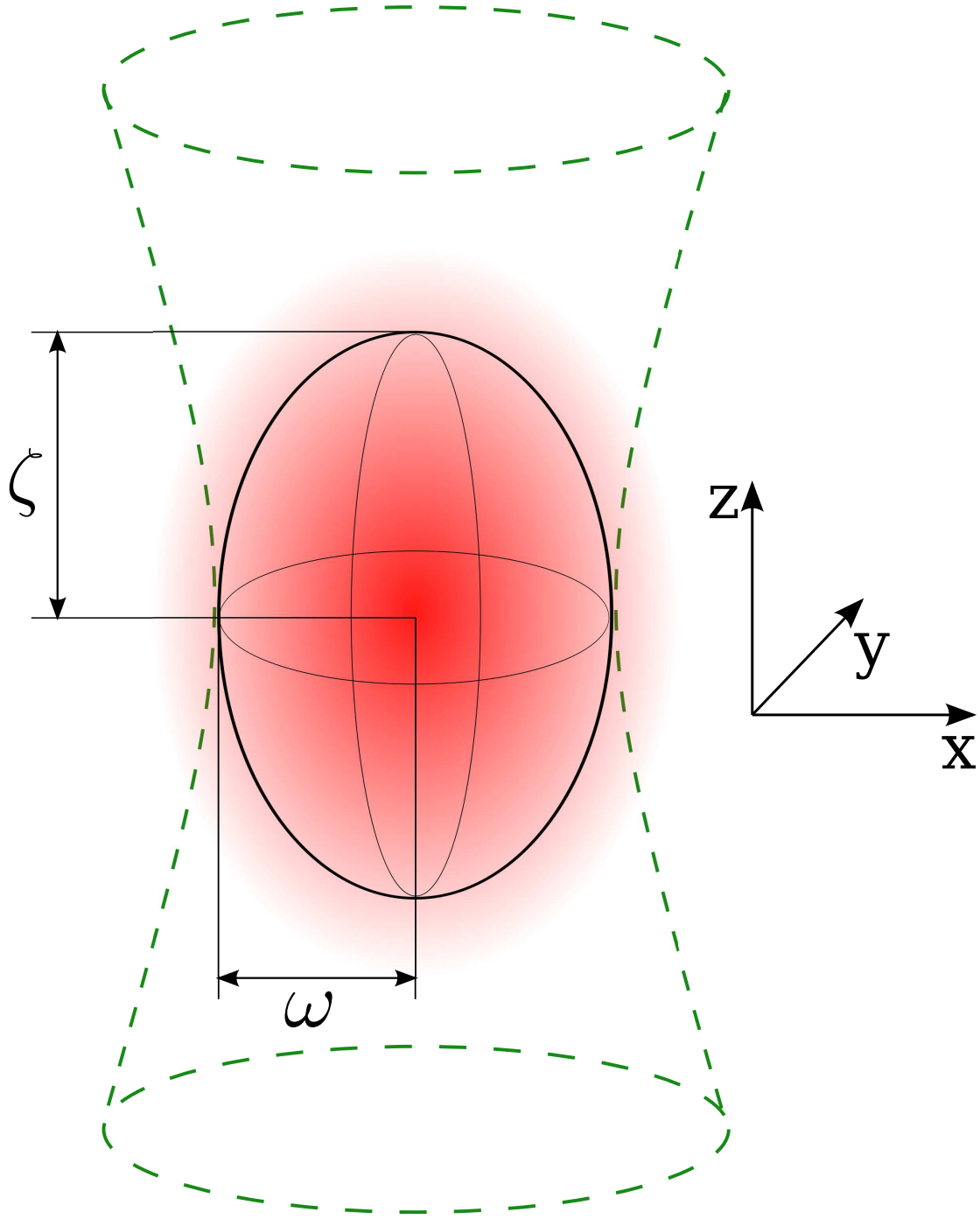

Figure 7: The model of the focal volume described by the three dimensional Gaussian function (cf. Eq.(1.3.5)). Dimensions of the observed volume (ellipsoid) are limited by the value of the fluorescence intensity and the radius ω and the half length ζ are points at space at which the intensity of fluorescence decreases to the value of e^{-2} of its maximal value.

---

of the FV, at time t, the total signal of the fluorescence is given by the following integral:

$$F(t) = B \int \mathrm{MDE}(\boldsymbol{r})\, C(\boldsymbol{r}, t)\, dV \tag{1.3.6}$$

where $C(\boldsymbol{r},t)$ is a distribution of the molecules inside the focal volume and dV denotes integration over the entire volume of the considered FV, $dV = d^3\boldsymbol{r}$. $\delta C(\boldsymbol{r},t)$ is the deviations of the concentration from the average value $\langle C\rangle$:

$$\delta C(\boldsymbol{r},t) = C(\boldsymbol{r},t) - \langle C\rangle \tag{1.3.7}$$

By substitution of Eq.(1.3.7) into Eq.(1.3.6) we obtain:

$$\begin{aligned} F(t) = B\int \text{MDE}(\boldsymbol{r})\left(\langle C\rangle + \delta C(\boldsymbol{r},t)\right)dV = \\ = B\int MDE(\boldsymbol{r})\langle C\rangle\, dV + B\int MDE(\boldsymbol{r})\,\delta C(\boldsymbol{r},t)\,dV \end{aligned} \tag{1.3.8}$$

Average concentration $\langle C\rangle$ is independent on the position in the sample. Thus one can write:

$$F(t) = B\langle C\rangle\int MDE(\boldsymbol{r})\,dV + B\int MDE(\boldsymbol{r})\,\delta C(\boldsymbol{r},t)\,dV \tag{1.3.9}$$

Let us now transform Eq.(1.3.3) in a following manner:

$$F(t) = \langle F\rangle + \delta F(t) \tag{1.3.10}$$

By comparing Eqs.(1.3.9) and (1.3.10) one can find that

$$\delta F(t) = B\int MDE(\boldsymbol{r})\,\delta C(\boldsymbol{r},t)\,dV \tag{1.3.11}$$

Therefore the autocorrelation function, used in the fluorescence correlation spectroscopy is defined as follows:

$$G(\tau) = \frac{B^2 \int\int \text{MDE}(\boldsymbol{r})\,\text{MDE}(\boldsymbol{r}')\,\langle \delta C(\boldsymbol{r},0)\,\delta C(\boldsymbol{r}',\tau)\rangle\, dV\,dV'}{\left(B\langle C\rangle \int \text{MDE}(\boldsymbol{r})\,dV\right)^2} = \\ = \frac{1}{\langle C\rangle^2} \frac{\int\int \text{MDE}(\boldsymbol{r})\,\text{MDE}(\boldsymbol{r}')\,\langle \delta C(\boldsymbol{r},0)\,\delta C(\boldsymbol{r}',\tau)\rangle\, dV\,dV'}{\left(\int \text{MDE}(\boldsymbol{r})\,dV\right)^2} \quad (1.3.12)$$

In Eq.(1.3.12), $\boldsymbol{r}'$ shows the position of the fluorophore at time $t = \tau$. Note that coefficient B cancels due to the fact that brightness of the fluorophore does not depend on the position. The term:

$$\langle \delta C(\boldsymbol{r},0)\,\delta C(\boldsymbol{r}',\tau)\rangle \quad (1.3.13)$$

is the correlation of the fluctuations of the concentration at the point $\boldsymbol{r}$ with respect to the position $\boldsymbol{r}'$ at time equal τ, and for $\tau = 0$, correlation of fluctuation of the concentration (Eq.(1.3.13)) occurs only if the same position is considered [19, page 341]. Namely when $\boldsymbol{r} = \boldsymbol{r}'$. Therefore Eq.(1.3.13) gives:

$$\langle \delta C(\boldsymbol{r},0)\,\delta C(\boldsymbol{r}',0)\rangle = \langle C\rangle\,\delta(\boldsymbol{r}-\boldsymbol{r}') \quad (1.3.14)$$

where $\delta(\boldsymbol{r}-\boldsymbol{r}')$ is the Dirac delta [19, page 341] function of the following properties.

$$\delta(-x) = \delta(x) \quad (1.3.15)$$

$$\int f(x)\,\delta(x-a)\,dx = f(a) \quad (1.3.16)$$

Using Eq.(1.3.12) and Eqs.(1.3.14) to (1.3.16) we obtain:

$$G(0) = \frac{1}{\langle C \rangle} \frac{\int \mathrm{MDE}^2(\boldsymbol{r})\, dV}{\left(\int \mathrm{MDE}(\boldsymbol{r})\, dV\right)^2} \tag{1.3.17}$$

The dimension of the second term of the right side of Eq.(1.3.17) is the inverse of the volume [20]:

$$\frac{\int \mathrm{MDE}^2(\boldsymbol{r})\, dV}{\left(\int \mathrm{MDE}(\boldsymbol{r})\, dV\right)^2} = \frac{1}{V} \tag{1.3.18}$$

therefore the value of the ACF at $\tau = 0$ is the average number of molecules in the FV (N).

$$G(0) = \frac{1}{\langle C \rangle} \frac{1}{V_{\mathrm{eff}}} = \frac{1}{N} \tag{1.3.19}$$

V_{eff} is the effective volume and for Gaussian shape of the FV, and it is defined [18, page 804] as:

$$V_{\mathrm{eff}} = \pi^{3/2} \omega^2 \zeta \tag{1.3.20}$$

One should keep in mind, however, that exact value of the effective volume in FCS experiments is generally unknown and Eq.(1.3.20) is only an estimate [18]. For the sample in which the average concentration of fluorophore equals $\langle C \rangle$, and the confocal volume equals V_{eff}, value of the autocorrelation function for $\tau = 0$ is the inverse number of molecules present in the confocal volume. $G(0)$ is called the amplitude of the ACF.

Three dimensional diffusion

Assume that the volume of the considered sample is significantly larger than FV. In addition, the concentration of the fluorophore in the sample satisfies the assumption of infinite dilution. In such case changes of the concentration of the fluoprophore in time can be described by the second Fick's law and it can be written as a differential form of Eq.(1.2.2):

$$\frac{\partial C\left(\boldsymbol{r},t\right)}{\partial t}=D\boldsymbol{\nabla}^{2}C\left(\boldsymbol{r},t\right) \tag{1.3.21}$$

Where D is the diffusion coefficient of the fluorophore. Using Eqs.(1.3.7) and (1.3.21), and the multiple Fourier transform operation which was described by Lakowicz [19, page 354], the correlation of fluctuations of concentration is given by the following equation [19, page 355]:

$$\left\langle \delta C\left(\boldsymbol{r},0\right)\delta C\left(\boldsymbol{r}',\tau\right)\right\rangle =\left\langle C\right\rangle \left(4\pi D\tau\right)^{\frac{3}{2}}\exp\left[-\frac{\left|\boldsymbol{r}-\boldsymbol{r}'\right|^{2}}{4D\tau}\right] \tag{1.3.22}$$

Eq.(1.3.22) can be regarded as the probability of finding molecule in the position $\boldsymbol{r}$ at time equal t, if position of the same molecule at $t=0$ is $\boldsymbol{r}'$. Free diffusion of the entities, apart of the Fick's laws (Eqs.(1.2.1) and (1.2.2)) and SSE equation (Eq.(1.2.12)), is also described by Einstein-Smoluchowski equation describing the mean square displacement of diffusing fluorophore in time:

$$\left|\boldsymbol{r}-\boldsymbol{r}'\right|^{2}=2\mathrm{d}Dt \tag{1.3.23}$$

where t is a time and d is a dimensionality of the diffusion process. The displacement of molecules occurring in the XY plane is important for FCS signal. The time that a molecule spends in the FV described by Eqs.(1.3.5) and (1.3.20), according to Eq.(1.3.23) is equal to:

$$\tau_{\mathrm{D}} = \frac{\omega^2}{4D} \tag{1.3.24}$$

Here τ_{D} is time of diffusion across FV, of the fluorophore through the focal volume with lateral radius equal ω. Now putting Eqs.(1.3.22) and (1.3.24) into Eq.(1.3.12) we obtain the ACF for three dimensional diffusion given by the following relation:

$$G(\tau) = G(0)\frac{1}{1+\frac{\tau}{\tau_{\mathrm{D}}}}\frac{1}{\sqrt{1+\kappa^2\frac{\tau}{\tau_{\mathrm{D}}}}} \tag{1.3.25}$$

where κ is the ratio of the half length ζ and the radius ω of the FV (Figure 7, Eq.(1.3.26)).

$$\kappa = \frac{\zeta}{\omega} \tag{1.3.26}$$

Photophysics of the fluorophore

As noted in the previous two paragraphs, changes of the concentration of fluorescent molecules, caused by their diffusion, produces a fluorescence signal fluctuations. From these fluctuations, information concerning the diffusion of molecules through the FV is obtained. However, not only diffusion can cause fluctuations in fluorescence. For example, phenomena related to the photophysics, also may cause such fluctuations. Moreover, the timescale of fluctuations arising from photophysics of the molecule is

comparable with the time scale corresponding to the diffusion of fluorescent molecules. The phenomenon of fluorescence occurs in the time scale of the order of nano seconds. One can compare this time scale, with the average time of diffusion of the fluorescent molecule through the focal volume with radius $\omega = 0.2$ μm. As an example let us take rhodamine B for which diffusion coefficient D at room temperature is of the order of 420 $\mu\text{m}^2\text{s}^{-1}$ [21] and $\tau_{\text{D}} = 23.8$ μs. Fluorescence process, although discrete in the nanosecond time scale, in diffusion time scale may be considered as continuous one. On the contrary, another photophysical phenomenon described in section 1.3.1 – phosphorescence occurs on time scale which is comparable with times of diffusion across the FV. When transition between electronic states S_1 and T_1 occurs, fluorescent molecule may be regarded as a dark molecule (due to the forbidden character of the transition $T_1 \rightarrow S_0$). The molecule is in the T_1 state and does not emit photons. Kinetics of the phosphorescence can be described by the Jabłoński diagram which was discussed in details in section 1.3.1 (cf. Figure 3). Time at which molecule remain dark for the detector (is in the triplet state – τ_{T}) as well as the fraction of those molecules ($\mathbb{T}$) can be calculated from the rates of each step showed in Figure 3 – Eqs.(1.3.27) and (1.3.28) [18, page 816].

$$\frac{1}{\tau_{\text{T}}} = \text{k}_{\text{T}\rightarrow\text{S}} + \frac{\text{k}_{01}\text{k}_{\text{S}\rightarrow\text{T}}}{\text{k}_{01} + \text{k}_{10}} \tag{1.3.27}$$

$$\mathbb{T} = \frac{\text{k}_{01}\text{k}_{\text{S}\rightarrow\text{T}}}{\text{k}_{01}\left(\text{k}_{\text{S}\rightarrow\text{T}} + \text{k}_{\text{T}\rightarrow\text{S}}\right) + \text{k}_{\text{T}\rightarrow\text{S}}\left(\text{k}_{\text{S}\rightarrow\text{T}} + \text{k}_{10}\right)} \tag{1.3.28}$$

When transition to the triplet state for a given fluorophore occurs, the measurement cannot be analyzed with the ACF given by Eq.(1.3.25). The problem is simplified for

$\tau_{\mathrm{T}} < \tau_{\mathrm{D}}$. In such case the phosphorescence process can be described as a chemical reaction which kinetics is described by Eqs.(1.3.27) and (1.3.28). The ACF can be written as a product of the ACF for simple diffusion $G_{\mathrm{D}}(\tau)$ and an autocorrelation function for reaction of transition from singlet to triplet state (G_{T}) [18, page 816]:

$$G(\tau) = G_{\mathrm{D}}(\tau)\, G_{\mathrm{T}}(\tau) \tag{1.3.29}$$

where:

$$G_{\mathrm{T}}(\tau) = 1 + \frac{\mathbb{T}}{1-\mathbb{T}} \exp\left(-\frac{\tau}{\tau_{\mathrm{T}}}\right) \tag{1.3.30}$$

Therefore the ACF for the fluorescent molecules which undergo diffusion and which exhibit triplet state transitions is given by Eq.(1.3.31).

$$G(\tau) = \frac{1}{N}\left(1 + \frac{\mathbb{T}}{1-\mathbb{T}} \frac{1}{\exp\left(\frac{\tau}{\tau_{\mathrm{T}}}\right)}\right) \frac{1}{1+\frac{\tau}{\tau_{\mathrm{D}}}} \frac{1}{\sqrt{1+\kappa^2 \frac{\tau}{\tau_{\mathrm{D}}}}} \tag{1.3.31}$$

The fluorescence correlation spectroscopy has been already successfully applied to the measurements in polymer solutions [14, 22, 23], surfactant solutions [24, 25] or in biological systems [15, 26]. In each case, for correct performance of the measurements and its analysis, a correct model of the ACF should be used. In particular when the fluorophore which exhibit triplet states is investigated, Eq.(1.3.31) should be used for FCS analysis. On the contrary, for simple, three dimensional diffusion (without triplet states which can be observed for quantum dots or ATTO 488 dye), Eq.(1.3.25) is an appropriate model.

1.4 Complex liquids

The phrase "complex liquid" generally refers to the polymer solutions, thermotropic or lyotropic (surfactants) liquid crystals or colloidal solutions. The following section discusses the physical and chemical properties of complex liquids.

1.4.1 Introduction to polymer solutions

Polymers are macromolecules consisting of smaller subunits – monomers. Monomers are usually small molecules which after the reaction of polymerization create longer chains. Such chain should be sufficiently long so that the change of its length of one or a few monomers will not affect its physicochemical properties. One can define degree of polymerization which is given by equation: $M_{\mathrm{w}} = nM_{\mathrm{w}_0}$ where M_{w} is the weight averaged molecular weight of the polymer chain, n is the degree of polymerization, and M_{w_0} is the molecular weight of the monomer. In practice when $n > 10^2$ then the chain is called a polymer, otherwise it is an oligomer.

Let us consider a linear polymer chain whose monomers can freely rotate around monomer-monomer bond. The simplest measurable value describing the size of such polymer, is the gyration radius of the polymer coil. For considered polymer chain it is given by the following equation:

$$\left\langle R_{\mathrm{g}}^2 \right\rangle = \frac{1}{n} \sum_{i=1}^{n} \left\langle (\boldsymbol{R}_{\mathrm{i}} - \boldsymbol{R}_0)^2 \right\rangle \tag{1.4.1}$$

Here n is the number of segments, $\boldsymbol{R}_0$ is a vector pointing to the center of the mass, and $\boldsymbol{R}_n$ is a vector pointing the n-th segment. Eq.(1.4.1) originate from the model in which polymer segments can easily rotate. In this case, the radius of gyration of the polymer chain is proportional to the square root of the number of monomers. One of the disadvantages of this model is that the segments can occupy the same place in a space. To avoid such unphysical behavior another model of polymer chain – excluded volume model – was introduced. In excluded volume model polymer segments cannot occupy the same position.

Size of the polymer is proportional to the number of segments to the ν power. Namely:

$$R_{\mathrm{g}} \propto n^{\nu} \tag{1.4.2}$$

In practice, the monomers are considered as single segments, therefore, the radius of gyration is a function of molecular weight of the polymer M_{w}:

$$R_{\mathrm{g}} \propto M_{\mathrm{w}}^{\nu} \tag{1.4.3}$$

Both models do not include interactions of the polymer chain with a solvent molecules. Solvent molecules however, may have significant influence the structure of the polymer [27]. For example in so called good solvents, according to the rule *similia similibus solvuntur*, polymer segments have large affinity to the solvent molecules. Thus monomers of the polymer in a good solvent would prefer to be surrounded by solvent molecules rather than by other monomers. This causes that polymer chain spreads and

$\nu > 1/2$. On the other hand when polymer is dissolved in poor solvent, the monomers have small affinity to solvent molecules. Therefore monomers prefer to be surrounded by other monomers rather than by solvent molecules and polymer chain collapses and $\nu < 1/2$. Apart from the interactions between monomers and solvent, temperature also influence on the size of the polymer coil. For example it is possible to find such temperature in which affinity of monomers to the solvent is equal to the affinity to the other monomers. For this temperature $\nu = 1/2$ and it is called θ or Flory's temperature [28]. Below this temperature affinity of monomers to monomers is higher then monomer to solvent which results in contraction of the size of the coil. On the contrary when $T > \theta$, an opposite situation occur and polymer expands its size.

The structure of polymer solutions depending on the concentration of the polymer, can be divided into three regimes shown in Figure 8. The so-called *dilute regime*, in which each of the polymer chains, is a separate individual, and the average distance between chains is larger than the size of these chains (Figure 8**a**). The second (*semi-dilute* – Figure 8**b**), in which the chains begin to overlap, and the average distance between the chains becomes smaller than the size of chains in the solution. And finally the *concentrated* (Figure 8**c**), in which the chains are completely overlapped and it is impossible to distinguish the individual chains. It is assumed that the concentration at which the polymer chains begin to overlap (c^*) is given by the equation:

$$c^* = \frac{M_{\mathrm{w}}}{\frac{4}{3}\pi R_{\mathrm{g}}^3 N_{\mathrm{A}}} \tag{1.4.4}$$

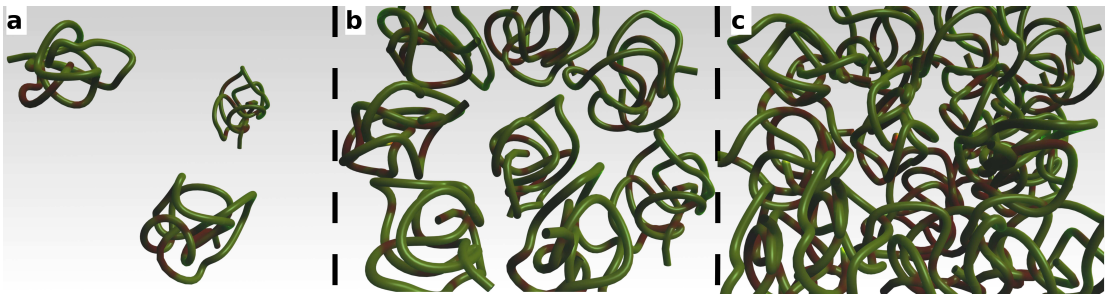

Figure 8: In polymer solutions one can distinguish three regimes describing given solution. **a** – *dilute* regime where polymer coils diffuse freely. Distances between polymers in this regime are big enough so that polymers do not interact. **b** – *semi-dilute* regime where polymers coils begin to overlap. The last (figure **c**) – *concentrated* regime where polymer chains are totally overlapped so that distinguishing between single chains is impossible.The transition between **a** and **b** occurs when the concentration c is equal to the overlap concentration c^*.

In order to describe the structure of the polymer solution in the semi-dilute regime, Pierre-Gilles de Gennes [29] introduced the concept of blob, characterizing the size of the part of the polymer chain, which is not overlapped with other chains and can be treated as an individual. Namely all monomers in the blob belong to a single chain. In other words one polymer chain can be divided into many blobs and each blob behave as a single chain and not as a part of a longer chain [30]. The linear dimension of the blob can be mathematically expressed as follows:

$$\xi = R_{\mathrm{g}} \left(\frac{c}{c^*} \right)^{-\beta} \tag{1.4.5}$$

where c is the concentration of the polymer in g·cm^{-3} and $\beta = \nu / (3\nu - 1)$ is an exponent related to excluded volume exponent, dependent on the solvent, i e. in a good solvents $\beta = 0.75$ whereas in θ solvents $\beta = 1$ [31]. Eq.(1.4.5) is also called a corre-

lation length and defines average distance between entanglement points of the polymer chain, or an average distance between the center of the mass of one chain, and the nearest monomer of the other chain as depicted in Figure 9.

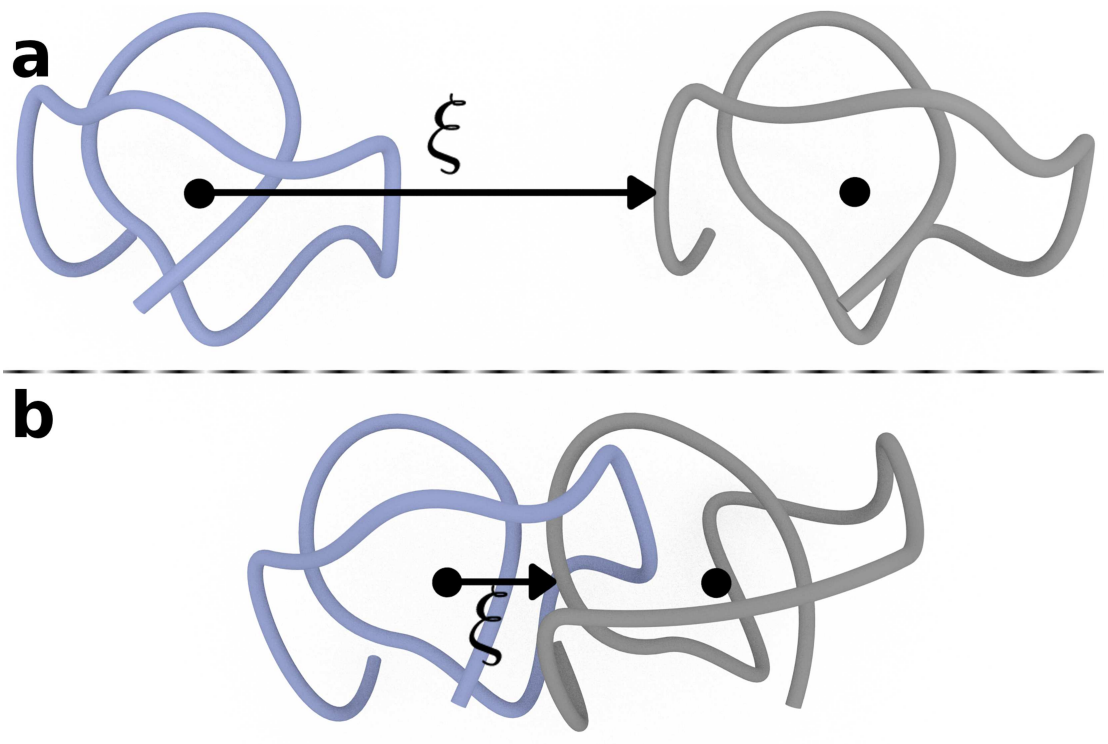

Figure 9: ξ in polymer solution can be define as the average distance between the center of mass of a polymer, and the nearest monomer belonging to another chain. For a dilute system, $\xi > R_{\mathrm{g}}$ and for concentrated systems $\xi < R_{\mathrm{g}}$. Black dots correspond to centers of the masses of the polymer chains.

1.4.2 Introduction to surfactant solutions

Another complex system, considered in this work is the solutions of surfactants. These compounds have affinity for two chemically different solvents, i.e., water and oil/air (amphiphilic compounds). Those molecules can be schematically represented as in Figure 10. Due to the amphiphilicity, surfactant molecules tend to incorporate on the

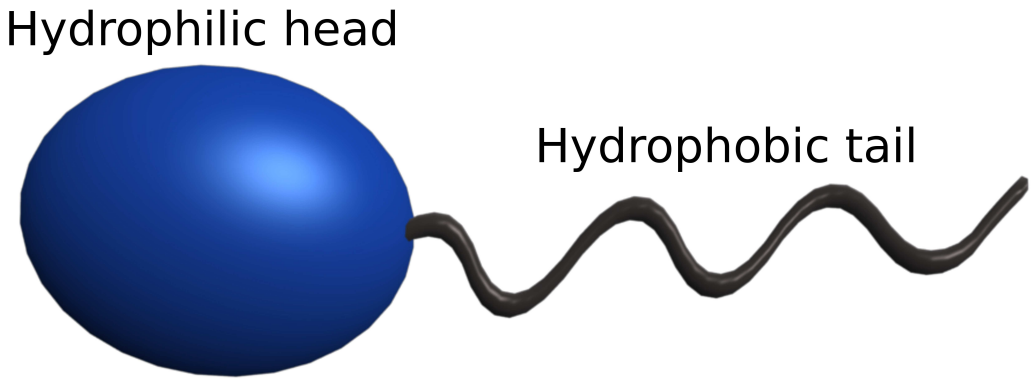

Figure 10: Schematic representation of the surfactant molecule. On the left hand hydrophilic part of molecule composed of chemical gropus with high afinity to water. On the opposite site hydrophobic tail, typically mostly of long alkyl chains (8-18 carbons).

interface between two phases and reduce the surface tension between them. The term surfactant is an acronym for surface active agents.

Properties of solutions of surfactants will be discussed below, based on the example of a system consisting of two immiscible liquids (water and oil). The molecules of surfactant dissolved in water, adsorb on the surface in such configuration which minimize their free energy. In other words, surfactants validate the rule: *similia similibus solvuntur*, and their hydrophilic head is immersed in water whereas hydrophobic tail is in the oil phase. Surfactants can be divided into three groups according to charge of the hydrophilic part. Namely, one can distinguish anionic (negatively charged), non-ionic (uncharged) and cationic (positively charged) surfactant molecules. Examples of the members of each group are presented in Figure 11.

Apart from the surface activity of surfactant molecules, another important property of those compounds should be discussed. When the concentration of the surfactant increases, molecules tend to self-organize. Above certain concentration called critical

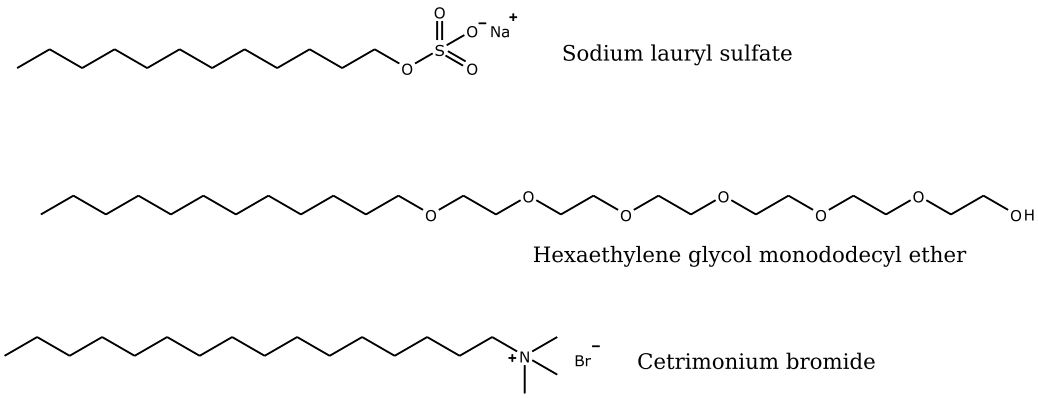

Figure 11: Examples of the surfactant molecules with different types of hydrophilic groups (two ionic and one non-ionic). Sodium dodecyl sulfate (SDS) represents anionic surfactant with negatively charged head group. Hexaethylene glycol monododecyl ether ($C_{12}E_6$) is an uncharged molecule. Cetrimonium bromide is a member of the positively charged (cationic) surfactants.

micelle concentration (CMC) surfactant molecules form micelles. When concentration of the surfactant molecules $C =$ CMC, various physicochemical properties of the surfactant solutions rapidly change their dependence on concentration. For example, surface tension between two immiscible liquids approaches a constant, when $C \rightarrow$ CMC, as in Figure 12. Micelles are formed due to repulsive interactions between hydrophobic part of the surfactant molecule and water. System aim to minimize contact of nonpolar alkyl chains with polar water molecules. Therefore hydrophilic – polar parts of surfactant molecules create a specific shell which encloses hydrophobic alkyl chains and separates them form water. Surfactant micelles may differ in shape which is determined by the shape of the molecule itself. Three types of micelles are observed: *spherical* – (Figure 13**a**) – whose concentrated solution can be regarded as a solution of colloids (Figure 13**d**); *rigid-elongated* – (Figure 13**b**) – concentrated solution create network of stiff rods (Figure 13**e**); *long and flexible* – (Figure 13**c**) – create a polymer-like network (Figure 13**f**). When concentration of surfactant molecules is further increased,

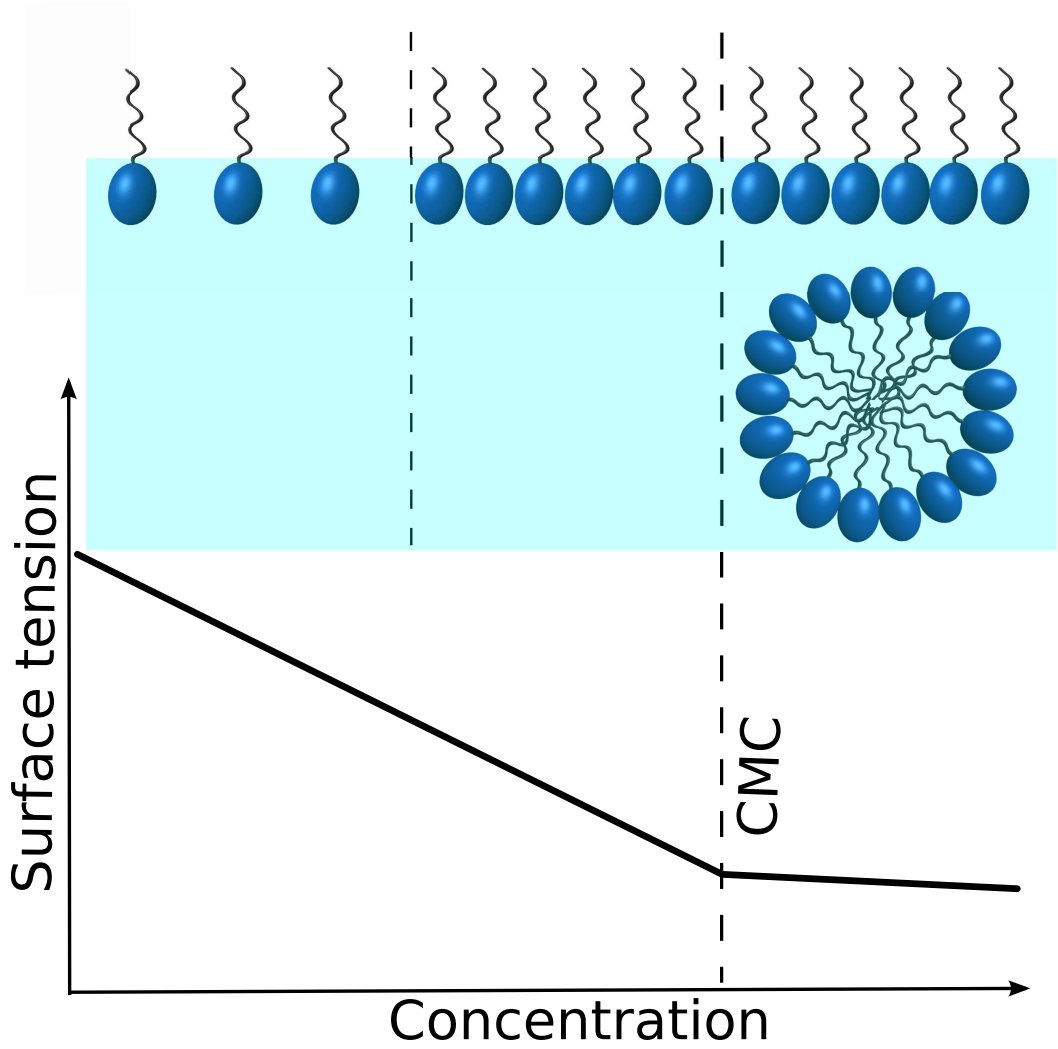

Figure 12: Dependence of the surface tension of aqueous surfactant solution on concentration of surfactant molecules (following reference [32, page 42]). Below CMC surfactant molecules incorporate on the interface between two phases. Increase of concentration cause increase of the surfactant molecules in the surface of the aqueous phase which lead to decrease of surface tension between immiscible phases. Above CMC addition of surfactant molecules lead to formation of micelles in the bulk. Concentration of surfactant molecules on the surface does not change dramatically and may be treat as constant. This results in small changes in the surface tension of the surfactant solution.

---

micelles reorganize into ordered structures. Those structures create autonomous phases (mesophases) with long range order. In these phases there is no ordering in the close neighborhood of molecules, but structures created by those molecules exhibit ordering.

Typical mesophases in surfactant systems are:

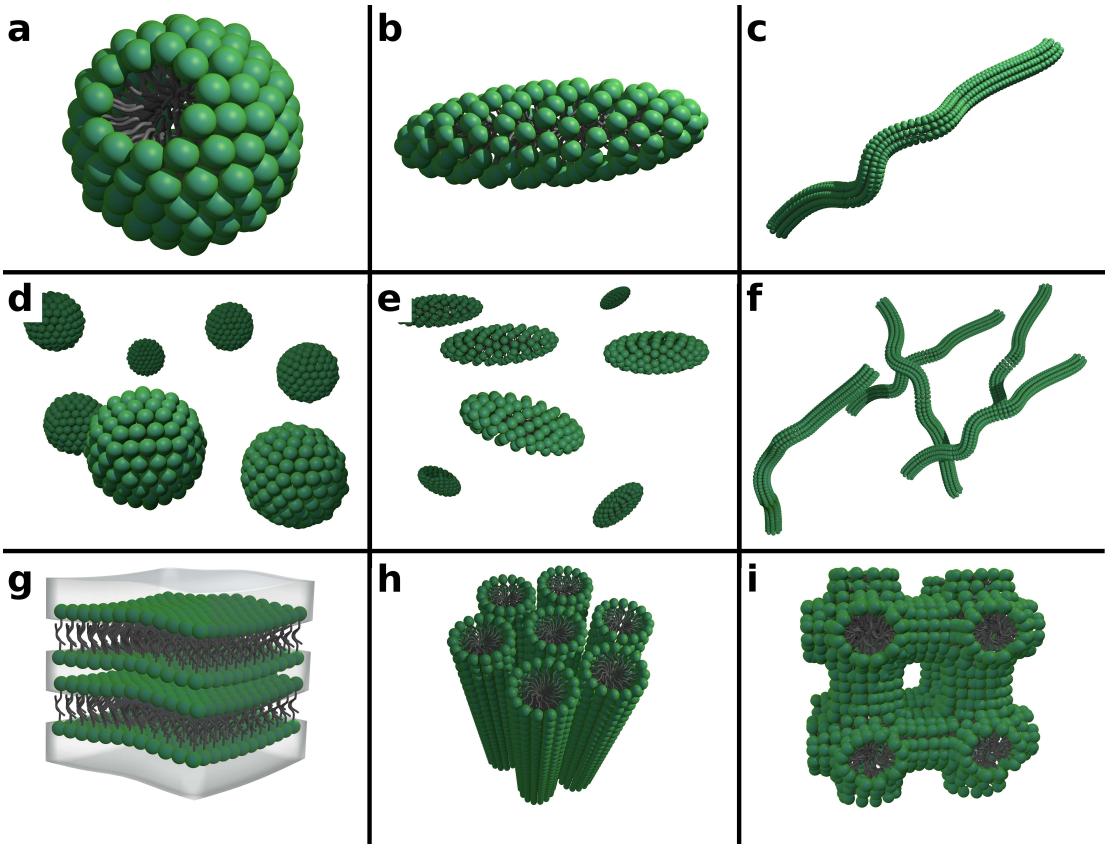

Figure 13: Various types of micelles **a** – spherical, **b** – elongated rigid micelles, **c** long and flexible aggregates. For each micelle type, properties of their concentrated solutions will be different. For example solutions of spherical micelles can be treated as the solution of hard spheres (**d**). Elongated rigid micelles will form network which can be described as a network of Pick-up sticks (**e**). Finally solution of long and flexible micelles can be described as polymer network – **f**. For higher concentrations of surfactant molecules ordered phases occurs: i.e. lamellar phase (**g**), hexagonal phase (**h**) and cubic – bicontinuous phase (**i**) or even more complex structures as it was described by Garstecki et al. [33].

- lamellar – in which ordered layers are created by molecules arranged perpendicularly to those layers,
- hexagonal – where surfactant molecules create columns
- cubic – where bicontinuous structure is crated

In this work only micellar solutions are discussed, properties of surfactant mesophases will be further omitted.

1.4.3 Introduction to viscosity of complex liquids

Viscosity of dilute solutions

The following section will discuss the viscosity of complex liquids. Namely, I will discuss empirical laws, explaining the changes in the viscosity of complex liquids depending on the concentration of obstacles that form the complex liquid.

The simplest equation for viscosity of suspension of colloids at high dilution was proposed by Einstein at the beginning of the XX-th century [34, 35].

$$\frac{\eta}{\eta_0} = 1 + \frac{5}{2}\phi = 1 + \frac{5}{2} n_{\mathrm{v}} \frac{4}{3} \pi r_{\mathrm{p}}^3 \tag{1.4.6}$$

Eq.(1.4.6) describes relative viscosity of the solution of non interacting spheres in the solution. η and η_0 denote viscosity of the solution and of the solvent respectively. ϕ is the volume fraction of the hard spheres, n_{v} is a number of spheres per unit volume and r_{p} is a hydrodynamic radius of the spheres. Eq.(1.4.6) shows how much the viscosity of the solvent increases after addition of a given volume fraction of spherical particles. Factor $5/2$ is so-called the intrinsic viscosity $[\eta]$ which in general is defined by Eq.(1.4.7)

$$[\eta] = \lim_{\phi \to 0} \frac{\eta - \eta_0}{\eta_0 \phi} \tag{1.4.7}$$

In practice this value for hard spheres and for other particles may different dramatically (from 2.14 to 4.7) as was shown by Arrhenius [36].

Equation which describes viscosity of polymer solutions, was developed by Hug-

gins [37]. It represents relative viscosity dependence on the concentration of polymer – C.

$$\frac{\eta}{\eta_0} = 1 + [\eta]\, C + k\, [\eta]^2\, C^2 + \cdots \tag{1.4.8}$$

where k is a constant characteristic for a given solute/solvent system. Additionally k is the same for solutions of different polymer homologous series in a given solvent [37].

Nano and macroscopic viscosity of concentrated solutions

Research carried out on concentrated solutions of polymers showed that the viscosity experienced by small probes can not be described by laws, proposed for dilute solutions. For example Schachman et al.[38] showed that small and large solutes sedimenting in a solution of DNA differ dramatically in sedimentation coefficients. Those and similar investigations on diffusion in polymer matrices and their viscosity [38–52], led to the empirical equation describing relation between the viscosity experienced by the nanoscopic probes and their radius r_{p},

$$\eta = \eta_0 exp\left(K r_{\mathrm{p}}^{\mu} c^{v}\right) \tag{1.4.9}$$

here η_0 is the viscosity of the solvent (i.e. water). K is a constant, c denotes the concentration of the polymer.

Recent investigations on polymer solutions [23] have introduced a concept of nanoviscosity. The nanoviscosity is the viscosity experienced by the nanoscopic probe during

its movement through the polymer matrix. Eq.(1.4.9) was replaced by more general scaling form of viscosity (Eqs.(1.4.10) and (1.4.11)) [23].

$$\frac{\eta}{\eta_0} = exp\left(\left(\frac{d_\mathrm{p}}{b\xi}\right)^a\right) \qquad \text{for } d_\mathrm{p} \ll R_\mathrm{g} \tag{1.4.10}$$

$$\frac{\eta}{\eta_0} = exp\left(\left(\frac{R_\mathrm{g}}{b\xi}\right)^a\right) \qquad \text{for } R \gg R_\mathrm{g} \tag{1.4.11}$$

Here ξ is the correlation length interpreted as the average distance between entanglement points in polymer network (Eq.(1.4.5) – Section 1.4.1), R_g is the radius of gyration of polymer coil, and d_p is a diameter of the probe. a is an exponent of the order of 1. The physical meaning of the exponent a (a constant of order 1) is still under discussion and as was shown by Odijk [51] it may vary from system to system. Eqs.(1.4.10) and (1.4.11) are valid only in extreme cases for: $d_\mathrm{p} \ll R_\mathrm{g}$ and for $d_\mathrm{p} \gg R_\mathrm{g}$. Eqs.(1.4.10) and (1.4.11) provide a uniform description of viscosity experienced by nano probes (Eq.(1.4.10)) and macroscopic viscosity experienced by macroscopic probe – Eq.(1.4.11) These equations connect the nanoviscosity experienced by the small probes (Eq.(1.4.10)) with the macroscopic viscosity of the polymer solutions – Eq.(1.4.11). Additionally Eqs.(1.4.10) and (1.4.11) show that one can expect a crossover length scale above which the probe experiences the macroscopic viscosity of the solution. Eq.(1.4.9) transform into the form of Eq.(1.4.10) with constants K, μ, and v given by following equations:

$$K = (2bR_\mathrm{g}c^*)^{-a} \tag{1.4.12}$$

$$\mu = a \tag{1.4.13}$$

$$v = \beta a \tag{1.4.14}$$

Since Eqs.(1.4.10) and (1.4.11) are valid in extreme cases only, one can treat them as limiting cases. However, both equations exhibit physical inconsistency. Namely, according to Eqs.(1.4.10) and (1.4.11) when size of the probe approach to infinity, the viscosity scales with R_{g}/ξ. On the contrary when size of the probe goes to zero, the viscosity scales with the diameter of the probe divided by ξ. One can ask a question: *Why for nanoscopic probes, the experienced viscosity is dependent on the* ***diameter*** *of the probe while for macroscopic ones on the* ***radius of gyration*** *of the polymer? Why the viscosity is not dependent only on the diameter, or only on the radius of gyration, no matter in what length scale is measured? What if the probe have the same size as the polymer, constituting the solution?* Eqs.(1.4.10) and (1.4.11) do not give answers to these questions. Therefore I propose new scaling form of the viscosity which unite **all length scales**.

To solve the problem of inconsistency of boundaries (Eqs.(1.4.10) and (1.4.11)), let us replace the radius of gyration of the polymer and the diameter of the probe, by the effective hydrodynamic radius R_{eff}, defined as follows:

$$\frac{1}{R_{\mathrm{eff}}^2} = \frac{1}{R_{\mathrm{h}}^2} + \frac{1}{r_{\mathrm{p}}^2} \tag{1.4.15}$$

Where R_{h} is the hydrodynamic radius of the polymer and r_{p} is the hydrodynamic radius of the probe. I propose the following scaling equation, have the following form:

$$\eta_{\mathrm{eff}} = \eta_0 \, exp\left[\left(\frac{R_{\mathrm{eff}}}{b\xi}\right)^a\right] \tag{1.4.16}$$

Here η_{eff} is the effective viscosity experienced by the probe of hydrodynamic radius r_{p}. One can find that in the limit of $r_{\mathrm{p}} \gg R_{\mathrm{h}}$ Eq.(1.4.16) becomes Eq.(1.4.11) with R_{g} replaced by R_{h}. In the opposite limit ($r_{\mathrm{p}} \ll R_{\mathrm{h}}$) Eq.(1.4.16) becomes Eq.(1.4.10) with d_{p} replaced by r_{p}. The novelty of Eq.(1.4.16) is in the combination of hydrodynamic properties of the probe (r_{p}) and co-solute (R_{h}) with the structural property of the network (ξ). Eqs.(1.4.10) and (1.4.11) reflect only structural properties of the matrix liquid (gyration radius R_{g} and ξ). Validity of Eq.(1.4.16) was examined for various physically different systems, described in following sections of this dissertation.

2 Experimental section

2.1 Materials

Diffusion of different probes in aqueous solutions of polymer was studied and further analysis of viscosity of those solutions was performed. For preparation of investigated solutions, linear and flexible polymer poly(ethylene glycol) (PEG) (cf. Figure 14**a**) was used. Solutions were prepared using phosphate buffer of pH 7 prepared ac-

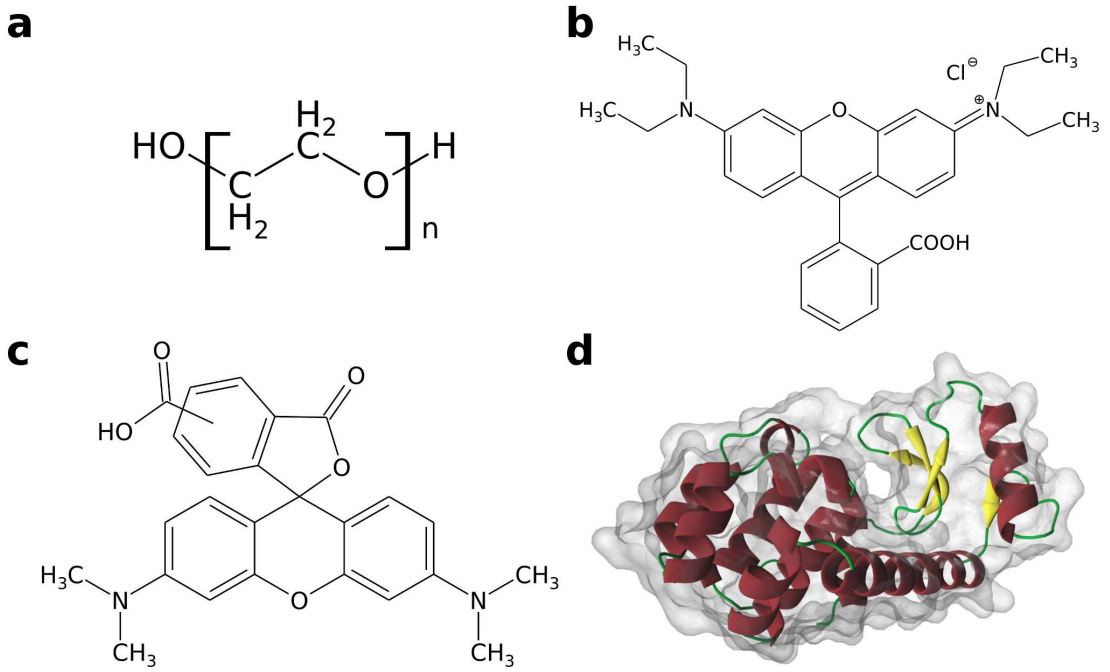

Figure 14: Materials used in experiments. Figure **a** illustrate structure of the polymer (poly(ethylene glycol). **b** – chemical structure of the rhodamine B used as a free dye. **c** – fluorescent dye – TAMRA (5(6)-Carboxytetramethylrhodamine) – used for labeling of proteins. Cartoon of the protein – lysozyme (**d**) used in the experiments. Lysozyme cartoon was created with the use of PyMOL software [53] using the crystalographic structure "4LZM" [54].

cording to recipe described elsewhere [55, page 113]. For buffer preparation deionized water (15 MΩ) was used. Viscosity of the buffer (η_0) at 25°C was equal to 1.08±0.04

mPa·s. Apart of PEG solutions, data for another systems were also analyzed. Dr Kaloian Koynov and dr Jędrzej Szymański kindly provided their experimental data of diffusion in polystyrene/acetophenone and aqueous, micellar solutions of the surfactant hexaethylene glycol monododecyl ether ($C_{12}E_6$). Provided data were analyzed in the same manner as experimental data for PEG solutions.

As it was discussed in the section 1.4.1, gyration (R_{g}) and hydrodynamic (R_{h}) radii of the polymer can be expressed as a function of the molecular weight. For PEG R_{g} and R_{h} are given by following formulae [56]:

$$R_{\mathrm{g}} = 0.0215\ M_{\mathrm{n}}^{0.58} \tag{2.1.1}$$

$$R_{\mathrm{h}} = 0.0145\ M_{\mathrm{n}}^{0.57} \tag{2.1.2}$$

Here M_{n} is a number averaged molecular weight of the polymer. Characteristics of the polymers used in discussed experiments are given in Table 1. As probes in FCS measurement Rhodamine B (RhB, cf. Figure 14**b**) with hydrodynamic radius $r_{\mathrm{p}} = 0.58$ nm and fluorescently labeled protein were used. Protein – lysozyme was labeled with (5-(and-6)-carboxytetramethylrhodamine) (TAMRA, cf. Figure 14**c**). Lysozyme (Figure 14**d**) is a small protein of molecular weight of 14 600 g/mol. Hydrodynamic radius of the lysozyme (r_{p}) is equal to 1.9 nm [57].

In the solutions of PS in the acetophenone dr Kaloian Koynov studied diffusion of following probes: N-(2,6-diisopropylphenyl)-9-(p-styryl)perylene-3,4-dicarboximide (PMI) with $r_{\mathrm{p}} = 0.53$ nm, PMI labelled polystyrene (PMI-PS 34 000 and PMI-PS

Table 1: Characteristics of poly(ethylene glycol) used in studied solutions

Symbol	M_n or M_w (g/mol)	R_g (nm)	R_h (nm)
PEG 400	325[a]	0.6[b]	0.4[c]
PEG 6 000	3 461[a]	2.4[b]	1.5[c]
PEG 20 000	10 944[a]	4.7[b]	2.9[c]
PEG 35 000	15 040[a]	5.7[b]	3.5[c]
PEG 600 000	276 862[a]	30.8[b]	18.3[c]
PEG 8 000 000[d]	7 019 190[a]	115.8[b]	201[c]
PS 34 000	34 000[e]	5.8[f]	4.4[f]
PS 220 000	220 000[e]	14.9[f]	11.5[f]
PS 255 000	255 000[e]	16.3[f]	12.5[f]

[a] Number averaged molecular weight M_n
[b] Calculated according to Eq.(2.1.1)
[c] Calculated according to Eq.(2.1.2)
[d] Data obtained form reference 23
[e] Weight averaged molecular weight M_w
[f] Hydrodynamic and gyration radii were determined according to the procedure described elsewhere [22]

255 000 – cf. Table 1).

Apart of the polymer solutions experimental data kindly provided by dr Jędrzej Szymański was analyzed. Dr Szymański studied the viscosity of surfactant solutions ($C_{12}E_6$) using probes listed in Table 2.

Table 2: Characteristics of probes used by dr Szymański in $C_{12}E_6$ solutions

Probe	r_p (nm)	Probe	r_p (nm)
Water	0.14	Apoferitin	6.9
TAMRA	0.85	QD[a]	12.5
Lysozyme	1.9	FSS[b]	35
Chymotrypsinogen	2.6	FSS[b]	57
Ovalbumin	3.4	FSS[b]	95
Bovine serum albumin	4.2		

[a] QD – Quantum dots
[b] FFS – Fluorescent silica spheres

Labeling of the lysozyme

Proteins were labeled with fluorescent dye – TAMRA[†] – according to the procedure

[†] 5-(and-6)-carboxytetramethylrhodamine

described by Dr. Szymański [55, page 39]. In order to remove unbound dye molecules, filtration of the protein solution with the 20 mM phosphate buffer (pH 7, 0.154 M NaCl) was performed. For the filtration the Millipore Amicon Ultra, centrifugal filter devices with the molecular weight cut-off 3kD were used. The filtration was necessary because the fluorescence signal originating from a free dye, could seriously diminish the signal from the dye bound to the protein. The filtration procedure was repeated about 50 times. Solution of lysozyme was then divided onto small portions (each equal 500 μL) and kept at -20°C. Before measurements sample of the protein solution was kept at room temperature in order to melt the solution.

2.2 Methods

Sample preparation

Small amount of investigated solution containing no fluorescent dye was placed into the eppendorf vial. Concentrated solution of fluorescent probes ($\sim 10^{-7}$ M) was added to the investigated solution in such volume which allow to obtain 100 fold dilution of fluorescent probes. Solutions of viscosity comparable to the viscosity of buffer ($\eta \approx \eta_0$) were blended by slowly pipetting the solution up and down. Solutions with viscosity $\eta \gg \eta_0$ were mixed by the end of the pipette an leave to equilibrate for around an hour. After mixing, 200 μL of the solution was transported into the sample container (8 Chambered Coverglass – Lab-Tek®) and analyzed.

FCS experimental setup

Fluorescence correlation spectroscopy experiments discussed in this work were performed using commercially available inverted NIKON EZ-C1 confocal microscope. Confocal setup was additionally equipped with PicoHarp 800 FCS setup made by PicoQuant. Water immersion objective with numerical aperture equal 1.2 and magnification $60\times$ was used in fluorescence correlation spectroscopy measurements. During measurements the power of the laser was set at constant level.The point of measurement of the power of the laser beam was situated just before the objective. For laser power measurements, an external power meter (PM100 made by THORLABS) was used. As the source of collimated light, HeNe laser of wavelength 543 nm was used. Before each measurement a drop of filtered, deionized water was used as the immersion medium between sample coverglass and the objective. During measurements focal volume was at constant distance ($h = 10$ μm) from the edge of the coverglass (see Figure 15).

Falling ball viscometry

In order to determine the macroscopic viscosity of PEG 400*, falling ball viscometer KF10 from RheoTec (Germany) was used. Tube of the viscometer was filled with investigated solution and a ball was put into the tube. During measurement, ball's falling time was measured. For each investigated solution, 10 to 15 measurements

*Macroscopic viscosity of PEG 6 000, 20 000, and 35 000, was measured by M.Sc. Urszula Rak, who kindly provided the data.

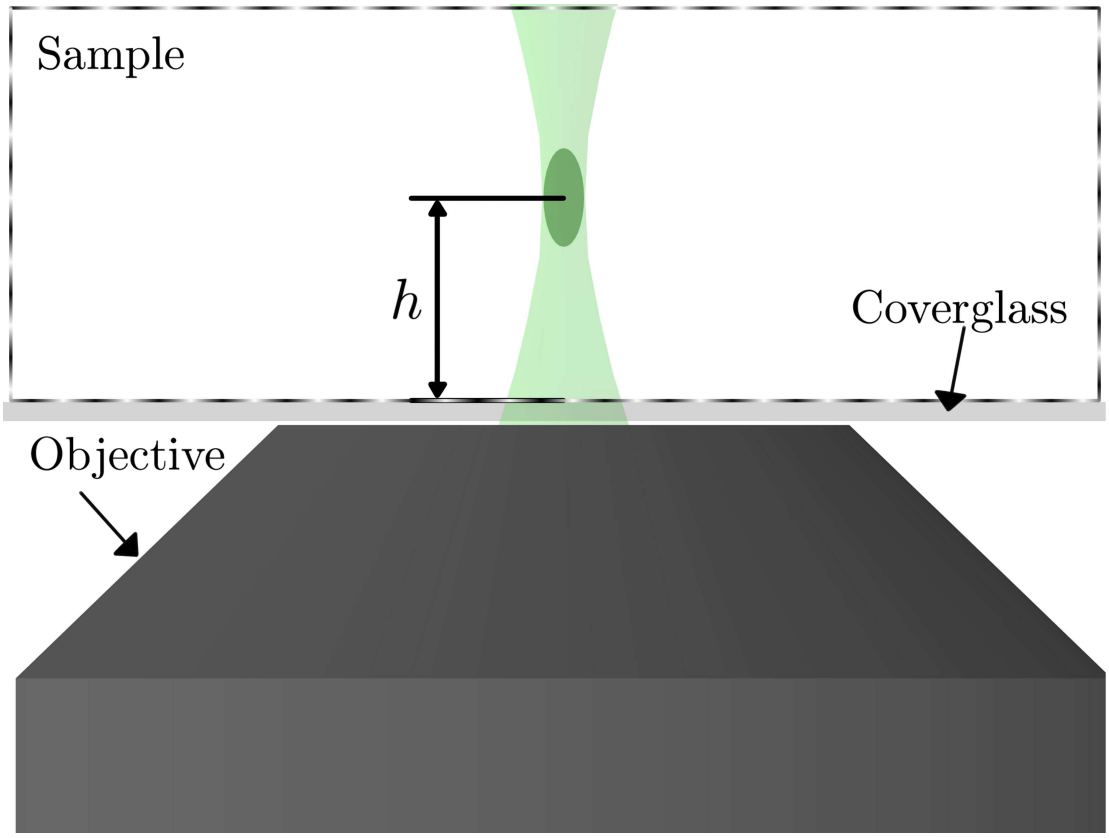

Figure 15: Laser beam is focused in a sample at a distance $h = 10$ μm from the edge of the coverglass.

were performed. Viscosity was calculated according to the following equation.

$$\eta = t\,(\rho_1 - \rho_2)\,K \tag{2.2.1}$$

Here η is a dynamic viscosity of the investigated solution in mPa·s, t is ball's falling time in seconds, ρ_1 is a density of the ball in g/cm^3, obtained from the test certificate provided by the manufacturer . ρ_2 denotes the density of the investigated solution (g/cm^3). K (mPa·cm^3/g) is the ball constant obtained from the test certificate provided by the manufacturer. Obtained viscosities of investigated solution were averaged.

Density of investigated solution (ρ_2) was determined as follows. Solution was equi-

librated in water bath in order to obtain temperature equal to temperature of viscosity measurement (25°C). Next the polymer solution was transferred into the volumetric flask and weighted with the analytic balance. From the difference between the weight of the empty and the filed flask, the weight of the fluid and the density was calculated.

FCS calibration and experimental procedure

Most of modern microscope objectives are strongly dedicated to one specific experimental medium i.e. water. For biological or biochemical measurements which are performed in water or in a buffer solution, influence of changes in the refractive index of a system is negligible. In polymer systems, however, changes the refractive index of solutions with increasing polymer concentration are significant and must be considered.

Each FCS experiment performed in the buffer solution was preceded by calibration based on diffusion of the RhB in water. Diffusion coefficient of the RhB in water at 25°C is equal D_0' = 420 μm^2/s [21]. For each measurement from 10 to 20 autocorrelation curves were acquired and averaged. An average autocorrelation curve was then analyzed. From fitting of Eq.(1.3.25), diffusion time τ_{D} of the RhB as well as the structure parameter – κ – was obtained. From τ_{D} and D_0' radius of the focal volume ω was determined according to Eq.(1.3.24). Parameters ω and κ were used in further analysis in order to determine the diffusion coefficient of probes in the investigated solutions.

FCS measurements in polymer solutions however, required more sophisticated method of the calibration. In case of polymer solutions, their refractive index exceeds the re-

fractive index of water. In addition, it increases with concentration of polymer (Figure 16). Shape of the focal volume strongly depends on the refractive index of the investigated solution [58]. The procedure of calibration in polymer solutions is given below.

Number of molecules is proportional to the volume $N = CN_AV$. Here C is a

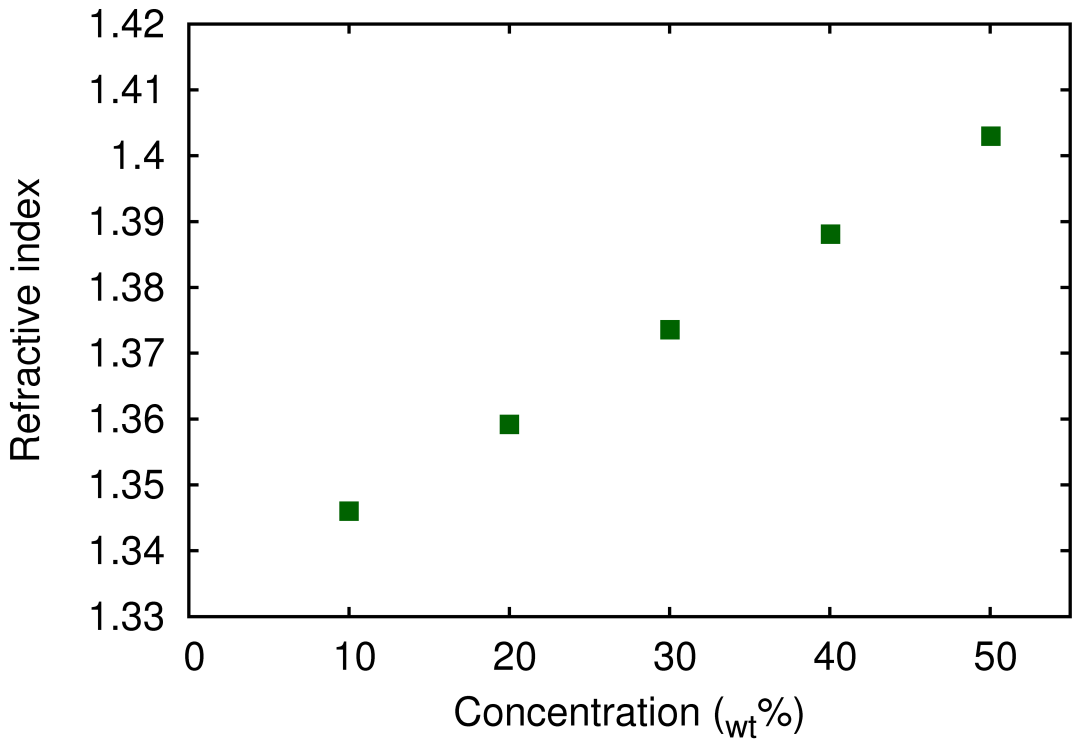

Figure 16: Changes of the refractive index of PEG 400 with concentration the polymer. Measurements were performed with standard Abbe refractometer (manufactured by Carl-Zeiss, Germany). Errors were smaller than symbols used in the plot

concentration of fluorescent molecules in mols per liter. Under assumption of Gaussian shape of the detection volume, one can find that it is possible to determine the effective volume by preparing a series of different concentration of the fluorophore. In discussed experiments an effective volume (V_{eff} – Eq.(1.3.20)) was determined from a slope of the plot of N against C ($N\,(C)$). For each investigated polymer solution, series of fluorophore concentration was investigated and the effective volume was calculated. Such

calibration method allow to avoid an error caused by changes of the effective volume due to changes of the refractive index of solution.

Measurements with lysozyme were carried out in the same polymer concentration as for calibration measurements. Therefore, from the effective volume (V_{eff}) obtained in calibration measurements and from κ, and ω, the diffusion coefficient of the probe in the investigated solution was determined.

Fluctuation dissipation theorem

Viscosity experienced by the probe in given solution can be directly calculated from its relative diffusion coefficient. According to the Stokes-Sutherland-Einstein equation (Eq.(1.2.12)), one can find that:

$$\frac{\eta}{\eta_0} = \frac{D_0}{D} \tag{2.2.2}$$

Eq.(2.2.2) however, is valid only when the fluctuation-dissipation theorem (FDT) is valid [59]. In particular fluctuation-dissipation theorem implies that when the system is in thermal equilibrium, the system response to external disturbance, is the same as on the spontaneous fluctuations. More generally, citing the words of Kubo [59], FDT can be expressed as follows:

> "*The friction, or more generally the resistance of a given system, represents the method by which the external work is dissipated into microscopic thermal energy. The reverse process is the generation of random force as the result of thermal fluctuation.*"

The later can be expressed as the relation between electrophoretical mobility μ of the probe (dragged in the external electric field) and the diffusion coefficient of the same probe.

$$\mu = \frac{D}{kT} \tag{2.2.3}$$

Experimentally, in order to test validity of the FDT in the investigated solution, following relation should be examined.

$$\frac{\mu_0}{\mu} = \frac{\eta}{\eta_0} = \frac{D_0}{D} \tag{2.2.4}$$

Here μ is a mobility of the probe in the investigated solution, μ_0 is the mobility of same probe in a pure solvent, η is the viscosity of the examined solution and η_0 is the viscosity of pure solvent. By the analogy, D is the diffusion coefficient of the probe in the investigated solution and D_0 is a diffusion coefficient of the same probe in the pure solvent. In practice FDT can be examined via comparative analysis of relative electrophoretical mobility and DCR. For PEG system, such studies were done [23] and validity of the FTD was confirmed. Therefore Eq.(2.2.2) can be used directly for determination of the viscosity experienced by the investigated probes in the PEG solutions.

3 Results, data analysis, and discussion

3.1 Viscosity of complex liquids

Measurements of diffusion in poly(ethylene glycol) solutions

In order to determine viscosity of polymer solution at the nanoscale, FCS measurements of diffusion of RhB and lysozyme in the concentrated polymer solutions were performed. For each concentration 10-20 autocorrelation curves were acquired and further averaged. From the average autocorrelation function (Figure 17), diffusion time τ_D was determined for each polymer concentration. Next using variables obtained from calibration measurements (ω, κ), the diffusion coefficient D was determined. Apart from RhB and lysozyme, latex, fluorescent nanoparticles (25 nm in diameter) were

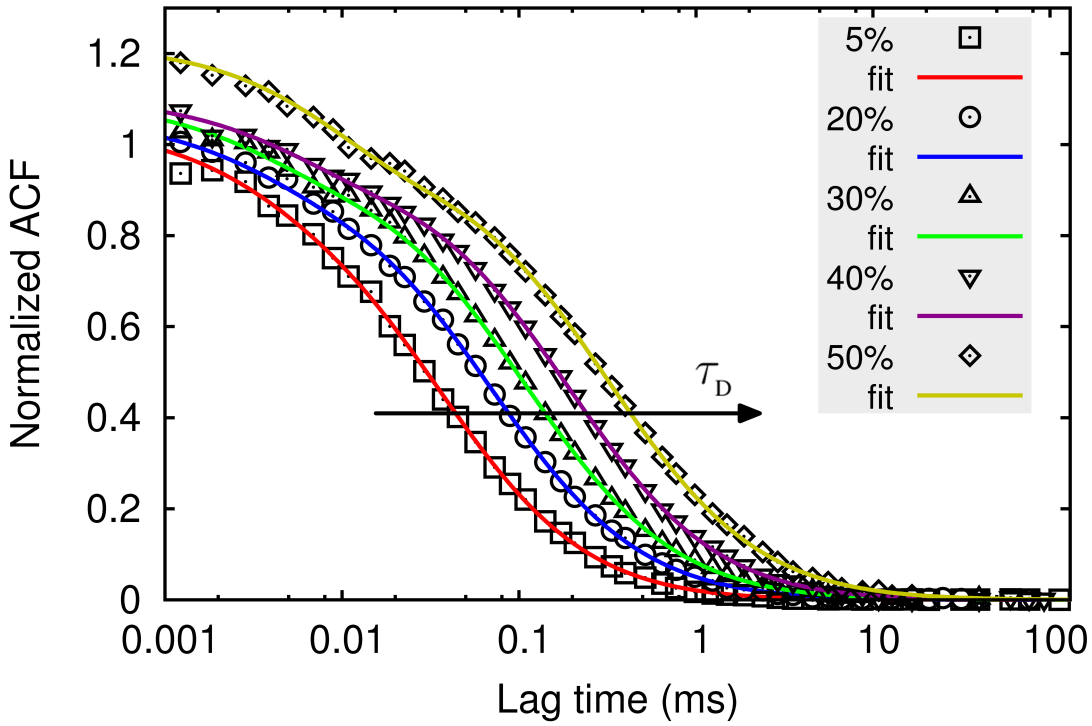

Figure 17: Normalized ACF ($G(\tau)/G(0)$) for five different concentartions of PEG 400. Diffusion time (decay time) increase with the concentration of the polymer.

used for diffusion measurements in PEG 600 000. Diffusion coefficients of probes were further related to the diffusion coefficient of given probe in a pure solvent. The diffusion coefficient ratio (DCR – D/D_0) for polymer solutions composed of polymers with different molecular weights, and for various probes are presented on Figure 18.

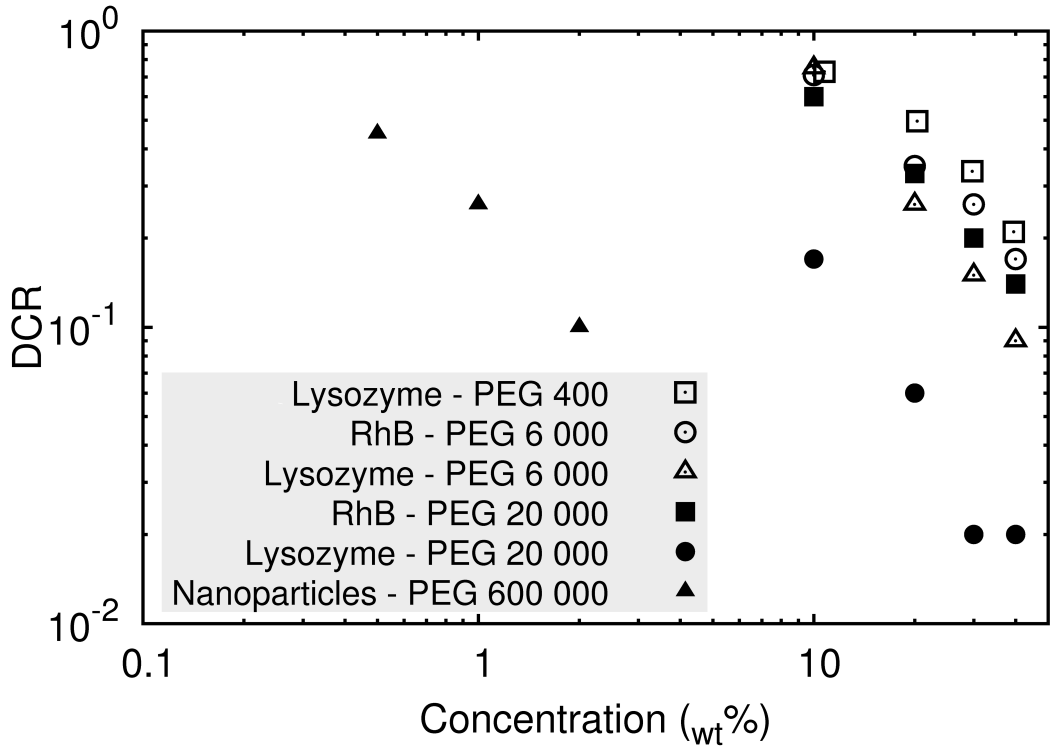

Figure 18: Diffusion coefficient ratio (DCR = D/D_0, D_0 – diffusion coefficient in water) obtained for different probes diffusing in various polymer systems.

3.1.1 Scaling form of the viscosity of complex liquids

In order to check validity of Eq.(1.4.16) proposed in section 1.4.3, viscosity of the following complex liquids was analyzed:

1. Aqueous solutions Poly(ethylene glycol).

2. Solutions of Polystyrene in acetophenone (Data of diffusion obtained from Dr Kaloyan Koynov).

3. Aqueous solutions of the surfactant $C_{12}E_6$ (Data obtained from Dr Jędrzej Szymański).

Results, and data analysis are given below.

Viscosity of poly(ethylene glycol) solutions

Measurements of the diffusion of RhB and of lysozyme performed in PEG solutions, as well as validity of the FDT discussed in section 2.2, allow to determine the viscosity experienced by the investigated probe in the examined solution. Viscosity experienced by the nanoscopic probe was further compared with macrosopic viscosity of given PEG solution. Figure 19 shows relative viscosity as a function of concentration of the polymer measured at different length scales. For PEG 400 viscosity measured by nanoscopic probe, is comparable with viscosity measured at the macroscale. On the other hand for longer polymers (higher molecular weight), viscosities measured with nanoscopic probes, exhibit much lower values in comparison to macroscopic viscosities. Furthermore for viscosities of both large polymers – PEG 6 000 and 20 000 –

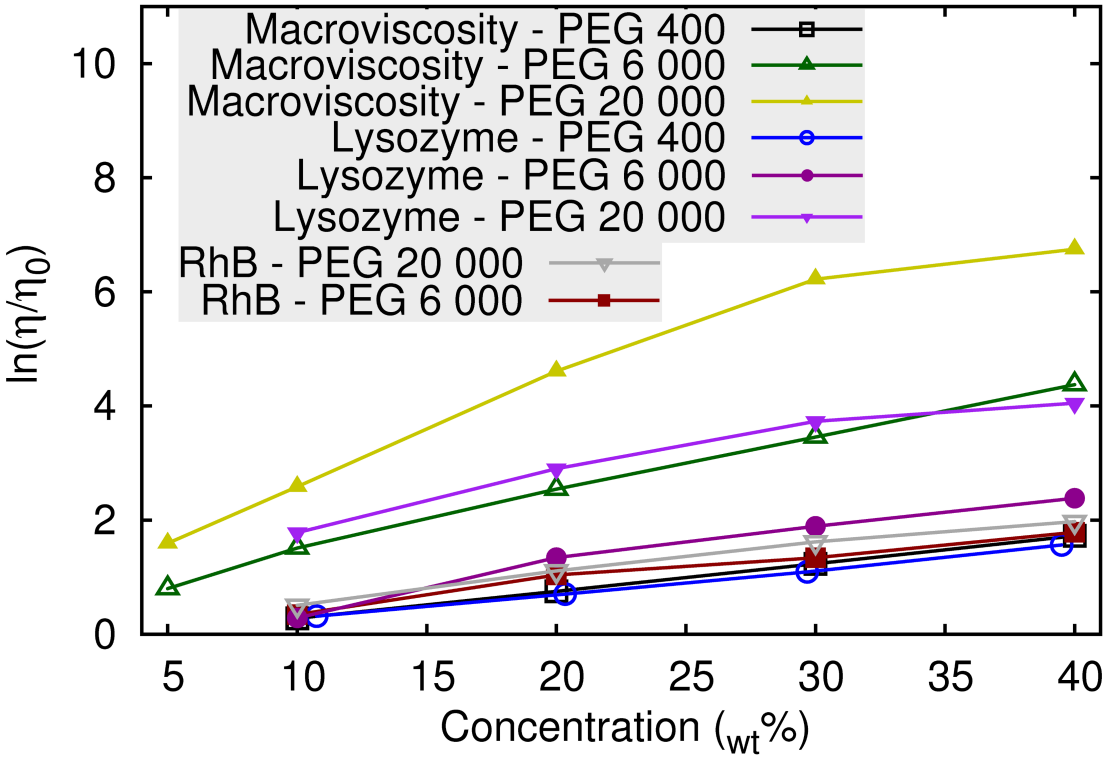

Figure 19: The logarithm of the viscosities of PEG solutions measured with different probes. For small polymer (PEG 400) macroscopic viscosity values cover with values measured with nanoscopic probe – lysozyme. On the contrary for longer polymers, PEG 6 000 or 20 000, the relative viscosity values are greatly below the macroscopic viscosity values. For all point errors were obtained at the level of 3-7% and were smaller than plotted symbols.

exhibit strong dependence on size of the probe. For example viscosity values measured with lysozyme are higher than those measured with rhodamine B and lower than macroscopic ones.

The viscosity of the complex liquid depends on the concentration of objects which create the fluid (polymer coils or micelles) and the size of the diffusant itself. Figures 20 to 22 visualize differences in the viscosities experienced by different probes. Viscosities as a function of the polymer or of the surfactant concentration for different ratios of hydrodynamic radii $r_{\mathrm{p}}/R_{\mathrm{h}}$ were plotted. Measurements of the viscosity in two solutions for different ratios of $r_{\mathrm{p}}/R_{\mathrm{h}}$ were carried out: one composed of PEG 400

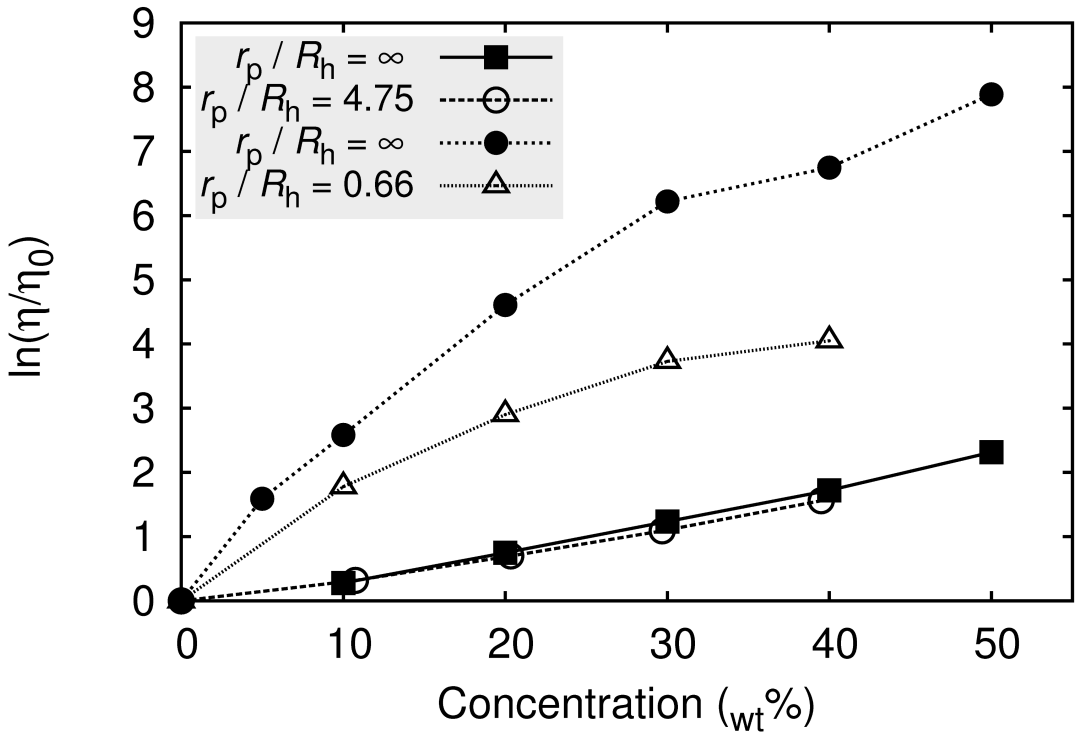

Figure 20: Viscosities of PEG solutions as a function of concentration measured with different nano probes. Figure shows macroscopic viscosity of low molecular weight oligomer PEG 400 (○, $r_\mathrm{p}/R_\mathrm{h}$ = ∞, $R_\mathrm{h} = 0.4$ nm), nanoscopic viscosity measured with a nano-probe (lysozyme) in the PEG 400 matrix (●, $r_\mathrm{p}/R_\mathrm{h}$ = 4.75, $r_\mathrm{p} = 1.9$ nm), macroscopic viscosity of PEG 20 000 (●, $r_\mathrm{p}/R_\mathrm{h}$ = ∞, $R_\mathrm{h} = 2.9$ nm) and one measured by diffusion of lysozyme in PEG 20 000 (△, $r_\mathrm{p}/R_\mathrm{h}$ = 0.66). For all point errors were obtained at the level of 3-7% and were smaller than plotted symbols.

($R_\mathrm{h} = 0.4$ nm) and of PEG 20 000 ($R_\mathrm{h} = 2.9$ nm) with lysozyme ($r_\mathrm{p} = 1.9$ nm) as the probe (Figure 20). When $r_\mathrm{p} < R_\mathrm{h}$ ($r_\mathrm{p}/R_\mathrm{h} < 1$) the probe diffused with nanoscopic viscosity lower than the macroscopic viscosity of the solution. The same probe in polymer solution composed of the smaller polymer coils (i.e. $r_\mathrm{p} > R_\mathrm{h}$; $r_\mathrm{p}/R_\mathrm{h} > 1$) experienced the macroscopic viscosity.

Viscosity of polystyrene solutions

In the PS 220 000 solutions ($R_\mathrm{h} = 11.5$ nm), probes such as PMI ($r_\mathrm{p} = 0.53$ nm) or fluorescently labeled polystyrene – PMI-PS 34 000 (with PMI as fluorophore) ex-

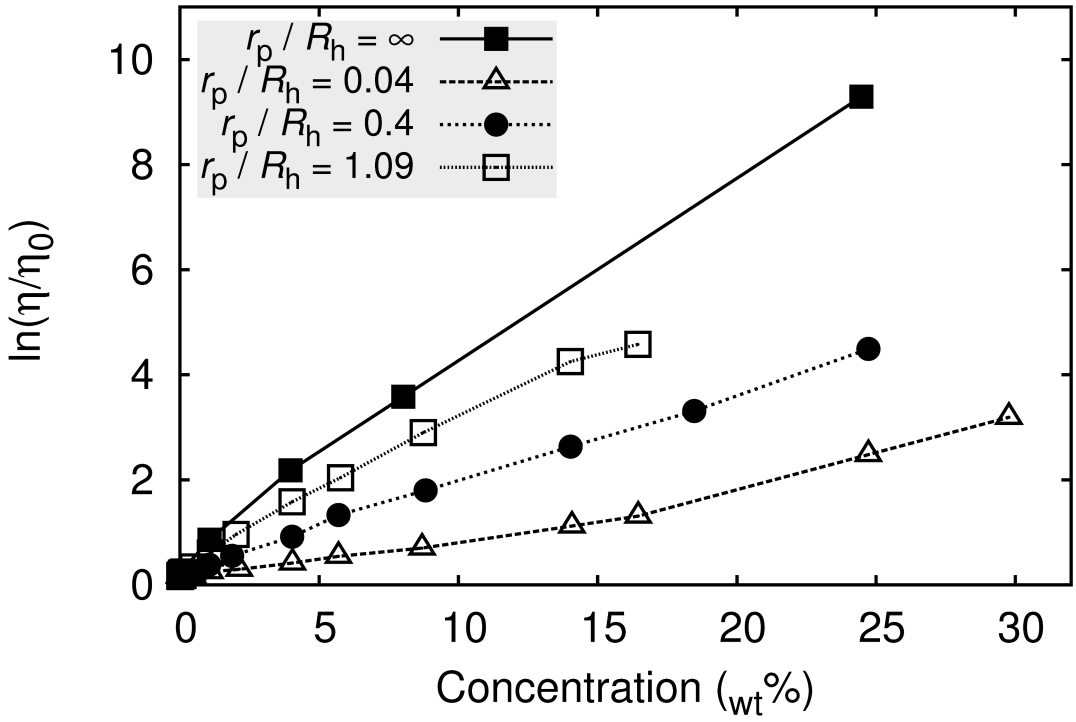

Figure 21: Viscosities of PS solutions as a function of concentration measured with different nano probes. Figure shows viscosity measured with different probes for solutions PS 220 000 in acetophenone. The following molecules were used as the probes: PMI (△, $r_\mathrm{p}/R_\mathrm{h}$ = 0.09, $r_\mathrm{p} = 0.53$ nm), PMI-PS 34 000 (●, $r_\mathrm{p}/R_\mathrm{h}$ = 0.4, $r_\mathrm{p} = 4.45$ nm) and PMI-PS 255 000 (□, $r_\mathrm{p}/R_\mathrm{h}$ = 1.09, $r_\mathrm{p} = 12.5$ nm). Macroscopic viscosity of PS 220 000 matrix is represented by ■ – ($r_\mathrm{p}/R_\mathrm{h} = \infty$, $R_\mathrm{h} = 11.5$ nm). For all point errors were smaller than plotted symbols.

perienced much lower viscosity than the macroscopic one (Figure 21). On the other hand r_p of the PMI-PS 255 000 was larger than the hydrodynamic radius R_h of the matrix obstacles. Surprisingly, PMI-PS 255 000 ($r_\mathrm{p} > R_\mathrm{h}$) experienced a viscosity lower than the macroscopic viscosity of the solution. *This result showed that* ***the crossover between the two regimes (nano- and macroscopic viscosity) could not be described with a sharp threshold determined by the radii of the probe and of the obstacles*** *(i.e. nanoscopic viscosity for $r_p/R_h < 1$ and macroscopic viscosity for $r_p/R_h > 1$.*

Viscosity of $C_{12}E_6$ solutions

Figure 22 shows the data obtained for $C_{12}E_6$ solutions [57] for three different probes (lysozyme $r_p = 1.9$ nm, apoferitin $r_p = 6.9$ nm, and nanoparticles $r_p = 57$ nm). The diffusion coefficient of the nanoparticles ($r_p \gg R_h$, $r_p/R_h = \infty$) was related to the macroscopic viscosity and all other probes to the nanoscopic one. When $r_p < R_h$ (lysozyme) or $r_p \geqslant R_h$, (apoferitin) the probe experienced nanoscopic viscosity – much lower than the macroscopic viscosity.

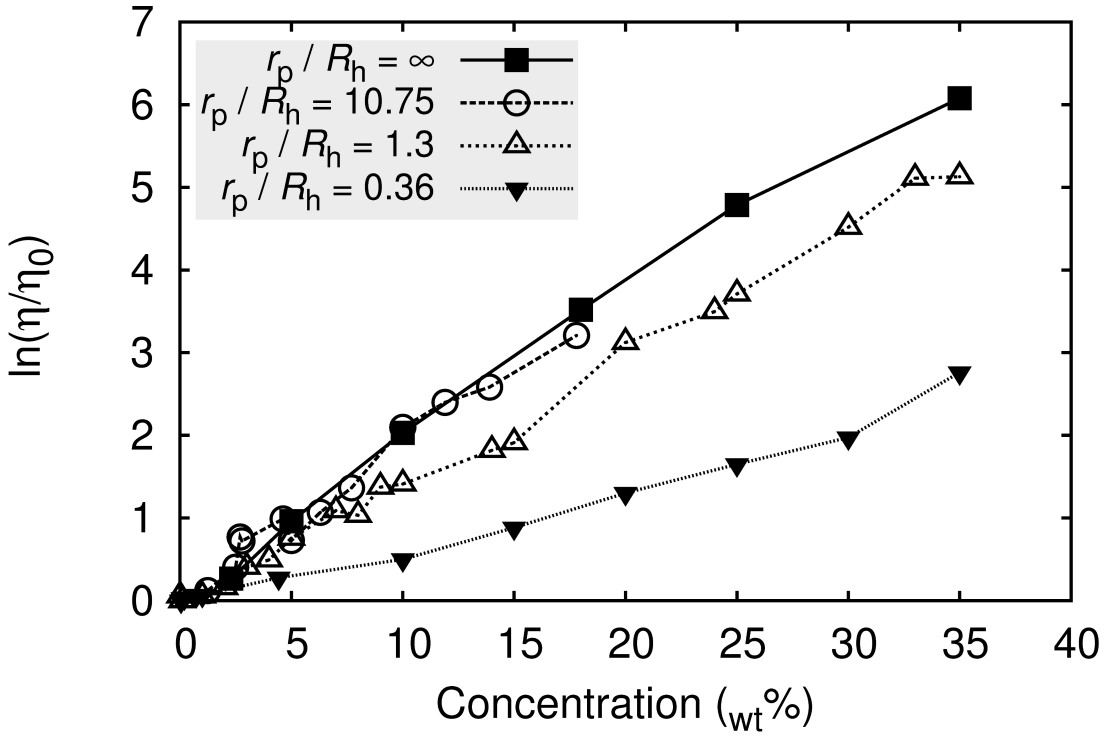

Figure 22: Viscosities of $C_{12}E_6$ solutions as a function of concentration measured with different nano probes. Figure shows viscosity of aqueous solutions of rigid micelles $C_{12}E_6$. Macroscopic viscosity (■,r_p/R_h = ∞, $R_h = 5.3$ nm) and viscosities measured with different probes: fluorescent particles (○, r_p/R_h = 10.75, $R_h = 57$ nm), apoferitin (△, r_p/R_h = 1.3, $r_p = 6.9$ nm) and lysozyme (▼, r_p/R_h = 0.36, $r_p = 1.9$ nm). For all point errors were smaller than plotted symbols.

3.1.2 Validation of the scaling formula

Table 3 presents effective hydrodynamic radii R_{eff} for different probes used in Figures 20 to 22. From the data included in Table 3 and from Eq.(1.4.15), the crossover

Table 3: Relation between hydrodynamic radii of the obstacles and the probes for different systems shown in Figures 20 to 22

Matrix/Probe	R_{h} (nm)	r_{p} (nm)	$r_{\text{p}}/R_{\text{h}}$	R_{eff} (nm)
PEG 20 000 – Macroscopic viscosity	2.9	∞	∞	2.9
PEG 20 000 / Lysozyme	2.9	1.9	0.66	1.6
PEG 400 – Macroscopic viscosity	0.4	∞	∞	0.4
PEG 400 / Lysozyme	0.4	1.9	4.75	0.4
PS 220 000 – Macroscopic viscosity	11.5	∞	∞	11.5
PS 220 000 / PMI	11.5	0.5	0.04	0.5
PS 220 000 / PMI-PS 34 000	11.5	4.5	0.4	4.2
PS 220 000 / PMI-PS 255 000	11.5	12.5	1.09	8.5
$C_{12}E_6$ – Macroscopic viscosity	5.3	∞	∞	5.3
$C_{12}E_6$ / Lysozyme	5.3	1.9	0.36	1.8
$C_{12}E_6$ / Apoferitin	5.3	6.9	1.3	4.2
$C_{12}E_6$ / Particles	5.3	57	10.75	5.3

criterion i.e. a criterion which states at what length scale the probes starts to experience the macroscopic viscosity can be formulated as follows.

Criterion 1. *The probe diffusing in the complex liquid experiences macroscopic viscosity of this liquid when R_{eff} defined by Eq.(1.4.15) is approximately equal to R_h. On the contrary when $R_{eff} \to r_p$, the probe experiences nanoscopic viscosity.*

For practical reasons when $r_{\text{p}} > 4R_{\text{h}}$ the viscosity experienced by the probe is very close (within 1-5%) to the macroscopic viscosity according to Eq.(1.4.15).

Figures 23 to 24 presents viscosity values scaled with the factor R_{eff}/ξ in PEG –

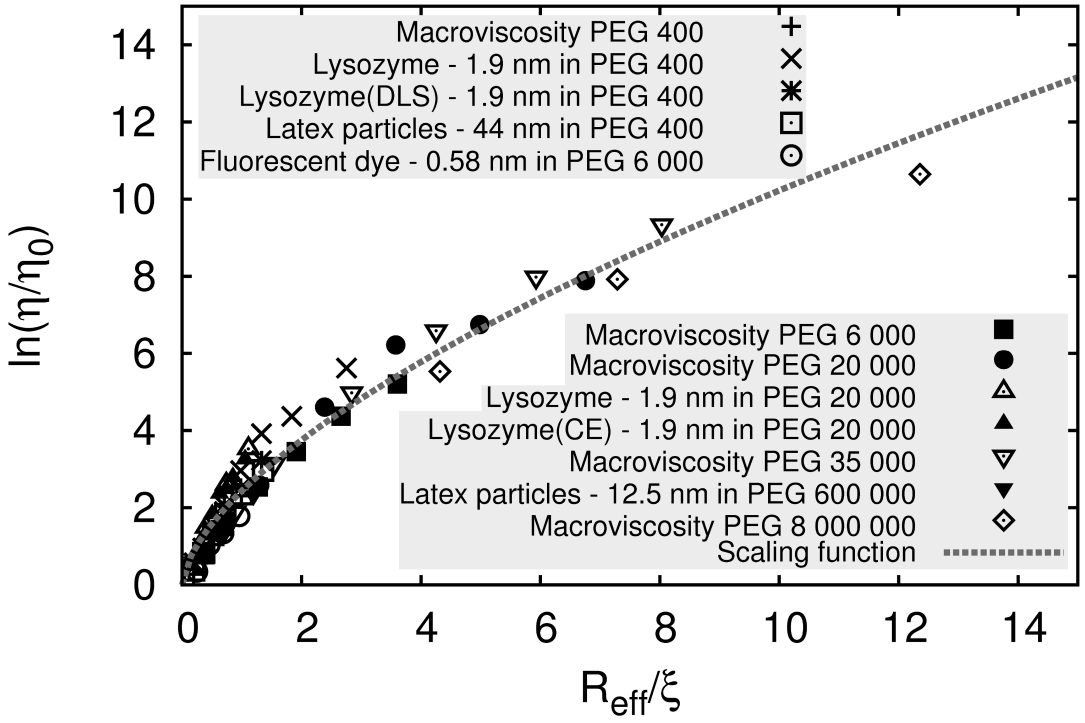

Figure 23: Scaled viscosity of PEG solutions divided by the viscosity of water at 25 °C (relative viscosity). Figure shows scaling plot for the logarithm of relative viscosity measured for different probes in aqueous solutions of PEG. All presented data follows the same curve given by equation (Eq.(1.4.16)) with parameters $a = 0.62 \pm 0.02$ and $b = 0.24 \pm 0.02$ (cf. Eq.(1.4.5)).

Figure 23, and in PS solutions – Figure 24. In all plots the data fall into the same master curve defined by Eq.(1.4.16), same for the macroscopic probes (falling ball viscometer) and for the nano probes (proteins or dyes). The scaling law describes the viscosity experienced by the proteins (compact structures similar to hard spheres – Figure 23) and labeled polymer coils (entangling with polymer coils crating a fluid – Figure 24).

The universality of the scaling law was tested by application to the solutions of elongated rigid micelles as shown in Figure 25. In studied system, above critical micelle concentration the surfactants aggregate forming elongated, ellipsoidal micelles of

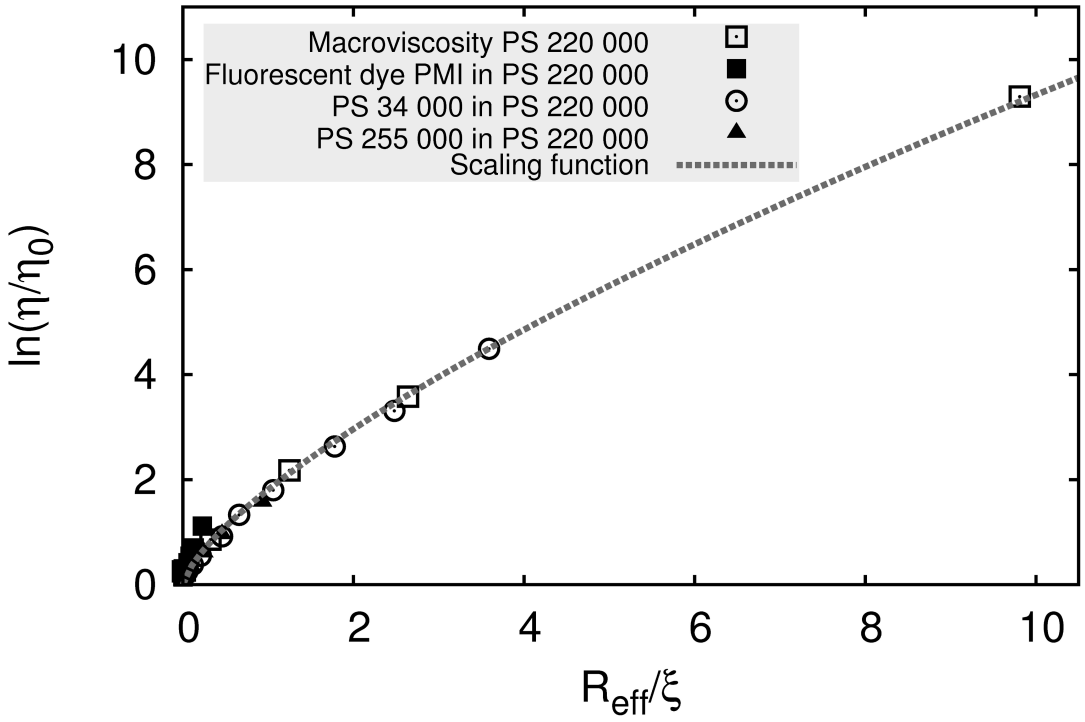

Figure 24: The logarithm of relative viscosity measured for different probes in PS solutions in acetophenone. The data follows the same curve given by equation (Eq.(1.4.16)) with parameters $a = 0.71 \pm 0.1$ and $b = 0.43 \pm 0.02$.

length L [24]. Further increase of concentration causes the micelles to overlap. In this system the correlation length ξ (Eq.(1.4.5)) is defined by the distance between two touching points of micelles. It is a similar definition to the one used in polymer solutions where ξ is defined as the distance between entanglement points of polymer coils. In micellar systems the correlation length should be defined by Eq.(1.4.5).

$$\xi = L\,(c/c^*)^{-\beta} \tag{3.1.1}$$

Here L is the length of the micelles. The overlap concentration in the solution of rigid micelles (with length much larger than their diameter) is given by $c^* = 3A_{\mathrm{n}}M_{\mathrm{w}}/\left(N_{\mathrm{A}}L^3\right)$,

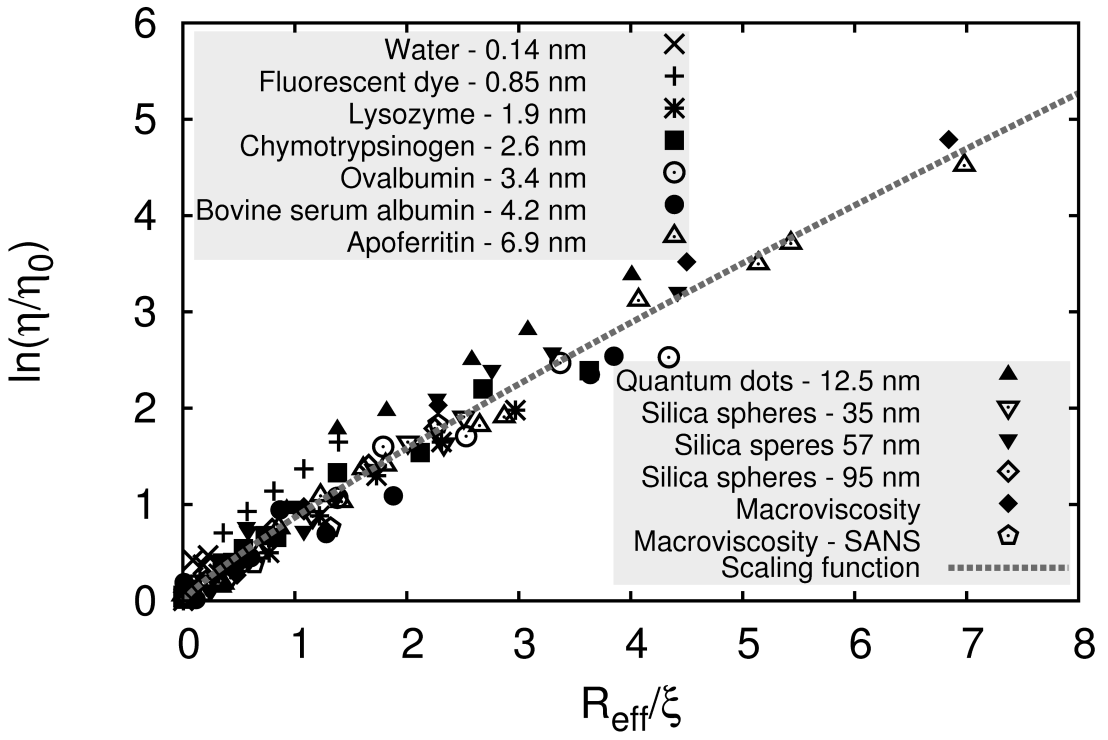

Figure 25: Scaled viscosity of $C_{12}E_6$ consisting of rigid micelles. All data follows the same curve given by equation (Eq.(1.4.16)) with parameters $a = 0.87 \pm 0.02$ and $b = 1.18 \pm 0.04$.

where A_{n} is an average number of surfactants in a micelle (aggregation number) and M_w is the molecular weight of the surfactant. In surfactant system β was found equal 1. The viscosity data scaled with R_{eff}/ξ for the micellar solution (Figure 25) follows the same curve given by Eq.(1.4.16) as in the case of the polymer solutions. Those results confirm validity of proposed scaling law (Eq.(1.4.16)) for complex liquids.

3.2 Viscosity of the cytoplasm of mammalian cells

The mobility of proteins and other solutes is one of the main regulating factors in processes taking place in living cells. However, the measurements of the self diffusion coefficients of proteins and small molecules in E.coli [60], HeLa [61, 62], and Swiss 3T3 [63] cells, could not be explained via the SSE equation and the macroscopic viscosity. Luby-Phelps et al. [63] performed fluorescence recovery after photobleaching (FRAP) measurements of fluorescently labeled dextrans in Swiss 3T3 muscle cells. They described the data via the diffusion coefficient ratio (DCR), calculated as the ratio of the coefficient of self diffusion of solutes in the cytoplasm to the self diffusion in water. They observed that DCR decreased with increasing size of the probes up to the size of 14 nm. For probes larger than 14 nm DCR had an approximately constant. FRAP measurements preformed on CHO[†] cells by Verkman group suggested that translational mobility of Green Fluorescence Protein (GFP) was determined mostly by the concentration of cellular obstacles [64]. Lukacs [62] studied the mobility of DNA fragments (from 21 up to 6000 bp) in the cytoplasm of HeLa cells. Fragments longer than 3000 bp presented unexpectedly low mobility. On the contrary in a nucleus, diffusion of all investigated DNA fragments was strongly hindered and did not change with size of diffusing entities. Dauty et al. [61] compared self diffusion coefficients (SDC) of fluorescently labeled DNA fragments diffusing in the solutions of polymerized actin with SDC obtained *in vivo* in HeLa cells. They postulated that it was the cytoskeletal network of actin filaments that hindered the diffusion of probes in the cytoplasm.

[†]Chinese hamster ovary

Studies on viscoelastic properties of polymerized actin solutions were reported in numerous works. Most of them, however, consider length scales of probes from 1 to 100 μm [65–69]. These studies showed that the viscoelastic properties of the actin network is determined by amount of bundles and cross-linkers connecting actin filaments [65, 66, 68]. Additionally, various theoretical models mimicking the cytoskeleton behavior [70] have been proposed. Also an opposite approach (bio materials which mimic polymers) has been established recently [71].

Each of the systems described in section 3.1 had only one type of crowding agent (objects which crowd the environment, micelles or polymers) that formed the complex liquid. Viscosity in these systems depended on two length scales: correlation length ξ and an effective hydrodynamic radius R_{eff}. In cells apart from the cytoskeleton and actin filaments one – can find lots of cytoplasmic proteins and other macromolecules and organelles which crowd the environment [72]. Comparison of *in vitro* measurement, performed in the solutions of polymerized actin, with *in vivo* measurements in cells, show that the self diffusion of small (few to tens of nanometers) probes in cells is hindered by the cytoskeleton network [61]. On the other hand studies of diffusion of proteins in protein solutions [73] suggest that viscosity of such solutions may be only slightly higher than the viscosity of water. Therefore in cells one could expect that diffusion of probes will depend on viscosity which is a product of both viscosities (viscosity of the protein solution and of the viscosity of cytoskeleton network). In this case I expect that the effective viscosity of the system should depend on the properties of all types of crowding agents. In particular I expect that the protein solution exhibits

viscosity – η_{matrix} and that the actin filament network is responsible for large change of the viscosity according to the exponential factor $exp\left[(R_{\text{eff}}/\xi)^a\right]$ (similarly as for complex liquids). I assume that the viscosity of the composite solution of proteins and actin filaments can be described by the following scaling law:

$$\eta = A\eta_0 exp\left[(R_{\text{eff}}/\xi)^a\right] \tag{3.2.1}$$

where $\eta_{\text{matrix}} = A\eta_0$, R_{eff} is defined by Eq.(1.4.15) and A is a constant of the order of 1.

I re-analyze the data of diffusion in a cytoplasm of human cancer cells (HeLa) cells for various probes: DNA, [61] water, [8] EGFP [74] and nano diamonds [75]. I also re-analyzed diffusion data of fluorescent dye [76] and dextrans [63] in Swiss 3T3 mammalian cells (mouse muscle cells). Variables such as hydrodynamic radius of the probes (r_{p}) were partially available in the literature. However, for the analysis of diffusion of DNA , the hydrodynamic radius of DNA was determined separately. Robertson et al.[77] studied diffusion of linear DNA fragments in buffer solutions. From those data an empirical equation for the hydrodynamic radius of DNA fragment as a function of its molecular weight was determined as follows.

From the diffusion coefficient of given DNA fragment, hydrodynamic radius r_{p} of the equivalent sphere was calculated according to Stokes-Sutherland-Einstein equation. Under assumption that molecular weight of a single base pair is equal $M_{\text{bp}} = 650$ g/mol, the molecular weight M of DNA fragments was estimated. The hydrodynamic radius

r_{p} of the DNA chain depends on its molecular weight (see also Eq.(2.1.2), page 48).

$$r_{\mathrm{p}} = kM^{\epsilon} \tag{3.2.2}$$

Here k is a constant and ϵ is the exponent. In order to obtain values of k and ϵ the $\log(r_{\mathrm{p}})$ was plotted against $\log(M)$ (Figure 26). From Figure 26 the exponent $\epsilon = 0.57$

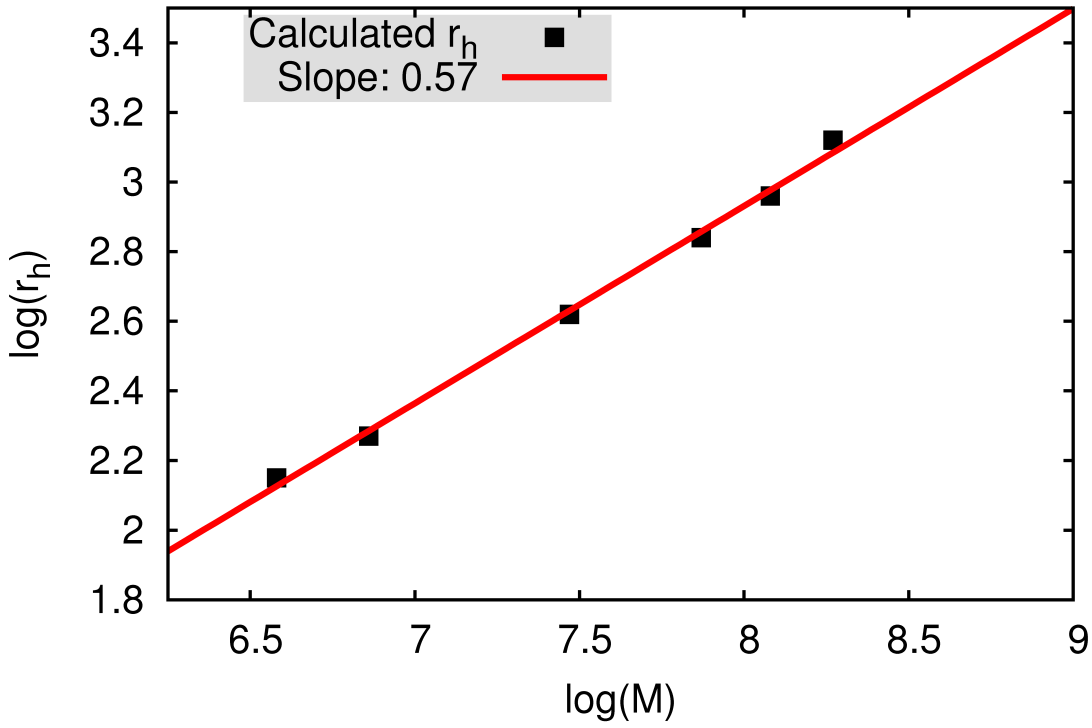

Figure 26: Hydrodynamic radius of the equivalent sphere for DNA fragments as a fuction of molecular weight M of DNA. The linear fit on the log-log scale gives the slope equal 0.57.

was obtained (value of the slope). In order to determine the value of k, r_{p} as a function of $M^{0.57}$ was plotted (Figure 27). The value of the slope in Figure 27 correspond to the constant k. This analysis allowed to formulate equation describing dependence of the

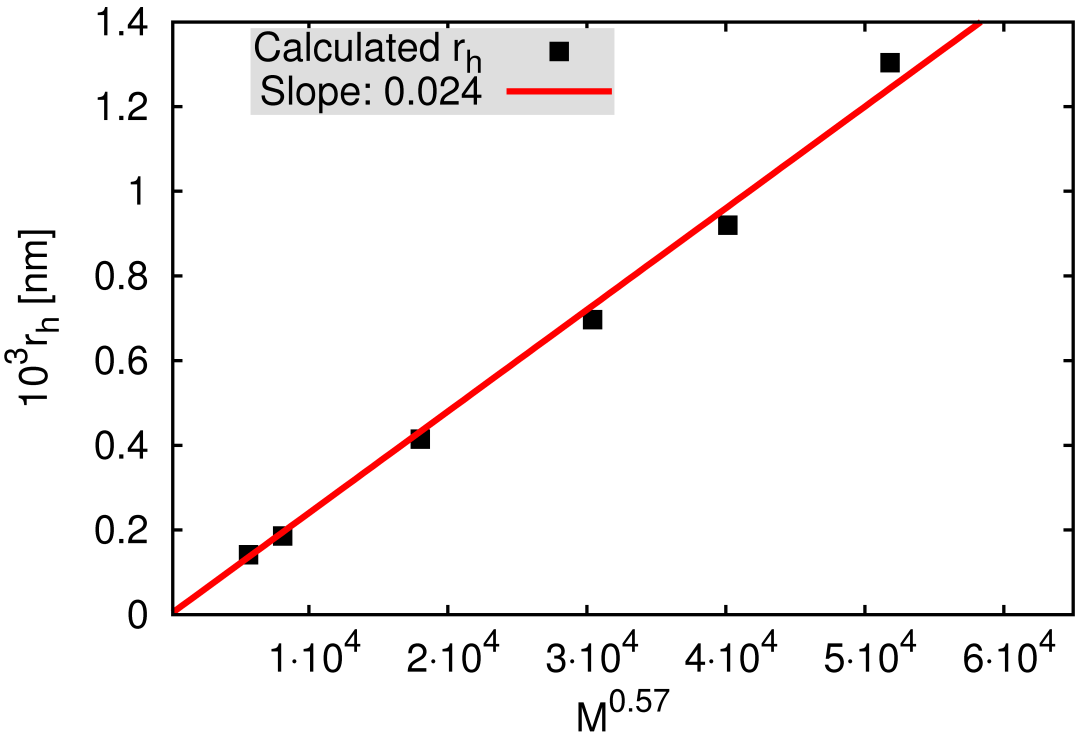

Figure 27: Hydrodynamic radius of the equivalent sphere for DNA fragments as a function of molecular weight of DNA ($M^{0.57}$). The linear fit gives slope equal 0.024.

equivalent hydrodynamic radius of DNA chain on the molecular weight of its chain.

$$r_{\mathrm{p}} = 0.024\ M^{0.57}\ [\mathrm{nm}] \tag{3.2.3}$$

Hydrodynamic radii and viscosities experienced by all investigated probes together with the cell type are listed in Table 4. In order to fit the data of the viscosity of the cytoplasm, Eqs.(1.4.15) and (3.2.1) were combined, and the following form of the scaling law was obtained:

$$\ln\left(\frac{\eta}{\eta_0}\right) = \ln\left(A\right) + \left(\frac{\xi^2}{R_{\mathrm{h}}^2} + \frac{\xi^2}{r_{\mathrm{p}}^2}\right)^{-a/2} \tag{3.2.4}$$

Table 4: Properties of the probes used in analysis

Probe	Cell type	r_{p} (nm)	η/η_0	Reference
H_2O	HeLa	0.14	1.5	Ref. 8
EGFP	HeLa	2	1.35	Ref. 74
DNA	HeLa	5.44	4.8	Ref. 61 and Eq.(3.2.3)
DNA	HeLa	13.7	6.37	Ref. 61 and Eq.(3.2.3)
DNA	HeLa	34.4	7.09	Ref. 61 and Eq.(3.2.3)
DNA	HeLa	50.7	17.95	Ref. 61 and Eq.(3.2.3)
Nano diamonds	HeLa	80	32.5	Ref. 75
DNA	HeLa	94.3	36.3	Ref. 61 and Eq.(3.2.3)
BCECF	Swiss 3T3	0.3	3.7	Ref. 76
Dextran	Swiss 3T3	2.2	5.1	Ref. 63
Dextran	Swiss 3T3	3.1	5.6	Ref. 63
Dextran	Swiss 3T3	4.2	5.8	Ref. 63
Dextran	Swiss 3T3	4.7	6.1	Ref. 63
Dextran	Swiss 3T3	6.2	6.8	Ref. 63
Dextran	Swiss 3T3	7	8.0	Ref. 63
Dextran	Swiss 3T3	9.4	14.5	Ref. 63
Dextran	Swiss 3T3	24.3	12.8	Ref. 63
Dextran	Swiss 3T3	38.6	24.6	Ref. 63

Here ξ, A, a and R_{h} (equivalent hydrodynamic radius of obstacles) were fitting parameters. b constant from Eq.(3.2.1) was included into ξ. Figures 28 and 29 shows the viscosity experienced by the probes listed in Table 4. The data obtained for living cells were fitted with Eq.(3.2.4). I found that in HeLa cells the viscosity of the matrix $\eta_{\mathrm{matrix}} = A\eta_0 = (1.3 \pm 0.3) \cdot \eta_{\mathrm{water}} = 0.9$ mPa·s. When the radius of the probe exceeds the correlation length ξ one should expect a sudden increase in the values of the viscosity measured with the probe. For HeLa cells, the correlation length was equal $\xi = 5 \pm 4$ nm. Furthermore for $\xi < r_{\mathrm{p}} < R_{\mathrm{h}}$ viscosity values increased with the radius of the probe. When $r_{\mathrm{p}} > R_{\mathrm{h}}$ a plateau in the value of viscosity plotted against r_{p} was observed. For $r_{\mathrm{p}} \gg R_{\mathrm{h}}$ the values of viscosity correspond to the macroscopic viscosity. It is assumed that R_{h} correspond to the mean value of the hydrodynamic radii of the obstacles. In the cytoplasm of HeLa cells $R_{\mathrm{h}} \approx 86$ nm. Value

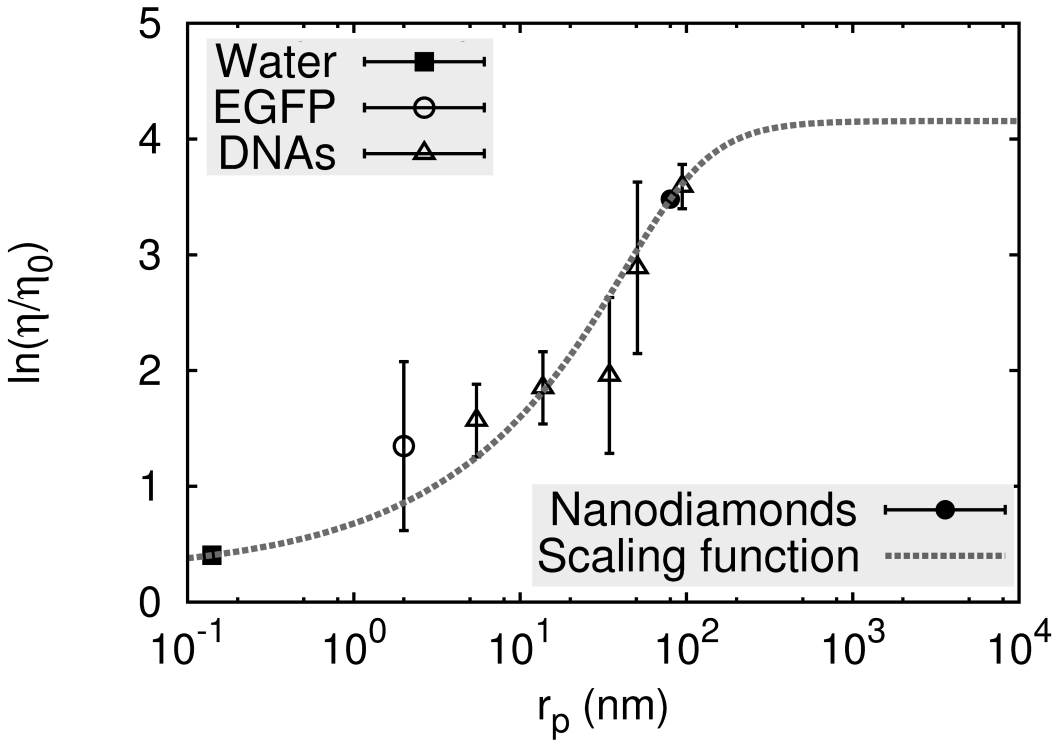

Figure 28: Viscosity of cell cytoplasm divided by the viscosity of water at 37 °C, as a function of the probe radius in HeLa cells. Figure shows data of viscosity measured with different probes such as water [8], EGFP [74], DNA fragments [61], and nanodiamonds [75]. Viscosity data was fitted with equation Eq.(3.2.4). It has been found that η_{matrix} was equal $(1.3 \pm 0.3) \cdot \eta_{\text{water}}$. Correlation length $\xi = 5 \pm 4$ nm, $R_{\text{h}} \approx 86$ nm and $a = 0.49 \pm 0.22$.

---

of exponent a for this type of cells (obtained from fitting of Eq.(3.2.4)) is equal to $a = 0.49 \pm 0.22$. Analogous parameters obtained from fits for Swiss 3T3 cells were equal $\eta_{\text{matrix}} = A\eta_0 = (2.9 \pm 0.6) \cdot \eta_{\text{water}} \approx 2.0$ mPa·s, $\xi = 7 \pm 2$ nm, $R_{\text{h}} \approx 30$ nm and $a = 0.62 \pm 0.36$. Under the assumption that the radius of the actin filament in HeLa cells is equal $r = 7$ nm [78], length of cellular obstacles can be calculated using the relation [79]:

$$R_{\text{h}} = \frac{L}{2s - 0.19 - 8.24s^{-1} + 12s^{-2}} \tag{3.2.5}$$

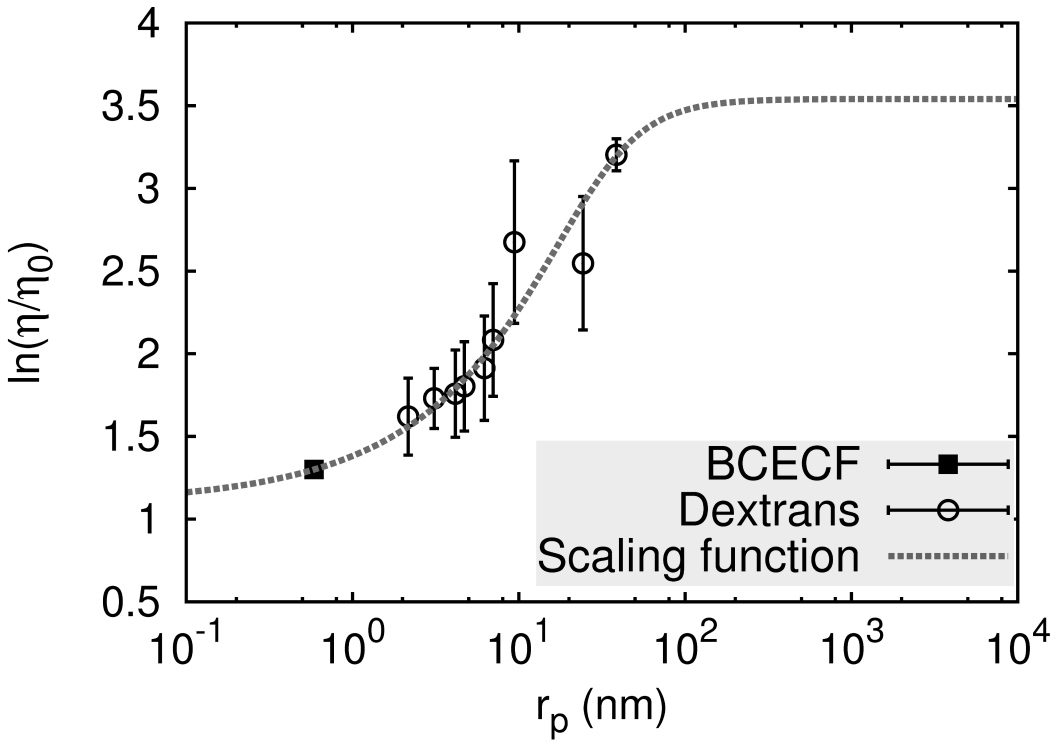

Figure 29: Viscosity of cell cytoplasm divided by the viscosity of water at 37 °C, as a function of the probe radius in Swiss 3T3 cells. Figure we presents data of viscosity measured with two different probes: small fluorescent particle BCECF [76] and dextrans of different molecular weights [63]. Viscosity data was fitted with equation Eq.(3.2.4). It has been found that $\eta_{\text{matrix}} = (2.9 \pm 0.6) \cdot \eta_{\text{water}}$, $\xi = 7 \pm 2$ nm, $R_{\text{h}} \approx 30$ nm and $a = 0.62 \pm 0.37$.

Here $s = \ln(L/r)$ and L is the length of the filament. The estimated obstacles' length was $L \approx 660$ nm in HeLa and ≈ 125 nm in Swiss 3T3 cells. The estimated filament length for cells seem reasonable when compared to the results of Dauty et al. [61] who measured the filaments to range from 100 to 500 nm. In addition presented analysis yields macroscopic viscosities for both cell types. For HeLa cells $\eta_{\text{macro}} \approx 64 \cdot \eta_{\text{water}} \approx 4.4{\cdot}10^{-2}$ Pa·s since for Swiss 3T3 cells $\eta_{\text{macro}} \approx 34{\cdot}\eta_{\text{water}} \approx 2.4{\cdot}10^{-2}$ Pa·s. These values are in agreement with the literature data of the cytoplasmic viscosity in an amoeba Dictyostelium Discoideum cells ($5 \cdot 10^{-2}$ Pa·s) [80]. According to the criterion that was proposed for complex liquids the probe will experience macroscopic viscosity when

$r_{\mathrm{p}} \geqslant 4R_{\mathrm{h}}$. One can estimate minimal hydrodynamic radius of the probe which would experience the macroscopic viscosity of the cytoplasm of HeLa and Swiss 3T3 cells. For HeLa cells hydrodynamic radius of such probe should exceeds 350 nm while for Swiss 3T3 cells $r_{\mathrm{p}} \geqslant 120$ nm.

3.3 Viscosity of the cytoplasm of *Escherichia coli*

Previous section discussed the viscosity of the cytoplasm of eukaryotic cells. The following section is devoted to the viscosity of the cytoplasm of the prokaryotic cells. In cells, many vital processes are controlled by diffusion. The main determinant of the diffusive transport in synthetic complex liquids and in the cytoplasm of living cells, is the viscosity of the liquid. The viscosity depends on the degree of crowding, i.e. the concentration of macromolecules constituting the liquid. The macromolecules (DNA and proteins) in prokaryotic cells occupy up to 30% of their volume [72]. Wang et al. [73] suggested that the main determinant of the transport in the cytoplasm of prokaryotic cells is the presence of proteins. Their *in vitro* measurements showed that the viscosity of protein solutions was not much (5 to 10 times) higher than the viscosity of water. On the other hand, many *in vivo* reports concerning diffusion of various probes in the cytoplasm of *E. coli*, suggest much larger values of viscosity of the cytoplasm [60, 81–92].

In the previous section it has been shown that the macroscopic viscosity of the cytoplasm of eukaryotic cells (human cancer cells - HeLa and Swiss 3T3 fibroblasts) can be thirty to sixty times higher than the viscosity of water [93] (cf. Figures 28 and 29) Moreover, the viscosity of the cytoplasm of mammalian cells is determined by the actin filaments forming the cytoskeleton. The viscosity of the cytoplasm of prokaryotic cells, for example, *Escherichia coli*, should be much higher than the macroscopic viscosity of the cytoplasm of mammalian cells since the cytoplasm of the prokaryotic cells is more compact and crowded (70% of water content) than the one in eukaryotic cells (90% of

water content). This observation is not consistent with the hypothesis of Wang et al. [73].

For the cytoplasm of mammalian cells it has been shown (section 3.2 and reference 93) that viscosity, which is effectively felt by objects diffusing in the cytoplasm is given by Eq.(3.2.4). In the case of mammalian cells, it has been found that objects whose hydrodynamic radius r_{p} is larger than the hydrodynamic radius of the actin filaments – R_{h} (86 nm for HeLa and 30 nm for Swiss 3T3 cells), will experience macroscopic viscosity of the cytoplasm (viscosity, which can be measured using a rheometer or a probe of macroscopic size). When $\xi < r_{\mathrm{p}} < R_{\mathrm{h}}$, the viscosity of the cytoplasm measured by a given probe, depends exponentially on r_{p} ($\xi = 5$ nm for HeLa and 7 nm for Swiss 3T3).

Here, I use literature data and Eq.(3.2.1) to determine the dependence of the viscosity of the cytoplasm of *Escherichia coli*, on the size of probes.

Viscosity felt by the probe can be calculated on the assumption that inverse of the relative diffusion coefficient (diffusion coefficient in water D_0 with respect to diffusion coefficient in the cytoplasm D) is equal to the relative viscosity (viscosity of the cytoplasm η with respect to the viscosity of water η_0): $D_0/D = \eta/\eta_0$. The length scale, which corresponds to a given viscosity value is determined by the size of the probe used in the particular measurement. On the basis of experimental data available in the literature concerning the diffusion coefficient of the macromolecules of known molecular weight (M_{w}), the inverse of the relative diffusion coefficient D_0/D was calculated. For proteins, diffusion coefficient in water (D_0 in $\mu\mathrm{m}^2/s$) is given by the following formula

[94, 95]:

$$D_0 = 8.34\frac{T}{\eta_0 M_{\mathrm{w}}^{1/3}} \tag{3.3.1}$$

where T is the temperature, η_0 is the viscosity of water in mPa·s (data taken from NIST database [96]). M_{w} is in g/mol. Using the SSE equation (Eq.(1.2.12)), we calculated the hydrodynamic radius of proteins. For plasmids D_0 was calculated according to the procedure described elsewhere [97, 98]. Relative viscosities and hydrodynamic radii of analyzed probes are summarized in Table 5.

Figure 30 shows a graph of the logarithm of relative viscosity as a function of hydrodynamic radius of the probe. From fit of Eq.(3.2.4) to the experimental data (Table 5), macroscopic viscosity of the cytoplasm as well as two crossover length scales – R_{h} and ξ has been found. We found that the value of the correlation length ξ is 0.33 ± 0.22 nm and the exponent a is equal to 0.45 ± 0.2. Unlike in the case of mammalian cells, the parameter A corresponding to the viscosity of the matrix η_{matrix}, for *E. coli* was equal to 1 which means that $\eta_{\mathrm{matrix}} = \eta_{\mathrm{water}} = \eta_0$ (cf. Eq.(3.2.1)). R_{h} was found equal to 46 ± 25 nm. This size is comparable to the size of the loops in the nucleoid, i.e., a strand of DNA, which is supercoiled due to the presence of proteins. Short-range structure of such individual, involves DNA fragments whose length does not exceed 1000 base pairs [99]. If we now assume that each of these chains is independent (similar to the assumption introduced by de Gennes for concentrated polymer solutions and the concept of blob that can be treated as a separate individual [27, 29]), its hydrodynamic radius R'_{h} will be about 49 nm. Surprising comparability of R_{h} and R'_{h} suggests

Table 5: Characteristics of the probes used in analysis. Table contains: name of the probes, molecular weights M_{w}, temperature T at which experiment was performed, logarithm of the relative viscosity, and hydrodynamic radius of the probes r_{p}.

Probe	M_{w} (kg/mol)	T	$\ln\left(\frac{\eta}{\eta_0}\right)$	r_{p} (nm)	Ref.
GFP[a]	27	293	2.4	2.63	Ref. 60
GFP[a]	27	293	3.1	2.63	Ref. 60
EYFP	27	293	2.4	2.62	Ref. 81
GFP-His6[a]	28	293	3.0	2.66	Ref. 60
cMBP-GFP[a]	72	293	3.2	3.65	Ref. 60
CheY-GFP[a]	41	293	2.7	3.03	Ref. 82
CFP-CheW-YFP	71	293	3.7	3.63	Ref. 81
CFP-CheR-YFP	86	293	3.5	3.88	Ref. 81
torA-GFP	30	310	2.6	2.73	Ref. 83
GFP[a]	27	293	2.1	2.63	Ref. 84
GFP	27	298	2.7	2.63	Ref. 85
torA-GFP2 [a]	57	293	2.1	3.38	Ref. 86
GFP2[a]	27	293	2.2	2.63	Ref. 86
torA-GFP2 [a]	57	293	2.0	3.38	Ref. 86
torA-GFP3 [a]	84	293	2.2	3.84	Ref. 86
torA-GFP4 [a]	111	293	2.2	4.22	Ref. 86
torA-GFP5 [a]	138	293	2.8	4.54	Ref. 86
AmiA-GFP[a]	58	293	3.6	3.4	Ref. 86
AmiA-GFP[a]	58	293	3.6	3.4	Ref. 86
$\mathrm{AmiA_{noSP}}$-GFP[a]	58	293	2.2	3.4	Ref. 86
NlpA-GFP[a]	55	293	3.4	3.34	Ref. 86
$\mathrm{NlpA_{noLB}}$-GFP[a]	55	293	3.2	3.34	Ref. 86
Glucose	0.42	293	2.1	0.53	Ref. 87
GFP	27	293	3.3	2.63	Ref. 87
$(\beta$ -Gal-GFP$)_4$	582	293	3.8	7.33	Ref. 87
GFP	27	298	2.7	2.63	Ref. 88
Water	0.018	301	0.1	0.14	Ref. 90
mRNA-GFP	6000	295	6.2	15.95	Ref. 91
Plasmid-GFP[a]	28000	293	9.4	346.89	Ref. 92

[a] No information about temperature at which measurement was performed, assumed 293 K.

that the main component crowding the cytoplasm is the nucleoid, i.e., parts of DNA. The macroscopic viscosity of the cytoplasm of *E. coli* estimated from Figure 30 is approximately 13 Pa·s (at 20°C) which is 13000 times higher than the viscosity of water. Objects whose hydrodynamic radius is larger than R_{h}, will experience the macroscopic viscosity. On the other hand, objects with a radius lower than ξ will experience the vis-

cosity that is similar to the viscosity of water. Macromolecules whose hydrodynamic

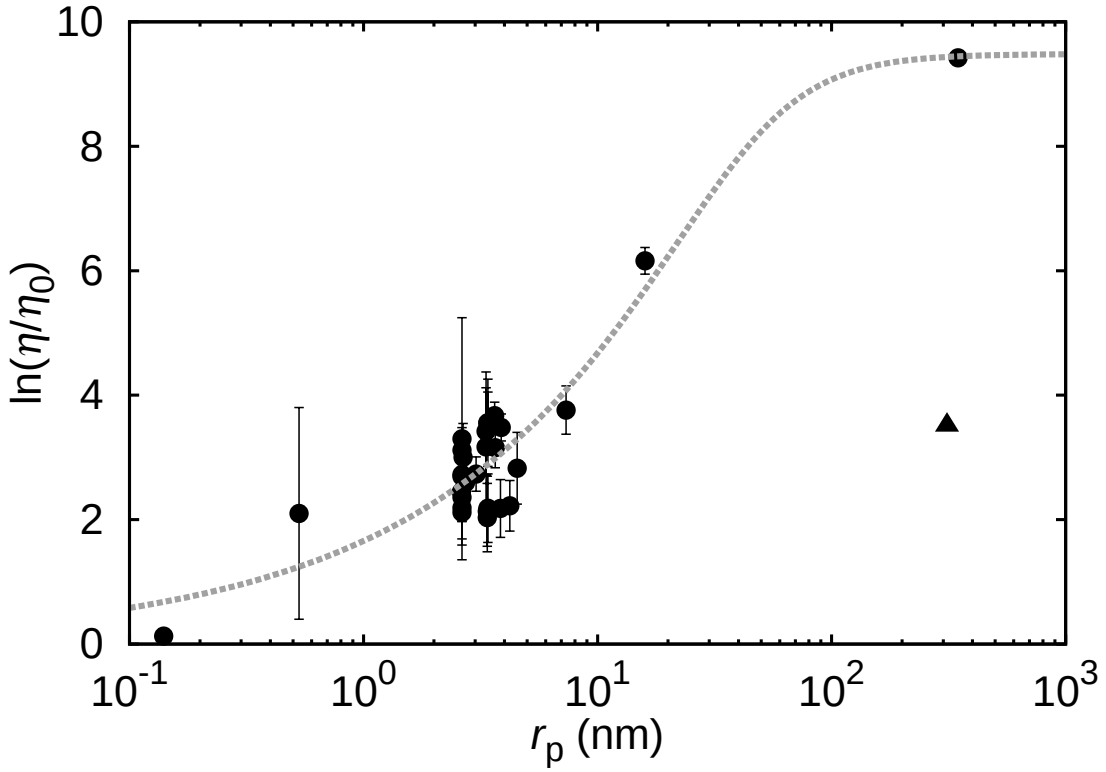

Figure 30: The logarithm of the relative viscosity experienced by probes diffusing in the cytoplasm of *E. coli*. Dashed line refers to the Eq.(3.2.4). Experimental data (•; Table 5) were fitted using the function given by Eq.(3.2.4). Based on the fitting of the available data we found, that the macroscopic viscosity of the cytoplasm is about 13 Pa·s (at 20°C). In addition, $R_{\mathrm{h}} = 46 \pm 25$ nm, ξ is 0.33 ± 0.22 nm, and $a = 0.45 \pm 0.2$. ▲ *refers to the calculated diffusion coefficient of a plasmid of molecular weight* 24 MDa [89]. Diffusion coefficient for this plasmid was calculated using the viscosity experienced by GFP. This led to significant overestimation of the diffusion coefficient in the cytoplasm and, consequently, to orders of magnitude underestimation of the viscosity experienced by the plasmid.

radius is between ξ and R_{h} will experience viscosity that increases exponentially with the hydrodynamic radius of the molecule under consideration. Additionally, in Figure 30, we placed the point showing the consequences of an incorrect assumption that the viscosity of the liquid is size independent (shown as ▲ in Figure 30). Derman et al. [89] estimated the diffusion coefficient of the plasmid with mass equal to 24 MDa. For the calculations they used the viscosity experienced by GFP in the cytoplasm of

E. coli. This assumption led to overestimated values of the diffusion coefficient and, consequently, to underestimated value of the viscosity experienced by this plasmid.

3.4 Viscosity of colloidal suspensions

3.4.1 Calculation of the effective viscosity of colloidal suspensions

In the case of spherical colloidal particles, that the diffusion coefficient of the particles can be described by the generalized SSE equation Eq.(3.4.1) [9]:

$$D = \frac{kT}{\mathrm{C}\pi\eta_{\mathrm{m}}r_{\mathrm{p}}} \tag{3.4.1}$$

where C is a constant. When size of the probe is much larger than the size of the objects constituting the liquid $\mathrm{C} = 6$ which correspond to so called stick boundary conditions. If the probes are smaller or their size is comparable to the size of the objects constituting the liquid, then $\mathrm{C} < 6$ is observed [7].

In the previous sections, I showed that the viscosity experienced by the probe diffusing among the objects of similar or bigger size, is expressed as the effective viscosity η_{eff}, which depends on the size of the probe. Hence, the factor influencing the value of the diffusion coefficient of those particles, is not a change of the coefficient C resulting from a change of boundary conditions, but the viscosity experienced by the probe η_{eff} which is much lower than the macroscopic viscosity η_{m}. The coefficient C should be constant and equal to 6, and the SSE equation should be written as follows:

$$D = \frac{kT}{6\pi\eta_{\mathrm{eff}}r_{\mathrm{p}}} \tag{3.4.2}$$

In fact, both, Eqs.(3.4.1) and (3.4.2) refer to the same value of the self diffusion coefficient, so they can be written as:

$$\frac{kT}{\mathrm{C}\pi\eta_{\mathrm{m}}r_{\mathrm{p}}} = \frac{kT}{6\pi\eta_{\mathrm{eff}}r_{\mathrm{p}}} \tag{3.4.3}$$

which gives:

$$\frac{6}{\mathrm{C}} = \frac{\eta_{\mathrm{m}}}{\eta_{\mathrm{eff}}} \tag{3.4.4}$$

Since the η_{m} and C can be determined independently, the effective viscosity experienced by the probe η_{eff} can be easily calculated according to Eq.(3.4.4).

3.4.2 Application of the scaling law to the literature data

In section 3.1 viscosity of the solutions of polymers and of elongated rigid micelles was studied. Scaling formula of the viscosity (Eq.(1.4.16)) was successfully applied to the viscosity data of $C_{12}E_6$ micellar solution. Therefore we may expect that laws governing the entangled complex system should be applicable to untangled system composed of rigid spherical objects. In the following section application of Eq.(1.4.16) to the solution of rigid spheres (literature data of Segrè et al. [9]) will be discussed

Segrè et al. [9] studied the viscosity of the solutions of polymethylmetacrylate (PMMA) particles in *cis*-decaline. The hydrodynamic radius of those particles was $r_{\mathrm{p}} = 247$ nm. In addition authors investigate the self diffusion of those particles in their own solution. Measurements were performed for volume fractions ranging from $\phi \to 0$ to 0.494. The viscosity of the colloidal solution calculated from the self diffusion of

the particles was much lower than the macroscopic viscosity of given solution. Differences between the macroscopic viscosity and the effective viscosity experienced by the particles can be explained by the size dependent viscosity. When size of the probe decreases to the nano scale, viscosity starts to depend on the size of the probe and of the size of the particles which create the solution.

Viscosity of polymer solution is described by the exponential function of the effective hydrodynamic radius R_{eff} and of the correlation length ξ. For the solution of colloidal particles one can expect similar dependence however ξ need to be adopted to the non overlapping rigid objects. In polymer solutions correlation length is a function of the radius of gyration of the polymer coil and of the concentration of the polymer. The concentration ratio (c/c^*) define how much the polymer coils are entangled with each other. Namely, when the polymer concentration c is less than c^*, the polymers behave like individual particles (dilute regime). When $c > c^*$, then the polymer chains begin to overlap with each other, and the higher c, the more chains are overlapped. Since ξ is a function of c/c^*, therefore ξ determine how far from the center of the mass of one selected polymer chain are monomers of the other chain. Although in colloidal solutions composed of spherical particles, entangling is not observed, the definition of the ξ should be similar and can be described as a distance from the center of the mass of one colloidal particle to the point in space where one will find surface of the other colloidal particle as shown in Figure 31. In the solution of polymers the ratio c/c^* can be expressed as the ratio of the volume of the polymer and the volume of the solvent, because $c^* = M_{\text{w}}/N_{\text{A}}V_{\text{p}}$, where M_{w} is molecular weight of the polymer, and V_{p} is a

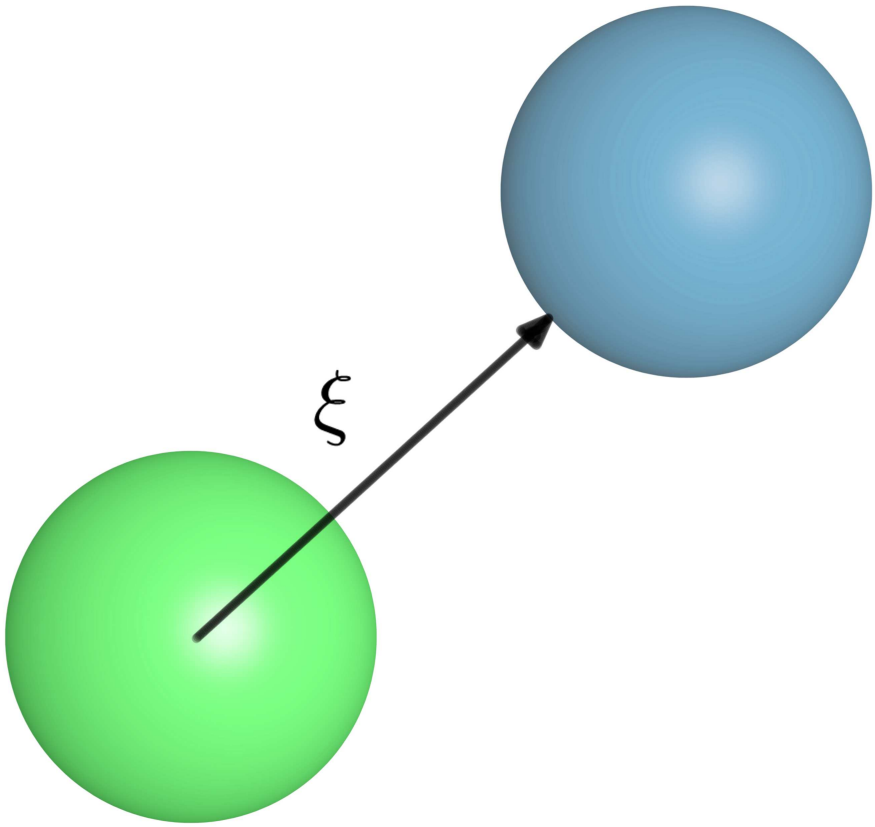

Figure 31: Graphical definition of ξ for colloidal system composed of hard spheres. ξ can be ascribed as a distance from the center of the mass of one colloidal particle to the point in space where one will find surface of the other colloidal particle.

volume of a single coil of the polymer. Though one will obtain:

$$\frac{c}{c^*} = \frac{m}{V_\mathrm{s}}\frac{V_\mathrm{p}N_\mathrm{A}}{M_\mathrm{w}} = \frac{m}{V_\mathrm{s}}\frac{V_\mathrm{p}N_\mathrm{A}N}{mN_\mathrm{A}} = \frac{m}{V_\mathrm{s}}\frac{V_\mathrm{p}}{m} = \frac{V_\mathrm{p}}{V_\mathrm{s}} = \psi \tag{3.4.5}$$

Here V_s is the volume of the solvent, m is the total mass of the polymer, and N is the number of polymer coils (for $c = c^*$,$N = 1$). Using Eq.(3.4.5), ξ can be written as:

$$\xi = R_\mathrm{g}\psi^{-\beta} \tag{3.4.6}$$

For the solution of colloids, ψ is defined by the right side of Eq.(3.4.6) and is equal to $\phi/(1-\phi)$ where ϕ is the volume fraction. Let us assume that the exponent β for rigid colloidal particles equals 1 as for rigid elongated micelles discussed in section 3.1 (Eq.(3.1.1)). According to the scaling laws discussed in previous sections, the equation describing macroscopic viscosity ($r_{\mathrm{p}} \rightarrow \infty$; $R_{\mathrm{eff}} \rightarrow R_{\mathrm{h}}$) of the solution of colloidal particles will be given by the following formula.

$$\frac{\eta_{\mathrm{m}}}{\eta_0} = exp\left[\left(\frac{R_{\mathrm{h}}}{b\xi}\right)^a\right] = exp\left[\left(\frac{R_{\mathrm{h}}}{bR_{\mathrm{g}}}\psi\right)^a\right] \tag{3.4.7}$$

The radius of gyration of the homogeneous sphere can be expressed [100] as:

$$R_{\mathrm{g}} = \sqrt{3/5}R \tag{3.4.8}$$

Where R is the radius of the sphere. Under assumption of $R = R_{\mathrm{h}}$, the substitution of Eq.(3.4.8) into Eq.(3.4.7) gives:

$$\frac{\eta_{\mathrm{m}}}{\eta_0} = exp\left[\left(\frac{1}{b}\sqrt{\frac{5}{3}}\psi\right)^a\right] \tag{3.4.9}$$

Here we ask: *what is the viscosity experienced by the particle diffusing among other particles with the same size?* Accordingly to Eqs.(1.4.16) and (3.4.6) the effective viscosity should be expressed as:

$$\frac{\eta_{\mathrm{eff}}}{\eta_0} = exp\left[\left(\frac{R_{\mathrm{eff}}}{bR_{\mathrm{g}}}\psi\right)^a\right] \tag{3.4.10}$$

When the particles diffuse in their own solution $r_{\mathrm{p}} = R_{\mathrm{h}}$, the effective hydrodynamic radii (according to Eq.(1.4.15)) should be equal $R_{\mathrm{eff}} = R_{\mathrm{h}}\sqrt{2}/2$ and Eq.(3.4.10) transforms into:

$$\frac{\eta_{\mathrm{eff}}}{\eta_0} = exp\left[\left(\frac{\sqrt{2}}{2}\frac{R_{\mathrm{h}}}{bR_{\mathrm{g}}}\psi\right)^a\right] = exp\left[\left(\sqrt{\frac{5}{6}}\frac{\psi}{b}\right)^a\right] \tag{3.4.11}$$

This equation has been applied to literature data of viscosity of colloidal suspensions [9]. It turned out that Eq.(3.4.11) can not be directly applied to the description of literature data. However, another equation describing the effective viscosity experienced by probes diffusing in a concentrated solution of hard spheres has been proposed. In this equation, the effective hydrodynamic radius R_{eff} (Eq.(1.4.15)), was modified as follows:

$$\frac{1}{R_{\mathrm{eff}}^2} = \frac{1}{R_{\mathrm{h}}^2} + \frac{1}{\left(r_{\mathrm{p}} + \vartheta\right)^2} \tag{3.4.12}$$

Where $\vartheta = dr_{\mathrm{p}}\psi$ (d – constant). Eq.(3.4.12) is a consequence of the observations made by Lammanna et al. [101]. They studied the self-diffusion of the solvent (water) in the solution of proteins. They observed that the diffusion coefficient of the solvent can not be described by the SSE equation, unless the correction is included in the hydrodynamic radius of the solvent. Namely, the hydrodynamic radius of the solvent (small particles between large proteins) should depend on the concentration of proteins. It can be assumed that a similar relationship should be observed not only for the solvent, but also for other objects. Lamanna et al. [101] did not provide a mathematical form of this correction, therefore, in Eq.(3.4.12) the simplest form of the correction, expressed as the product of the concentration ψ and hydrodynamic radius r_{p} was adopted. As a re-

sult, the equation describing the effective viscosity experienced by the probe, diffusing in solution of colloids, will be expressed by the equation:

$$\frac{\eta_{\mathrm{d}}}{\eta_0} = exp\left[\left(\frac{R_{\mathrm{eff}}}{b\xi}\right)^a\right] = exp\left[\left(\sqrt{\frac{R_{\mathrm{h}}^2\left(r_{\mathrm{p}}+\vartheta\right)^2}{R_{\mathrm{h}}^2+\left(r_{\mathrm{p}}+\vartheta\right)^2}}\frac{\psi}{b}\right)^a\right] \tag{3.4.13}$$

Here η_{d} is the viscosity experienced by the probe with correction included in the hydrodynamic radius of the probe.

Figure 32 shows the experimental data obtained from the work of Segrè et al. [9].

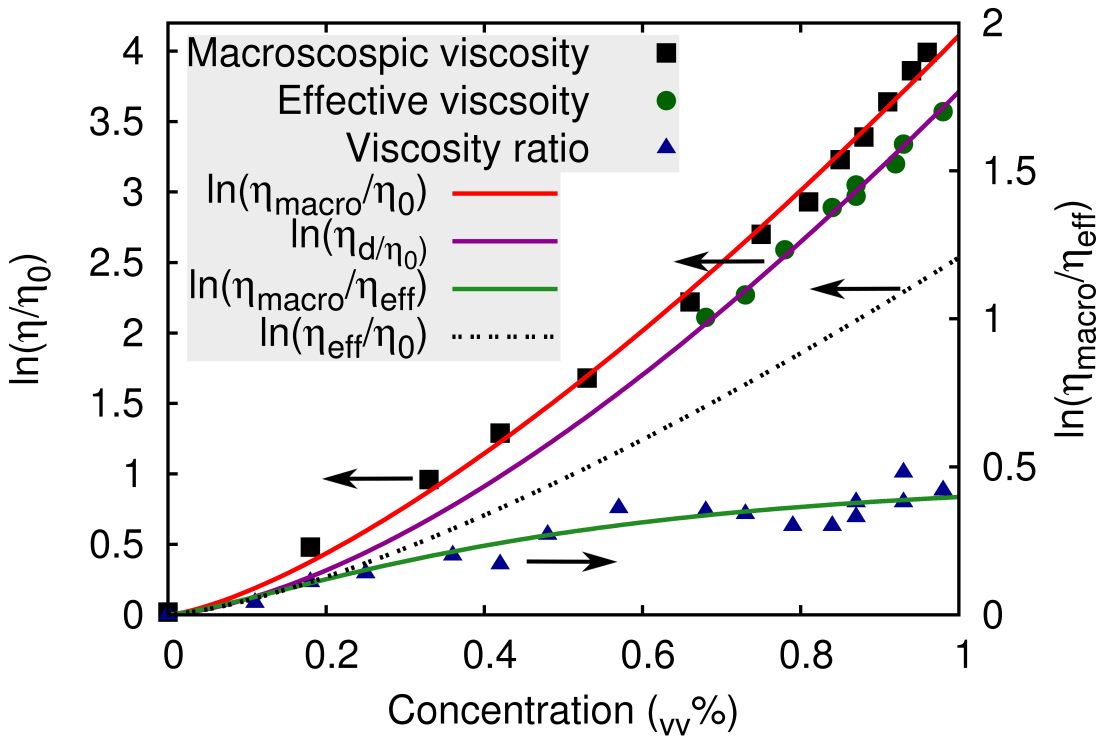

Figure 32: Figure shows viscosity data obtained from the work of Segrè et al. [9]. The macroscopic viscosity (■) was fitted with Eq.(3.4.9) with parameters: $a = 1.39 \pm 0.05$ and $b = 0.47 \pm 0.01$. The effective viscosity experienced by the probe (●) is described by Eq.(3.4.13) with same parameters as the macroscopic viscosity and with r_{p} enlarged by the $\vartheta = dr_{\mathrm{p}}\psi$, $d = 1.52 \pm 0.06$. The ratio of the macroscopic and effective viscosity (▲) follows the curve given by the ratio of Eqs.(3.4.9) and (3.4.13).

Macroscopic viscosity of the colloidal solution (■) was fitted with Eq.(3.4.9) (red, solid

curve). The parameters a and b were found equal to 1.39 ± 0.05 and 0.47 ± 0.01 respectively. We found that particles undergoing self-diffusion among the particles of same type, experience the effective viscosity (lower than macroscopic one – ●), however, size of the probe should be enlarged by the correction: $\vartheta\left(r_{\mathrm{p}}, \psi\right)$ (Eq.(3.4.13) – purple, solid curve). Parameter d in correction ϑ was found equal to 1.52 ± 0.06. The bottom, dark green, solid curve corresponds to the ratio between macroscopic viscosity (Eq.(3.4.9)) and effective viscosity (Eq.(3.4.13)). Experimental points (▲) obtained from the work of Segrè et al. [9], were calculated as shown in Section 3.4.1 (Eq.(3.4.4)).

The physical meaning of the ϑ (added to the hydrodynamic radius of the probe) is unclear. It may be, however, related to the distance at which the momentum is transferred during the motion of the probe through the solution. The scaling equations describing the viscosity of the solution of colloidal particles is only the rough estimation. More detailed studies are required in order to determine the effective viscosity experienced by the probe diffusing among rigid colloidal particles of same type.

4 Summary and conclusions

In presented work, the viscosity as a function of the size of the probe was discussed. The scaling law describing the viscosity for all length scales was proposed and was verified for different systems.

1. **In the synthetic complex liquids** such as solutions of polymers, or surfactants, viscosity depends significantly on the scale at which the measurement was made. In other words, it depends on the size of the probe used to measure the viscosity. We studied three different complex liquids. Two of them were solutions of flexible polymers, differing in solvent (aqueous solution of poly(ethylene glycol) and polystyrene dissolved in acetophenone). The third complex liquid was an aqueous solution of surfactant ($C_{12}E_6$) that creates a rigid elongated micelles. We have successfully used the equation Eq.(1.4.16) for all the mentioned complex liquids, which confirms universality of this equation. These results have very serious consequences because all measurements of viscosity, diffusion or electrophoretical mobility in complex liquids (via dynamic light scattering, capillary electrophoresis, chromatography and many others) should be treated very carefully when the probes are nanoscopic. The SSE equation can be applied to complex liquids at all length scales, with a proper account for the viscosity dependence on R_{eff} (Eq.(1.4.15)). Additionally viscosity experienced by the probes of a given r_{p} in a solution comprising obstacles of $R_{\mathrm{h}} = r_{\mathrm{p}}$ (polymer in polymers or micelle in micellar solution) is lower than the macroscopic viscosity of the

solution. Furthermore if the scaling form of the viscosity is known in a given system, one can use the SSE equation with the scale dependent viscosity to predict the self diffusion coefficient for any probe of known hydrodynamic radius. I suppose that this is the first model of viscosity that takes into account and unites both: the relationship between the probe and the obstacles (R_{eff} – Eq.(1.4.15)) as well as the structural properties of the matrix ($\xi(R_{\text{g}}, c)$ or $\xi(L, c)$) – introduced by Langevin and Rondelez [102].

2. **The viscosity of the cytoplasm of mammalian cells** was also analyzed. We found an analogous dependence, of the viscosity of the cytoplasm, on the size of the probe as in the case complex liquids. The results of this work are complementary to the work of Arcizet et al. [80], who proposed to probe the cytoplasm at the micrometer scale, and distinguished between active and passive transport [103]. In this work data concerning diffusion coefficients of probes with hydrodynamic radii below 100 nm were used. One can propose an experiment to probe all length scales (from nano to macro) and to determine, for investigated cell strain, scaling function of the viscosity across all length scales. Such experiment should be based on single molecule measurements (e.g. FCS) to probe nanoscopic length scale and on single particle tracking [80] to probe microscopic scale. Additionally sub-micrometer length scale (>100 nm) can be probed with the technique described by Wirtz [104]. In all techniques however, at which hydrodynamic radius of the probe is smaller than few hundreds of nanometers, results should be analyzed with scale dependent viscosity taken into account.

3. **Analysis of the viscosity of the cytoplasm of prokaryotic cells** was carried out. We found that the macroscopic viscosity of the cytoplasm of *E. coli* equals 13 Pa·s. This value is three orders of magnitude higher than the value estimated for mammalian cell cytoplasm, where the macroscopic viscosity was estimated to be $4.4 \cdot 10^{-2}$ Pa·s for HeLa cells and $2.4 \cdot 10^{-2}$ Pa·s for fibroblasts. The main reason for such a dramatic difference in the macroscopic viscosity of the cytoplasm of prokaryotic and of eukaryotic cells, results from the water content of the system. In mammalian cells, 90% of the volume is occupied by water while in *E. coli* only 70% [72]. In addition, the macroscopic viscosity difference is related to the type of objects that crowd the liquid. In the cytoplasm of mammalian cells the macroscopic viscosity was associated with actin filaments forming the cytoskeleton. In the cytoplasm of *E. coli* cells, main component responsible for the macroscopic viscosity value are loops of DNA, forming the nucleoid. The average distance between DNA chains in *E. coli* is roughly 28 nm [105, 106], while the correlation length ξ determined from fit, was about 0.3 nm. This result suggests that the threshold length scale that determines whether the probe experiences viscosity of water or much higher (ξ), originate from the presence of proteins and other macromolecules (smaller than DNA). Thus, viscosity of the cytoplasm of *E. coli* is influenced by presence of both: DNA (macro scale), and all other small macromolecules such as proteins or mRNA (nano scale).

4. The results obtained for **solutions of colloids**, suggests that the scaling function the viscosity is much more complicated than that proposed for polymer solutions.

It was shown that the hydrodynamic radius of the probe should be enlarged by the factor which depend on the concentration of the colloidal particles in the solution and of the size of the probe ($\vartheta = dr_{\mathrm{p}}\psi$) which is consistent with experimental observations made by Lamanna et al. [101]. In addition, the exponent a obtained from the fitting of Eqs.(3.4.10) and (3.4.13) to the experimental data [9] is consistent with experimental results, obtained by Porcar et al.[107]. The authors studied the self-diffusion of lysozyme in concentrated solution. They observed that the relative diffusion coefficient varies with the volume fraction of lysozyme with exponent 4/3. This value is close to the a exponent obtained in this work for colloidal suspensions, which was equal to 1.39 ± 0.05.

Further studies (experimental as well as theoretical) of the viscosity at the nano scale are mandatory in complex liquids as well as in other fluids. Also, examination, of the dependence of the nano scale viscosity, on the temperature is necessary. I suppose that the parameter b from the equation Eq.(1.4.16) is strongly related to the temperature at which the measurement is performed. Further experiments in this direction are needed in order to confirm or reject those suppositions.

References

[1] Graham, T. H. On the law of diffusion of gases. *Phyl. Mag.* **2**, 175–191,269–276,351–358 (1833).

[2] Fick, A. On liquid diffusion. *Phyl. Mag.* **10**, 30–39 (1855).

[3] Stokes, G. G. *Transactions of the Cambridge Philosophical Society*, volume IX. (1850).

[4] Sutherland, W. Ionization, ionic velocities, and atomic sizes. *Phil. Mag.* **3**, 161–177 (1902).

[5] Sutherland, W. A dynamical theory of diffusion for non-electrolites and the mollecular mass of albumin. *Phil. Mag.* **9**, 781–785 (1905).

[6] Einstein, A. On the motion of small particles suspended in a stationary liquid, as required by the molecular kinetic theory of heat. *Annalen der Physik* **17**, 549 (1905).

[7] Edward, J. Molecular volumes and Stokes-Einstein equation. *J. Chem. Educ.* **47**(4), 261–& (1970).

[8] Zhao, L., Sukstanskii, A. L., Kroenke, C. D., Song, J., Piwnica-Worms, D., Ackerman, J. J. H., and Neil, J. J. Intracellular water specific MR of microbead-adherent cells: HeLa cell intracellular water diffusion. *Magn. Reson. Med.* **59**(1), 79–84 (2008).

[9] Segre, P., Meeker, S., Pusey, P., and Poon, W. Viscosity and structural relaxation in suspensions of hard-sphere colloids. *Phys. Rev. Lett.* **75**(5), 958–961 (1995).

[10] Meechai, N., Jamieson, A., and Blackwell, J. Translational diffusion coefficients of bovine serum albumin in aqueous solution at high ionic strength. *J. Colloid Interface Sci.* **218**(1), 167–175 (1999).

[11] Rigler, R., Mets, U., Widengren, J., and Kask, P. Fluorescence correlation spectroscopy with high count rate and low background: analysis of translational diffusion. *Eur. Biophys. J.* **22**, 169–175 (1993).

[12] Herschel, J. F. W. On a case of superficial colour presented by a homogenous liquid internally colourless. *Philosophical Translation of the Royal Society of London* **135**, 143–145 (1845).

[13] Magde, D., Webb, W., and Elson, E. thermodynamic fluctuations in a reacting system - measurement by fluorescence correlation spectroscopy. *Phys. Rev. Lett.* **29**(11), 705–& (1972).

[14] Cherdhirankorn, T., Harmandaris, V., Juhari, A., Voudouris, P., Fytas, G., Kremer, K., and Koynov, K. Fluorescence Correlation Spectroscopy Study of Molecular Probe Diffusion in Polymer Melts. *Macromolecules* **42**(13), 4858–4866 (2009).

[15] Dauty, E. and Verkman, A. Molecular crowding reduces to a similar extent the diffusion of small solutes and macromolecules: measurement by flu-

orescence correlation spectroscopy. *J. Mol. Recognit.* **17**(5), 441–447 (2004). EMBO Workshop on Biological Implications of Macromolecular Crowding, Avila, SPAIN, JUN 14-18, 2003.

[16] Haustein, E. and Schwille, P. Ultrasensitive investigations of biological systems by fluorescence correlation spectroscopy. *Methods* **29**(2), 153–166 (2003).

[17] Kask, P., Piksarv, P., Mets, U., Pooga, M., and Lippmaa, E. fluorescence correlation spectroscopy in the nanosecond time range - rotational diffusion of bovine carbonic anhydrase-B. *Eur. Biophys. J. Biophys. Lett.* **14**(4), 257–261 (1987).

[18] Lakowicz, J. R. *Principles of Fluorescence Spectroscopy*. Springer, Baltimore, (2006).

[19] Lakowicz, J. R. *Topics in fluorescence spectroscopy*, volume 1. Kluwer Academic / Plenum Publishers, (1999).

[20] Enderlein, J., Gregor, I., Patra, D., Dertinger, T., and Kaupp, U. Performance of fluorescence correlation spectroscopy for measuring diffusion and concentration. *ChemPhysChem* **6**(11), 2324–2336 (2005).

[21] Gendron, P.-O., Avaltroni, F., and Wilkinson, K. J. Diffusion Coefficients of Several Rhodamine Derivatives as Determined by Pulsed Field Gradient-Nuclear Magnetic Resonance and Fluorescence Correlation Spectroscopy. *J. Fluoresc.* **18**(6), 1093–1101 (2008).

[22] Cherdhirankorn, T., Best, A., Koynov, K., Peneva, K., Muellen, K., and Fytas,

G. Diffusion in Polymer Solutions Studied by Fluorescence Correlation Spectroscopy. *J. Phys. Chem. B* **113**(11), 3355–3359 (2009).

[23] Hołyst, R., Bielejewska, A., Szymański, J., Wilk, A., Patkowski, A., Gapiński, J., Żywociński, A., Kalwarczyk, T., Kalwarczyk, E., Tabaka, M., Ziębacz, N., and Wieczorek, S. A. Scaling form of viscosity at all length-scales in poly(ethylene glycol) solutions studied by fluorescence correlation spectroscopy and capillary electrophoresis. *Phys. Chem. Chem. Phys.* **11**(40), 9025–9032 (2009).

[24] Gapiński, J., Szymański, J., Wilk, A., Kohlbrecher, J., Patkowski, A., and Hołyst, R. Size and Shape of Micelles Studied by Means of SANS, PCS, and FCS. *Langmuir* **26**(12), 9304–9314 (2010).

[25] Szymański, J., Patkowski, A., Gapiński, J., Wilk, A., and Holyst, R. Movement of proteins in an environment crowded by surfactant micelles: Anomalous versus normal diffusion. *J. Phys. Chem. B* **110**(14), 7367–7373 (2006).

[26] Schwille, P., Korlach, J., and Webb, W. Fluorescence correlation spectroscopy with single-molecule sensitivity on cell and model membranes. *Cytometry* **36**(3), 176–182 (1999).

[27] Doi, M. *Introduction to polymer physics*. Oxford University Press, (1997).

[28] Przygocki, W. and Włochowicz, A. *Fizyka Polimerów*. Wydawnictwo Naukowe PWN SA, (2001).

[29] de Gennes, P. *Scaling concept in polymer physics*. Cornell University Press, (1979).

[30] Galina, H. *Fizykochemia polimerów*. Oficyna Wydawnicza Politechniki Rzeszowskiej, (1998).

[31] Cheng, Y., Prud'homme, R., and Thomas, J. Diffusion of mesoscopic probes in aqueous polymer solutions measured by fluorescence recovery after photobleaching. *Macromolecules* **35**(21), 8111–8121 (2002).

[32] Holmberg, K., Jönsson, B., Kronberg, B., and Lindman, B. *Surfactant and polymers in aqueous solution*. John Willey & Sons, Ltd, 2nd edition, (2004).

[33] Garstecki, P. and Holyst, R. Scattering patterns of self-assembled gyroid cubic phases in amphiphilic systems. *J. Chem. Phys.* **115**(2), 1095–1099 (2001).

[34] Einstein, A. A new determination of molecular dimensions. *Annalen der Physik* **19**, 289 (1906).

[35] Einstein, A. Correction to my paper, "a new determination of molecular dimensions". *Annalen der Physik* **34**, 591 (1911).

[36] Arrhenius, S. The viscosity of solutions. *Biochem. J.* **11**(2), 112 (1917).

[37] Huggins, M. L. The viscosity of dilute solutions of long-chain molecules. iv. dependence on concentration. *J. Am. Chem. Soc.* **64**(11), 2716–2718 (1942).

[38] Schachman, H. and Harrington, W. On viscosity measurements in the ultracentrifuge. *J. Am. Chem. Soc.* **74**(15), 3965–3966 (1952).

[39] Rodbard, D. and Chrambac.A. Estimation of molecular radius, free mobility, and valence using polyacrylamide gel electrophoresis. *Anal. Biochem.* **40**(1), 95–& (1971).

[40] Kosar, T. and Phillips, R. Measurement of protein diffusion in dextran solutions by holographic-interferometry. *AICHE JOURNAL* **41**(3), 701–711 (1995).

[41] Laurent, T., Bjork, I., Persson, H., and Pietruszkiewicz, A. On interaction between polysaccharides and other macromolecules .2. transport of globular particles through hyaluronic acid solutions. *Biochim. Biophys. Acta* **78**(2), 351–& (1963).

[42] Laurent, T. and Pietruszkiewicz, A. Effect of hyaluronic acid on sedimentation rate of other substances. *Biochim. Biophys. Acta* **49**(2), 258–& (1961).

[43] Lin, T. and Phillies, G. Probe diffusion in poly(acrylic acid) water - effect of probe size. *Macromolecules* **17**(9), 1686–1691 (1984).

[44] Ngai, K. and Phillies, G. Coupling model analysis of polymer dynamics in solution: Probe diffusion and viscosity. *J. Chem. Phys.* **105**(18), 8385–8397 (1996).

[45] Ogston, A., Preston, B., Wells, J., Ogston, A., Preston, B., Snowden, J., and Wells, J. transport of compact particles through solutions of chain-polymers. *Proc. R. Soc. London Ser. A-Math. Phys. Eng. Sci.* **333**(1594), 297–316 (1973).

[46] Phillies, G., Ullmann, G., Ullmann, K., and Lin, T. Phenomenological scal-

ing laws for semidilute macromolecule solutions from light-scattering by optical probe particles. *J. Chem. Phys.* **82**(11), 5242–5246 (1985).

[47] Radko, S. and Chrambach, A. Mechanisms of retardation of rigid spherical particles with 3 to 1,085 nm radius in capillary electrophoresis, using buffered polyacrylamide (molecular weight 5 x 10(6)) solutions. *Electrophoresis* **17**(6), 1094–1102 (1996).

[48] Radko, S. and Chrambach, A. Electrophoresis of proteins in semidilute polyethylene glycol solutions: Mechanism of retardation. *Biopolymers* **42**(2), 183–189 (1997).

[49] Tokita, M., Miyoshi, T., Takegoshi, K., and Hikichi, K. Probe diffusion in gels. *Phys. Rev. E* **53**(2), 1823–1827 (1996).

[50] Wattenbarger, M., Bloomfield, V., Bu, Z., and Russo, P. Tracer diffusion of proteins in dna solutions. *Macromolecules* **25**(20), 5263–5265 (1992).

[51] Odijk, T. Depletion theory of protein transport in semi-dilute polymer solutions. *Biophys. J.* **79**(5), 2314–2321 (2000).

[52] Chrambach, A. and Rodbard, D. Polyacrylamide gel electophoresis. *Science* **172**(3982), 440–& (1971).

[53] Schrödinger, LLC. The PyMOL molecular graphics system, version 1.3r1. (2010).

[54] Bell, J., Wilson, K., Zhang, X., Faber, H., Nicholson, H., and Matthews, B. Comparison of the crystal-structure of bacteriophage t4-lysozyme at low, medium, and high ionic strengths. *Proteins* **10**(1), 10–21 (1991).

[55] Szymański, J. *Diffusion of proteins in the solutions of nonionic surfactants*. PhD thesis, Institute of Physical Chemistry of the Polish Academy of Sciences, (2006).

[56] Devanand, K. and Selser, J. Asymptotic-behavior and long-range interactions in aqueous-solutions of poly(ethylene oxide). *Macromolecules* **24**(22), 5943–5947 (1991).

[57] Szymański, J., Patkowski, A., Wilk, A., Garstecki, P., and Hołyst, R. Diffusion and viscosity in a crowded environment: From nano- to macroscale. *J. Phys. Chem. B* **110**(51), 25593–25597 (2006).

[58] Mueller, C. B., Eckert, T., Loman, A., Enderlein, J., and Richtering, W. Dual-focus fluorescence correlation spectroscopy: a robust tool for studying molecular crowding. *Soft Matter* **5**(7), 1358–1366 (2009).

[59] Kubo, R. Fluctuation-dissipation theorem. *Rep. Prog. Phys.* **29**(Part 1), 255 (1966).

[60] Elowitz, M., Surette, M., Wolf, P., Stock, J., and Leibler, S. Protein mobility in the cytoplasm of Escherichia coli. *J. Bacteriol.* **181**(1), 197–203 (1999).

[61] Dauty, E. and Verkman, A. Actin cytoskeleton as the principal determinant of

size-dependent DNA mobility in cytoplasm. *J. Biol. Chem.* **280**(9), 7823–7828 (2005).

[62] Lukacs, G., Haggie, P., Seksek, O., Lechardeur, D., Freedman, N., and Verkman, A. Size-dependent DNA mobility in cytoplasm and nucleus. *J. Biol. Chem.* **275**(3), 1625–1629 (2000).

[63] Luby-Phelps, K., Taylor, D. L., and Lanni, F. Probing the structure of cytoplasm. *J. Cell Biol.* **102**(6), 2015–2022 (1986).

[64] Swaminathan, R., Hoang, C., and Verkman, A. Photobleaching recovery and anisotropy decay of green fluorescent protein GFP-S65T in solution and cells: Cytoplasmic viscosity probed by green fluorescent protein translational and rotational diffusion. *Biophys. J.* **72**(4), 1900–1907 (1997).

[65] Bathe, M., Heussinger, C., Claaessens, M. M. A. E., Bausch, A. R., and Frey, E. Cytoskeletal bundle mechanics. *Biophys. J.* **94**(8), 2955–2964 (2008).

[66] Gardel, M., Valentine, M., Crocker, J., Bausch, A., and Weitz, D. Microrheology of entangled F-actin solutions. *Phys. Rev. Lett.* **91**(15) (2003).

[67] Liu, J., Gardel, M., Kroy, K., Frey, E., Hoffman, B., Crocker, J., Bausch, A., and Weitz, D. Microrheology probes length scale dependent rheology. *Phys. Rev. Lett.* **96**(11) (2006).

[68] Luan, Y., Lieleg, O., Wagner, B., and Bausch, A. R. Micro- and macrorheolog-

ical properties of isotropically cross-linked actin networks. *Biophys. J.* **94**(2), 688–693 (2008).

[69] Wong, I., Gardel, M., Reichman, D., Weeks, E., Valentine, M., Bausch, A., and Weitz, D. Anomalous diffusion probes microstructure dynamics of entangled F-actin networks. *Phys. Rev. Lett.* **92**(17) (2004).

[70] Mohrdieck, C., Dalmas, F., Arzt, E., Tharmann, R., Claessens, M. M. A. E., Bausch, A. R., Roth, A., Sackmann, E., Schmitz, C. H. J., Curtis, J., Roos, W., Schulz, S., Uhrig, K., and Spatz, J. P. Biomimetic models of the actin cytoskeleton. *Small* **3**(6, Sp. Iss. SI), 1015–1022 (2007).

[71] Schmoller, K. M., Fernandez, P., Arevalo, R. C., Blair, D. L., and Bausch, A. R. Cyclic hardening in bundled actin networks. *Nat. Commun.* **1** (2010).

[72] Goodsel, D. *The Machinery of life*. Copernicus Books, Springer Science+Business Media, 2nd edition, (2009).

[73] Wang, Y., Li, C., and Pielak, G. J. Effects of Proteins on Protein Diffusion. *J. Am. Chem. Soc.* **132**(27), 9392–9397 (2010).

[74] Ruan, Q., Chen, Y., Gratton, E., Glaser, M., and Mantulin, W. Cellular characterization of adenylate kinase and its isoform: Two-photon excitation fluorescence imaging and fluorescence correlation spectroscopy. *Biophys. J.* **83**(6), 3177–3187 (2002).

[75] Hui, Y. Y., Zhang, B., Chang, Y.-C., Chang, C.-C., Chang, H.-C., Hsu, J.-H.,

Chang, K., and Chang, F.-H. Two-photon fluorescence correlation spectroscopy of lipid-encapsulated fluorescent nanodiamonds in living cells. *Opt. Express* **18**(6), 5896–5905 (2010).

[76] Kao, H., Abney, J., and Verkman, A. Determinants of the translational mobility of small solute in cell cytoplasm. *J. Cell Biol.* **120**(1), 175–184 (1993).

[77] Robertson, R. M., Laib, S., and Smith, D. E. Diffusion of isolated DNA molecules: Dependence on length and topology. *Proc. Natl. Acad. Sci. U. S. A.* **103**(19), 7310–7314 (2006).

[78] Maupin, P. and Pollard, T. Arrangement of actin-filaments and myosin-like filaments in the contractile ring and of actin-like filaments in the mitotic spindle of dividing HeLa-cells. *Journal of ultrastructure and molecular structure research* **94**(1), 92–103 (1986).

[79] Vandesande, W. and Persoons, A. The size and shape of macromolecular structures - determination of the radius, the length, and the persistence length of rodlike micelles of dodecyldimethylammonium chloride and bromide. *J. Phys. Chem.* **89**(3), 404–406 (1985).

[80] Arcizet, D., Meier, B., Sackmann, E., Raedler, J. O., and Heinrich, D. Temporal Analysis of Active and Passive Transport in Living Cells. *Phys. Rev. Lett.* **101**(24) (2008).

[81] Kumar, M., Mommer, M. S., and Sourjik, V. Mobility of Cytoplasmic, Mem-

brane, and DNA-Binding Proteins in Escherichia coli. *Biophys. J.* **98**(4), 552–559 (2010).

[82] Cluzel, P., Surette, M., and Leibler, S. An ultrasensitive bacterial motor revealed by monitoring signaling proteins in single cells. *Science* **287**(5458), 1652–1655 (2000).

[83] Mullineaux, C., Nenninger, A., Ray, N., and Robinson, C. Diffusion of green fluorescent protein in three cell environments in Escherichia coli. **188**(10), 3442–3448 (2006).

[84] van den Bogaart, G., Hermans, N., Krasnikov, V., and Poolman, B. Protein mobility and diffusive barriers in Escherichia coli: consequences of osmotic stress. **64**(3), 858–871 (2007).

[85] Slade, K. M., Steele, B. L., Pielak, G. J., and Thompson, N. L. Quantifying Green Fluorescent Protein Diffusion in Escherichia coli by Using Continuous Photobleaching with Evanescent Illumination. *J. Phys. Chem. B* **113**(14), 4837–4845 (2009).

[86] Nenninger, A., Mastroianni, G., and Mullineaux, C. W. Size Dependence of Protein Diffusion in the Cytoplasm of Escherichia coli. *J. Bacteriol.* **192**(18), 4535–4540 (2010).

[87] Mika, J. T., van den Bogaart, G., Veenhoff, L., Krasnikov, V., and Poolman,

B. Molecular sieving properties of the cytoplasm of Escherichia coli and consequences of osmotic stress. **77**(1), 200–207 (2010).

[88] Konopka, M. C., Shkel, I. A., Cayley, S., Record, M. T., and Weisshaar, J. C. Crowding and confinement effects on protein diffusion in vivo. *J. Bacteriol.* **188**(17), 6115–6123 (2006).

[89] Derman, A. I., Lim-Fong, G., and Pogliano, J. Intracellular mobility of plasmid DNA is limited by the ParA family of partitioning systems. *Mol. Microbiol.* **67**(5), 935–946 (2008).

[90] Jasnin, M., Moulin, M., Haertlein, M., Zaccai, G., and Tehei, M. Down to atomic-scale intracellular water dynamics. *EMBO REPORTS* **9**(6), 543–547 (2008).

[91] Golding, I. and Cox, E. RNA dynamics in live Escherichia coli cells. *Proc. Natl. Acad. Sci. U. S. A.* **101**(31), 11310–11315, AUG 3 (2004).

[92] Campbell, C. S. and Mullins, R. D. In vivo visualization of type II plasmid segregation: bacterial actin. laments pushing plasmids. *J. Cell Biol.* **179**(5), 1059–1066 (2007).

[93] Kalwarczyk, T., Zięba cz, N., Bielejewska, A., Zaboklicka, E., Koynov, K., Szymański, J., Wilk, A., Patkowski, A., Gapiński, J., Butt, H.-J., and Hołyst, R. Comparative analysis of viscosity of complex liquids and cytoplasm of mammalian cells at the nanoscale. *Nano Letters* **11**(5), 2157–2163 (2011).

[94] He, L. and Niemeyer, B. A novel correlation for protein diffusion coefficients based on molecular weight and radius of gyration. *Biotechnol. Prog.* **19**(2), 544–548 (2003).

[95] Young, M., Carroad, P., and Bell, R. Estimation of diffusion-coefficients of proteins. *Biotechnol. Bioeng.* **22**(5), 947–955 (1980).

[96] for the Properties of Water, I. A. and Steam. Revised release on the iaps formulation 1985 for the viscosity of ordinary water substance, (1997).

[97] Hou, S., Ziebacz, N., Kalwarczyk, T., Kaminski, T. S., Wieczorek, S. A., and Holyst, R. Influence of nano-viscosity and depletion interactions on cleavage of DNA by enzymes in glycerol and poly(ethylene glycol) solutions: qualitative analysis. *Soft Matter* **7**(7), 3092–3099 (2011).

[98] Seils, J. and Pecora, R. Dynamics of a 2311-base-pair superhelical dna in dilute and semidilute solutions. *Macromolecules* **28**(3), 661–673 (1995).

[99] Pettijohn, D. E. *Modulation of chemical composition and other parameters of the cell by growth rate*, volume 1 of *The Nucleoid*, 158–166. ASM Press., Washington DC (1996).

[100] Sorensen, C. and Shi, D. Guinier analysis for homogeneous dielectric spheres of arbitrary size. *Opt. Commun.* **178**(1-3), 31–36 (2000).

[101] Lamanna, R., Delmelle, M., and Cannistraro, S. Solvent Stokes-Einstein Vi-

olation In Aqueous Protein Solutions. *Phys. Rev. E* **49**(6, Part b), 5878–5880 (1994).

[102] Langevin, D. and Rondelez, F. Sedimentation of large colloidal particles through semidilute polymer-solutions. *Polymer* **19**(8), 875–882 (1978).

[103] Brangwynne, C. P., Koenderink, G. H., MacKintosh, F. C., and Weitz, D. A. Cytoplasmic diffusion: molecular motors mix it up. *J. Cell Biol.* **183**(4), 583–587 (2008).

[104] Wirtz, D. Particle-Tracking Microrheology of Living Cells: Principles and Applications. *Ann. Rev. Biophys.* **38**, 301–326 (2009).

[105] Berg, O. G., Winter, R. B., and von Hippel, P. H. Diffusion-driven mechanisms of protein translocation on nucleic acids. 1. models and theory. *Biochemistry* **20**(24), 6929–6948 (1981).

[106] Li, G.-W., Berg, O. G., and Elf, J. Effects of macromolecular crowding and DNA looping on gene regulation kinetics. *Nat. Phys.* **5**(4), 294–297 (2009).

[107] Porcar, L., Falus, P., Chen, W.-R., Faraone, A., Fratini, E., Hong, K., Baglioni, P., and Liu, Y. Formation of the Dynamic Clusters in Concentrated Lysozyme Protein Solutions. *J. Phys. Chem. Lett.* **1**(1), 126–129 (2010).